Error probability in digital fiber optic communication systems

th e

Error probability in digital fiber optic communication systems

by

A. M. J. Koonen

E I N D H O V E N U N I V E R S I T Y O F T E C H N O L O G Y
Department of Electrical Engineering
Eindhoven The Netherlands

ERROR PROBABILITY IN DIGITAL FIBER OPTIC COMMUNICATION SYSTEMS

by

A.M.J. Koonen

TH-Report 79-E-99
ISBN 90-6144-099-8

Eindhoven
September 1979

ABSTRACT

The average bit error probability for a digital optical fiber system is numerically calculated using two receiver models. We analyze the influence of a number of important system parameters and of mBnB line coding. The decision threshold and the average avalanche gain are optimized to yield a minimum average bit error probability. Timing errors in the receiver are not considered, and we assume the shape of the received optical pulses to be known (rectangular or Gaussian). The equalization in the receiver is of the raised cosine type. A Gaussian approximation of the statistics of the signal at the threshold detector input is introduced. Average bit error probabilities are calculated using the exhaustive method.

Koonen, A.M.J.
ERROR PROBABILITY IN DIGITAL FIBER OPTIC COMMUNICATION SYSTEMS.
Eindhoven University of Technology, Department of Electrical Engineering, Eindhoven, The Netherlands. September 1979.
TH-Report 79-E-99

Present address of the author:

Ir. A.M.J. Koonen,
Philips' Telecommunicatie Industrie B.V.,
Afd. Voorontwikkeling Transmissie,
HUIZEN,
The Netherlands

CONTENTS

1. Introduction

Several years ago the optical fiber was introduced as an important new communication medium. It offers a lot of technical and economical advantages as compared with conventional metallic conductors like coaxial cables. For instance it weights less. It is thinner, more flexible, free of electromagnetic interferences, it has a larger bandwidth, and is composed of cheaper basic materials. Being an attractive solution to meet the growing need of information transmission capacity, it is the subject of many investigations and experiments.

An appropriate criterion to judge the quality of a digital transmission system is the average bit error probability. As far as error probability calculations are concerned, optical fiber systems distinguish themselves from coaxial systems by the fact, that at the photo detection process in the receiver a so-called shot noise is produced. This shot noise is non-stationary and signal-dependent. The receiver adds the usual stationary Gaussian noise. In coaxial systems only stationary, signal-independent noise plays a part.

Several methods to calculate the error probability of a digital optical transmission system have already been published. They all try to approximate the very complicated statistics of the signal at the threshold detector input in the receiver with more or less accuracy. An approach with Gaussian quadrature integration formules is possible [8], and also an "exact" calculation [1], a statistical simulation [1], a method based on the Chernoff-bound [1], and a method based on a Gaussian approximation [1,3,6]. The last method offers more insight into the influence of system parameter variations, and facilitates the implementation of line coding in the calculations. It gives fairly accurate results, but tends to underestimate the optimum threshold setting and overestimate the optimum average avalanche gain [1]. Following this method, we numerically calculate the average bit error probability using two receiver models. We analyze the influence of a number of important system parameters and of mBnB line coding.

To carry out error probability calculations, we have to define a system model (chapter 2). Using this a statistical signal analysis is derived (chapter 3). We introduce a linear receiver model (chapter 4). The very complicated statistics of the signal at the threshold detector input, needed for error probability calculations, may under certain circumstances be approximated by

Gaussian statistics (chapter 5). The signal dependence of the shot noise can be translated into interference by the neighboring symbols with the symbol under decision. We can deal with this interference using the so-called exhaustive method. This method scans all possible patterns of the relevant neighboring symbols. Using this method we shall calculate the average bit error probability with the aid of a digital computer. We consider the optimum setting of the decision threshold and of the average avalanche gain at the receiver (chapter 6), and the aspects of the so-called mBnB line coding (chapter 7). Using the previously mentioned receiver model, calculations of the average bit error probability are carried out (chapter 8). Timing errors at the sampler are not considered, and we assume the shape of the received optical pulses to be known (rectangular or Gaussian). The equalization in the receiver is of the raised cosine type. We analyze the influence of a number of important system parameters, and of line coding. The decision threshold and the average avalanche gain are optimized to yield a minimum average bit error probability. Similar calculations are carried out using a modified receiver model (chapter 9).

2. System model

The transmission of digital information over an optical fiber system can be described with the model shown in figure 2.1.

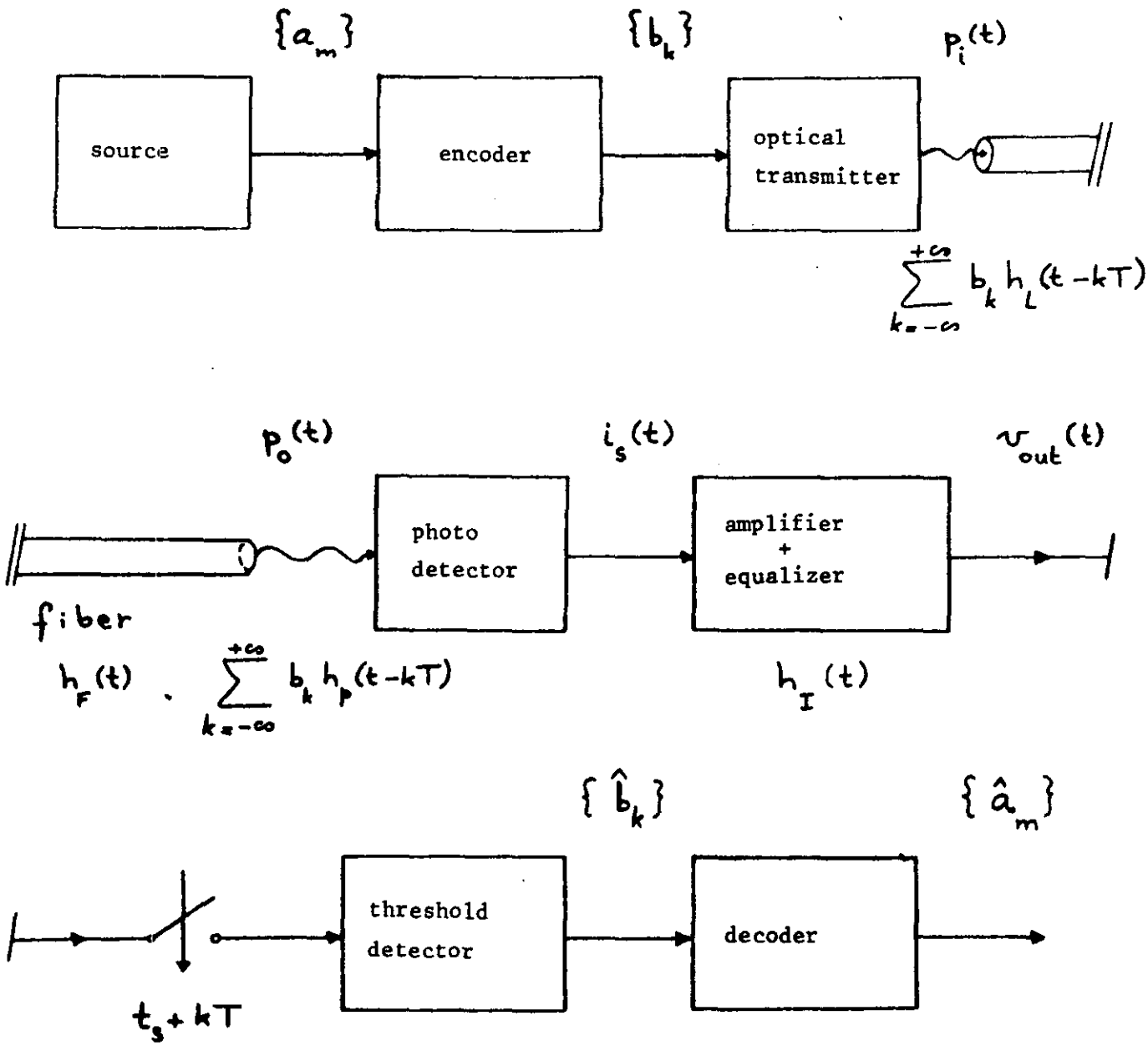

Figure 2.1. The transmission of digital information over an optical fiber system

The source produces a sequence of data symbols $\{a_m\}$.
In the encoder, the source signal is converted into a symbol sequence $\{b_k\}$ suitable for transmission with a signalling rate of $1/T$ symbols per second.

A laser diode or a light emitting diode (LED) is used as optical transmitter We prefer a laser diode because of its larger output power, smaller spectral bandwidth, faster response, and smaller divergence of the light beam. The modulation characteristic of a laser diode is non-linear. We may however specify the shape of the output optical pulses $h_L(t)$ in such a way that the laser output approximately is formed by a linear superposition of these pulses. The optical power, launched into the fiber, is

$$p_i(t) = \sum_{k=-\infty}^{+\infty} b_k . h_L(t-kT) \tag{2.1}$$

where $\int_{-\infty}^{+\infty} b_k . h_L(t-kT)dt$ is the energy of the k-th optical pulse, and $h_L(t) \geq 0$ for every t.

Introducing a linear approximation of the fiber baseband behavior [2], we denote its impulse response by $h_F(t)$. We obtain for the light power at the output of the fiber

$$p_o(t) = \sum_{k=-\infty}^{+\infty} b_k . h_p(t-kT) \tag{2.2}$$

where

$$h_p(t) \triangleq h_L(t) * h_F(t) \geq 0 \text{ for every } t$$

(* means convolution). Following Personick [3], we normalize the received optical pulse shape $h_p(t)$ so that

$$\int_{-\infty}^{+\infty} h_p(t)\, dt = 1 \tag{2.3}$$

making b_k equal to the energy in the k-th received optical pulse:

$$b_k \geq 0 \text{ for every integer } k \tag{2.4}$$

The photodetector converts $p_o(t)$ into an electrical current $i_s(t)$. For this purpose we take a PIN-photodiode or an avalanche photodiode (APD). We prefer an APD because of its internal amplification mechanism.

The amplifier and the equalizer convert $i_s(t)$ into an output voltage $v_{out}(t)$, which will be further analyzed in chapter 3. The joint impulse response of amplifier and equalizer is denoted by $h_I(t)$. The signal $v_{out}(t)$ is periodically

sampled at $t_s + kT$. From the sampled values, the threshold detector derives estimates $\{\hat{b}_k\}$ for the symbols $\{b_k\}$ being sent, using bit-by-bit detection. A decoder converts the sequence $\{\hat{b}_k\}$ into estimates $\{\hat{a}_m\}$ of the sequence produced by the source.

3. Statistical analysis of signals

3.1. Photodetector

Using an avalanche photodiode (APD) as photodetector, we describe its output current by a filtered non-uniform Poisson process [3,4]

$$i_s(t) = \sum_{i=1}^{N(t)} e g_i . h_s(t-t_i) \qquad (3.1)$$

where:

e : charge of an electron

g_i : random avalanche gain at random time t_i, i.e. the number of secondary electrons generated for a primary electron at t_i

$g.h_s(t)$: APD impulse response (ideal APD: $h_s(t) = \delta(t)$)

$$\int_{-\infty}^{+\infty} h_s(t)\, dt = 1$$

N(t) : the number of primary electrons generated during $(-\infty,t)$ for the incident photons

$$\Pr[N(t) = N] = \frac{\Lambda^N}{N!} . e^{-\Lambda} \quad \text{where } \Lambda \triangleq \int_{-\infty}^{t} \lambda(\tau)d\tau$$

N(t) is a non-homogeneous counting process with intensity $\lambda(t)$ given by

$$\lambda(t) = \frac{\eta}{h\nu} . p_o(t) + \lambda_o \qquad (3.2)$$

where

$h\nu$: energy in a photon

η : quantum efficiency of the detector

λ_o : dark current of the detector

Substituting (2.2) we obtain

$$\lambda(t) = \frac{\eta}{h\nu} . \sum_{k=-\infty}^{+\infty} b_k . h_p(t-kT) + \lambda_o \qquad (3.3)$$

The same model holds for a PIN photodiode, but without avalanche effect (so $g_i \equiv 1$).

3.2. Equalizer output signal

Let the duration of the photodiode response $h_s(t)$ be negligible as compared with the remaining time constants in the receiver circuitry. With the joint impulse response $h_I(t)$ of the amplifier and the equalizer, the equalizer output signal is

$$v_{out}(t) = x(t) + n_{th}(t) \tag{3.4}$$

where

$$x(t) = i_s(t) * h_I(t) \simeq \sum_{i=1}^{N(t)} eg_i . h_I(t-t_i)$$

represents a non-uniform filtered Poisson process with intensity $\lambda(t)$ according to (3.3), and where $n_{th}(t)$ represents additive thermal noise from the amplifier and the equalizer. This $n_{th}(t)$ is stationary and signal-independent, having a Gaussian probability density function (p.d.f.) with expectation

$$E[n_{th}(t)] = 0 \tag{3.5}$$

The signal $x(t)$ can be separated into its expectation $E[x(t)]$ and a non-stationary, signal-dependent, zero-mean shot noise $n_s(t)$

$$n_s(t) \triangleq x(t) - E[x(t)] \tag{3.6}$$

We are interested in the expectation and the variance of $v_{out}(t)$ at the decision time t_s. From $v_{out}(t_s)$ the threshold detector derives an estimate $\hat{b}_o$ for the symbol b_o being sent. In the following signal dependency will be indicated by a condition on the transmitted data sequence $B \triangleq \{b_k\}$. Using (3.3) we calculate for the expectation [3,4]

$$E[v_{out}(t_s)|B] = E[x(t_s)|B] = \int_{-\infty}^{+\infty} \lambda(\tau).E[eg.h_I(t_s-\tau)]d\tau$$

$$= \sum_{k=-\infty}^{+\infty} b_k.h_{out}(t_s-kT) + V_o \tag{3.7}$$

where

$h_{out}(t) \triangleq eG.\frac{\eta}{h\nu} . h_p(t) * h_I(t)$: equalized output pulse

$G \triangleq E[g]$: average avalanche gain

$V_o \triangleq eG.\lambda_o.H_I(o)$: dark current contribution

($H_I(f) = \mathcal{F}[h_I(t)]$, $\mathcal{F}$ denoting Fourier transformation).
Assuming the shot noise $n_s(t)$ and the thermal noise $n_{th}(t)$ to be uncorrelated, we calculate for the variance using (3.3) [3,4]

$$\begin{aligned} Var[v_{out}(t_s)|B] &= E[n_s^2(t_s)|B] + E[n_{th}^2(t)] \\ &= \int_{-\infty}^{+\infty} \lambda(\tau).E[(eg.h_I(t_s-\tau))^2]d\tau + E[n_{th}^2(t)] \\ &= \frac{h\nu}{\eta} \cdot F_e \cdot \sum_{k=-\infty}^{+\infty} b_k.z(t_s-kT) + Z_o + E[n_{th}^2(t)] \end{aligned} \qquad (3.8)$$

where

$F_e \triangleq E[g^2]/G^2$: excess noise factor

$z(t) \triangleq (\frac{eG\eta}{h\nu})^2 \cdot h_p(t) * h_I^2(t) = h_p(t) * h_1^2(t)$: shot noise variance function

$h_1(t) = \mathcal{F}^{-1}[H_1(f)] \triangleq \mathcal{F}^{-1}[H_{out}(f)/H_p(f)]$

$Z_o \triangleq \lambda_o.F_e.(\frac{h\nu}{\eta})^2 \int_{-\infty}^{+\infty} |H_1(f)|^2 df$: dark current contribution

($\mathcal{F}^{-1}$ denotes inverse Fourier transformation; $H_{out}(f) = \mathcal{F}[h_{out}(t)]$ and $H_p(f) = \mathcal{F}[h_p(t)]$). Furthermore $F_e = 1$ holds for a photo diode with a deterministic amplification.

3.3. Time normalization

In order to isolate the dependence on the time slot width T from the functions $h_p(t)$ and $h_{out}(t)$, we introduce time-normalized functions

$$h_p'(t) \triangleq T.h_p(t.T) \qquad H_p'(f) = \mathcal{F}[h_p'(t)] = H_p(f/T)$$

$$h_{out}'(t) \triangleq h_{out}(t.T) \qquad H_{out}'(f) = \mathcal{F}[h_{out}'(t)] = \frac{1}{T}.H_{out}(f/T) \qquad (3.9)$$

Formula (2.3) retains its validity for $h_p'(t)$:

$$\int_{-\infty}^{+\infty} h'_p(t)\,dt = H'_p(o) = 1 \tag{3.10}$$

Using (3.9) we can also obtain time-normalized equivalents for the functions $h_l(t)$ and $z(t)$:

$$h'_l(t) \triangleq h_l(t.T) \qquad H'_l(f) = \mathcal{F}[h'_l(t)] = \frac{1}{T}.H_l(f/T) = H'_{out}(f)/H'_p(f) \tag{3.11}$$

$$z'(t) \triangleq z(t.T) \qquad z'(t) = h'_p(t) * h'^2_l(t) \tag{3.12}$$

All these time-normalized functions and the corresponding spectra depend on the shapes of the spectra $H_p(f)$ and $H_{out}(f)$, but no longer on the time slot width T.

3.4. Transmitter alphabet

Because of the non-linear modulation characteristic of the optical transmitter (i.c. laser diode), we restrict ourselves in the following to a binary alphabet for the line symbols b_k:

$$b_k \text{ E } \{b_{min}, b_{max}\} \quad \text{where } 0 \leqslant b_{min} < b_{max} \tag{3.13}$$

We define an extinction EXT by

$$EXT \triangleq \frac{b_{min}}{b_{max}} \tag{3.14}$$

Thus imperfect modulation results in EXT > 0.
We normalize the line symbols b_k on the maximum energy b_{max} in a received optical pulse

$$b'_k \triangleq \frac{b_k}{b_{max}} \tag{3.15}$$

thereby introducing a normalized transmitter alphabet, equivalent with (3.13):

$$b'_k \text{ E } \{EXT, 1\} \quad \text{where EXT} \geqslant 0 \tag{3.16}$$

If the alphabet symbols b_{min} and b_{max} are equiprobable, the average received

optical power P_o is given by

$$P_o = 10 \cdot {}^{10}\log\left[\frac{b_{max}(1+EXT)}{2T.1\ mW}\right] \quad (dBm) \tag{3.17}$$

This formula applies to the case of a balanced line code, and to the case of straight binary transmission with equiprobable symbols.
Substituting (3.9) through (3.15) in (3.7) and (3.8), we obtain for the expectation and the variance of the equalizer output signal at the decision time t_s, respectively

$$E[v_{out}(t_s)|B] = b_{max} \sum_{k=-\infty}^{+\infty} b'_k . h'_{out}(\frac{t_s}{T} - k) + V_o \tag{3.18}$$

$$Var[v_{out}(t_s)|B] = \frac{h\nu}{\eta}.F_e.b_{max} \sum_{k=-\infty}^{+\infty} b'_k . z'(\frac{t_s}{T} - k) + Z_o + E[n^2_{th}(t)] \tag{3.19}$$

The dark current contributions are according to (3.7) through (3.11)

$$V_o = eG.\lambda_o.\frac{h\nu}{\eta}.\frac{1}{eG}.\frac{H_{out}(o)}{H_p(o)} = \lambda_o T.\frac{hf}{\eta}.H'_{out}(o) \tag{3.20}$$

$$Z_o = \lambda_o T.(\frac{h\nu}{\eta})^2.F_e.I_2 \tag{3.21}$$

where we have defined a weighting factor I_2 in agreement with [3] by

$$I_2 \triangleq \int_{-\infty}^{+\infty} |H'_{out}(f)/H'_p(f)|^2 df = \int_{-\infty}^{+\infty} |H'_1(f)|^2 df \tag{3.22}$$

This factor only takes into account the shape of the received optical pulse $h_p(t)$ and of the equalized output pulse $h_{out}(t)$. It is independent of the time slot width T, because it is expressed in the time-normalized spectra of these pulses. Note that both dark current contributions are inversely proportional to the signalling rate 1/T.

3.5. Worst case and best case data patterns

From (2.2) and (3.9) we have

$$h'_p(t) \geqslant 0 \quad \text{for every } t \tag{3.23}$$

so with (3.12)

$$z'(t) \geq 0 \quad \text{for every } t \tag{3.24}$$

Hence the signal contribution to the output variance (3.19), given a symbol under decision b_o, attains its maximum value if the neighboring symbols $\{b_{k,k\neq o}\}$ all have their maximum value. We therefore define with (3.13) a worst case pattern B'_{WC} of neighboring symbols by

$$B'_{WC} \triangleq \{b_{k,k\neq o} \equiv b_{max}\} \tag{3.25}$$

This pattern gives rise to the maximum noise power at the equalizer output at the decision time t_s given b_o, for which we write using (3.15) and (3.19)

$$\begin{aligned} NW\ (b_o) &\triangleq Var[v_{out}(t_s)|B'_{WC},b_o] \\ &= \frac{h\nu}{\eta}.F_e\{b_o.z'(\frac{t_s}{T}) + b_{max}\ (\sum_{k=-\infty}^{+\infty} z'(\frac{t_s}{T} - k)\ -z'(\frac{t_s}{T}))\} \\ &+ Z_o + E\ [n^2_{th}(t)] \end{aligned} \tag{3.26}$$

In a similar way we define with (3.13) a best case pattern B'_{BC} of neighboring symbols by

$$B'_{BC} \triangleq \{b_{k,k\neq o} \equiv b_{min}\} \tag{3.27}$$

which gives rise to the minimum noise power at the equalizer output

$$\begin{aligned} NB\ (b_o) &\triangleq Var[v_{out}(t_s)|B'_{BC},b_o] \\ &= \frac{h\nu}{\eta}.F_e.\{b_o.z'(\frac{t_s}{T}) + b_{min}.(\sum_{k=-\infty}^{+\infty} z'(\frac{t_s}{T} - k) - z'(\frac{t_s}{T}))\} \\ &+ Z_o + E[n^2_{th}(t)] \end{aligned} \tag{3.28}$$

3.6. Excess noise factor

We can express the excess noise factor F_e in the average avalanche gain G

and an APD ionisation constant k. Starting from an implicit expression for the moment generating function $M_g(s)$ of the avalanche gain g [10], we calculate F_e according to (see (3.8))

$$F_e = E[g^2]/G^2 = \frac{d^2M_g(s)}{ds^2}\Big|_{s=o} \Big/ \left[\frac{dM_g(s)}{ds}\Big|_{s=o}\right]^2 \tag{3.29}$$

which leads to

$$F_e = kG + (1-k).(2 - \frac{1}{G}) \tag{3.30}$$

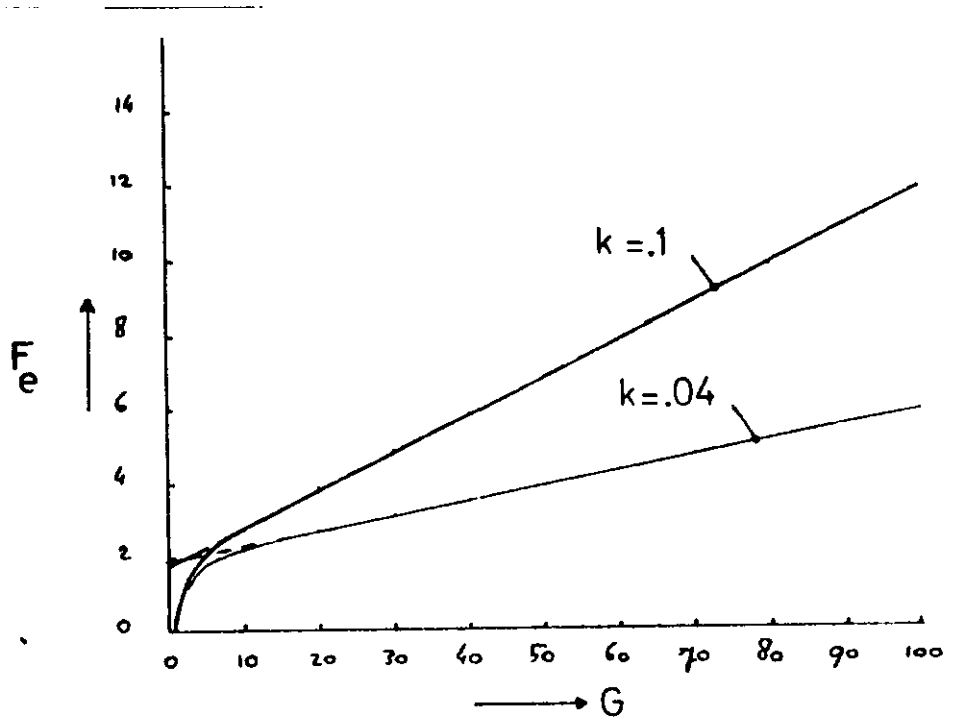

Figure 3.1. Excess noise factor F_e versus the average avalanche gain G with the APD ionisation constant k as a parameter

The constant k is the ratio of the probability per unit length of a hole (moving in the detector high field region) producing a collision, to the same quantity for electrons.
Figure 3.1 shows a plot of F_e versus G with k as a parameter. For large G (3.30) can be approximated by

$$F_e \simeq kG + 2.(1-k) \quad \text{if } G >> 1 \tag{3.31}$$

Personick uses in [3] the approximation

$$F_e \simeq G^x \tag{3.32}$$

suggesting x = .5 as a typical value of the excess noise exponent x for a silicon APD. If G ≃ 60, (3.32) approximates (3.30) fairly well by taking k = .1 (within 2% if G = 60 ($\pm$ 5%)).

4. Linear receiver model

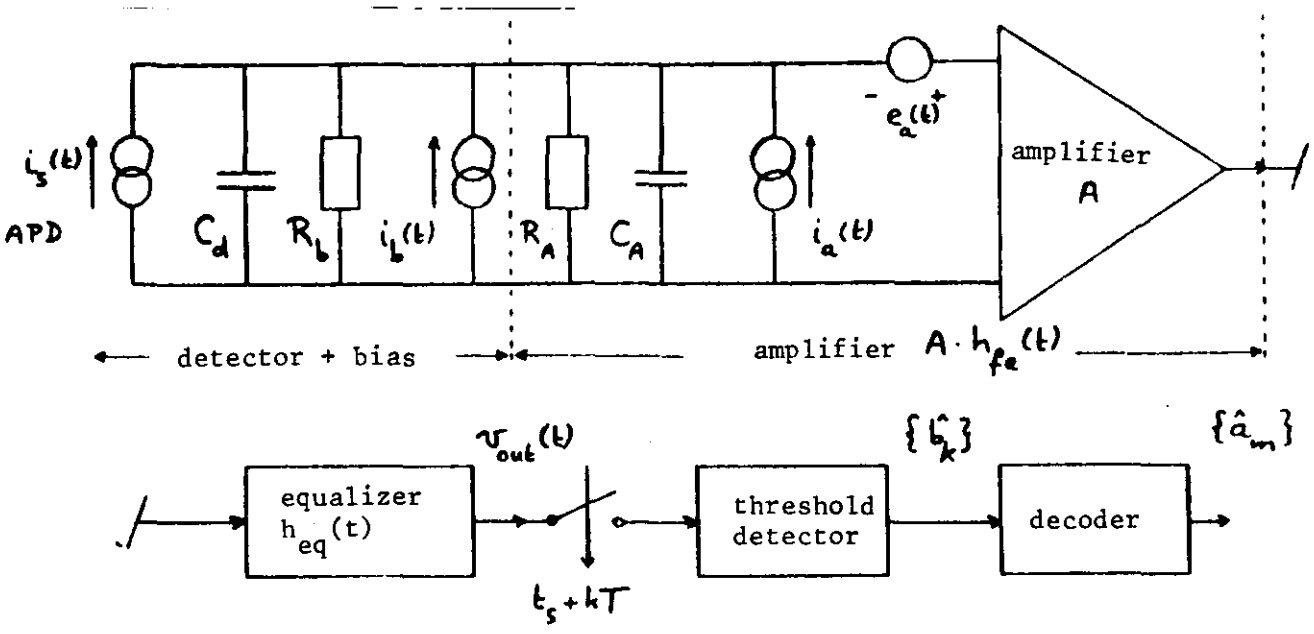

Figure 4.1. Receiver

Figure 4.1 shows a typical optical receiver in schematic form [3]. Here

R_b : APD biasing resistance
C_d : APD junction capacitance
$i_b(t)$: current noise source, associated with R_b
R_A : amplifier input resistance
C_A : amplifier input capacitance
$i_a(t)$: amplifier input current noise source
$e_a(t)$: amplifier input voltage noise source

The noise sources are assumed to be white, Gaussian, and uncorrelated. The amplifier gain A is assumed to be sufficiently high so that noises introduced by the equalizer are negligible. The equalizer impulse response $h_{eq}(t)$ is chosen such, that a received optical pulse $h_p(t)$ causes an equalized output pulse $h_{out}(t)$ free from intersymbol interference at $t = kT$ for every integer k:

$$h_{out}(kT) = \delta_k \tag{4.1}$$

where Kronecker symbol

$\delta_k = 1$ for $k = 0$
$= 0$ for integer k, $k \neq 0$.

4.1. Thermal noise power at the equalizer output

The thermal noise power at the equalizer output is given by [3]

$$E[n_{th}^2(t)] = \left(\frac{h\nu}{e\eta G}\right)^2 \cdot \left\{\left[\frac{2k\theta}{R_b} + \frac{S_E}{R_T^2} + S_I\right].TI_2 + S_E.(2\pi C_T)^2.\frac{I_3}{T}\right\} \qquad (4.2)$$

where

$2k\theta/R_b$: two-sided spectral noise density of $i_b(t)$ in A^2/Hz

S_E : two-sided spectral noise density of $e_a(t)$ in V^2/Hz

S_I : two-sided spectral noise density of $i_a(t)$ in A^2/Hz

$R_T = R_A // R_b$ (// denotes parallel connection)

$C_T = C_A + C_d$

Like I_2 the weighting factor I_3 takes into account only the shape of the received optical pulse $h_p(t)$ and of the equalized output pulse $h_{out}(t)$, and is independent of the time slot width T. We define I_3 in agreement with [3] by

$$I_3 \triangleq \int_{-\infty}^{+\infty} f^2.|H'_{out}(f)/H'_p(f)|^2 df = \int_{-\infty}^{+\infty} f^2.|H'_1(f)|^2 df \qquad (4.3)$$

To minimize $E[n_{th}^2(t)]$ R_b and R_A must be as large as possible, and C_d and C_A as small as possible.

According to (4.2) $E[n_{th}^2(t)]$ is inversely proportional to G^2. We define a thermal noise parameter Z_{th}, independent of G, by

$$Z_{th} \triangleq G^2.E[n_{th}^2(t)] = \left(\frac{h\nu}{e\eta}\right)^2.\left\{\left[\frac{2k\theta}{R_b} + \frac{S_E}{R_T^2} + S_I\right].TI_2 + S_E.(2\pi C_T)^2.\frac{I_3}{T}\right\} \qquad (4.4)$$

Thus Z_{th} (and $E[n_{th}^2(t)]$ also) consists of a term, proportional to I_2 and inversely proportional to the signalling rate 1/T, and of a term, proportional to I_3 and to 1/T. Hence at higher rates 1/T, Z_{th} is nearly proportional to 1/T:

$$Z_{th} \simeq \left(\frac{h\nu}{e\eta}\right)^2 S_E.(2\pi C_T)^2.\frac{I_3}{T} \text{ for large } 1/T \qquad (4.5)$$

Z_{th} is related to Z, defined in [3, part I, formula (30)], by

$$Z_{th} = \left(\frac{h\nu}{\eta}\right)^2.Z \qquad (4.6)$$

and to n_{therm}, defined in [6, p. 217] (where it is named n_{th}), being the thermal noise in the units of secondary electrons, by

$$Z_{th} = \left(\frac{h\nu}{\eta}\right)^2.n_{therm}^2 \qquad (4.7)$$

4.2. Received optical pulse shapes

We consider two families of received optical pulse shapes (time-normalized according to (3.9)):

a. rectangular pulses ($\alpha_r \lesssim 1$)

$$\begin{aligned} h'_p(t) &= 1/\alpha_r \qquad \text{for } |t| < \alpha_r/2 \\ &= 0 \qquad\quad \text{otherwise} \end{aligned} \qquad (4.8)$$

$$H'_p(f) = \sin(\alpha_r.\pi f)/(\alpha_r.\pi f)$$

b. Gaussian pulses

$$h'_p(t) = \frac{1}{\alpha_g.\sqrt{2\pi}} \cdot e^{-t^2/2\alpha_g^2}$$

$$H'_p(f) = e^{-2(\alpha_g.\pi f)^2} \qquad (4.9)$$

These pulses are shown by figure 4.2. Pulse narrowing leads to a proportional increase in pulse height, because of the pulse energy remaining constant (see (3.10)).

It is worth noticing that the assumption of rectangular received optical pulses makes sense only in the case of negligible fiber dispersion. A certain amount of fiber dispersion makes Gaussian pulses more plausible.

We define a normalized r.m.s. optical pulse width $\frac{\sigma}{T}$ by [3]

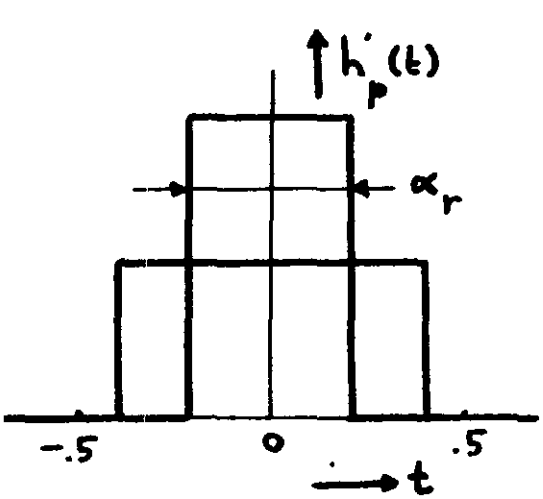

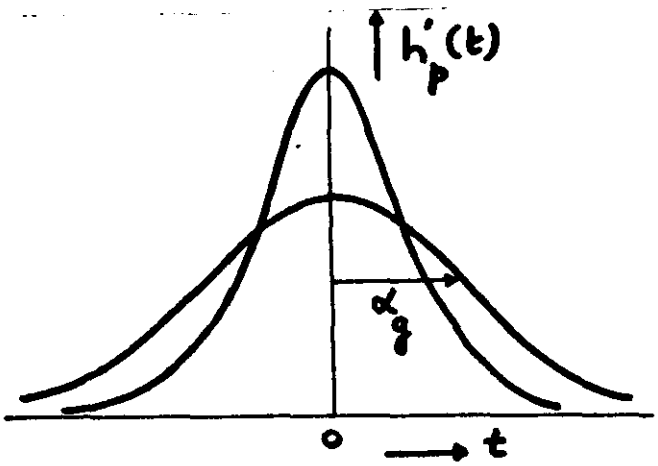

4.2.a. Rectangular ($\alpha_r \leq 1$) 4.2.b. Gaussian

Figure 4.2. Received optical pulse shapes (time-normalized)

$$\left(\frac{\sigma}{T}\right)^2 \triangleq \frac{1}{T^2} \cdot \left\{ \int_{-\infty}^{+\infty} t^2 . h_p(t)dt - \left[\int_{-\infty}^{+\infty} t . h_p(t)dt \right]^2 \right\}$$

$$= \int_{-\infty}^{+\infty} t^2 . h'_p(t)dt - \left[\int_{-\infty}^{+\infty} t . h'_p(t)dt \right]^2 \qquad (4.10)$$

Hence

$$\alpha_r = \sqrt{12} \cdot \frac{\sigma}{T} \quad \text{and} \quad \alpha_g = \frac{\sigma}{T} \qquad (4.11)$$

4.3. Equalized output pulse shapes

We consider two families of equalized output pulse shapes, both with a roll-off factor β ($0 \leq \beta \leq 1$), and time-normalized according to (3.9):

a. raised cosine pulses

$$h'_{out}(t) = \frac{\sin(\pi t).\cos(\beta\pi t)}{\pi t.[1-(2\beta t)^2]}$$

$$H'_{out}(f) = 1 \qquad \text{for } |f| < (1-\beta)/2$$

$$= \tfrac{1}{2}[1-\sin(\tfrac{\pi}{\beta}(|f| - \tfrac{1}{2}))] \quad \text{for } (1-\beta)/2 \leq |f| < (1+\beta)/2$$

$$= 0 \qquad \text{otherwise} \qquad (4.12)$$

b. "optimum" pulses

$$h'_{out}(t) = \frac{\sin(\pi t)}{\pi t}\{(1-\beta)\cos(\beta\pi t) + \frac{\sin(\beta\pi t)}{\pi t}\}$$

$$H'_{out}(f) = 1 \qquad \text{for } |f| < (1-\beta)/2$$

$$= 1 - |f| \qquad \text{for } (1-\beta)/2 \leq |f| < (1+\beta)/2$$

$$= 0 \qquad \text{otherwise} \tag{4.13}$$

These pulses with their spectra are shown by figure 4.3.
Both pulse types do not cause intersymbol interference (i.s.i.) at the sampling times t = k (integer k) according to (4.1). In addition the "optimum" pulses introduce for small timing errors a minimum amount of i.s.i. according to a mean squared error criterion [7,8].
In section 9.1 we will also consider raised cosine equalized output pulses with a rolloff factor $\beta > 1$.

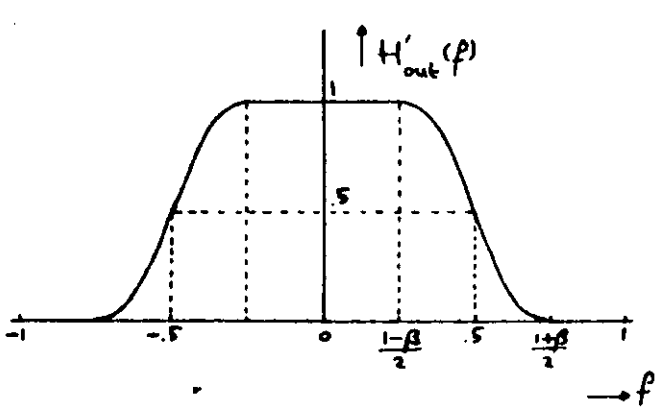

4.3.a. raised cosine spectrum $H'_{out}(f)$

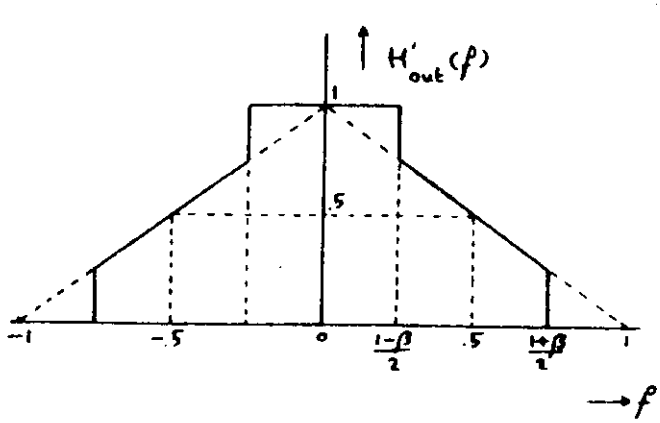

4.3.b. "optimum" spectrum $H'_{out}(f)$

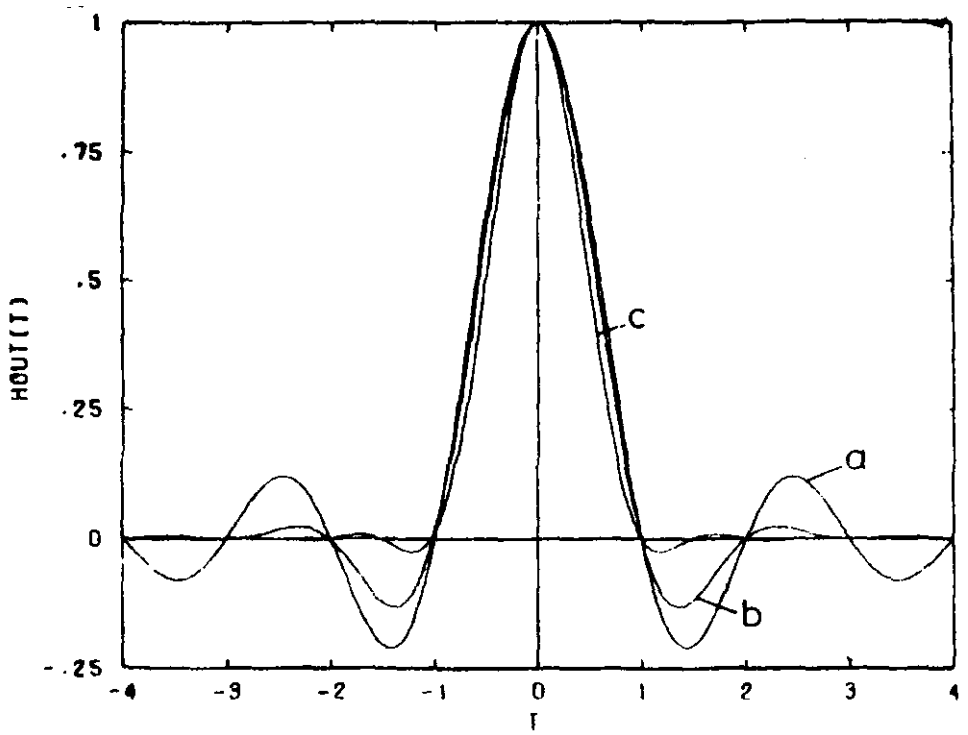

4.3.c. raised cosine time function $h'_{out}(t)$
(a: β = .1; b: β = .5; c: β = 1)

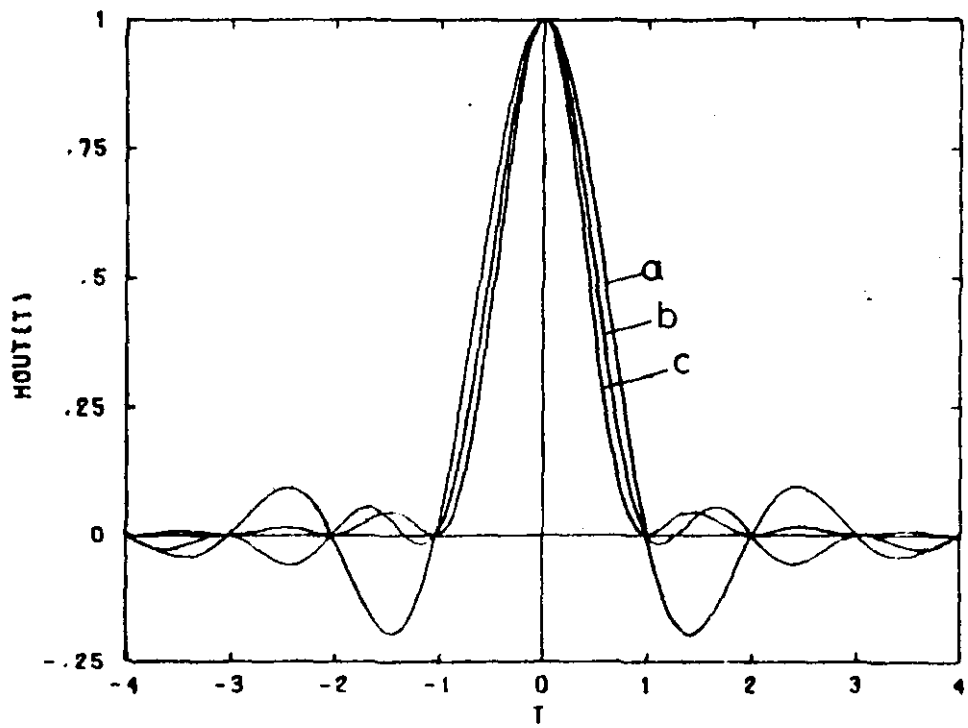

4.3.d. "optimum" time function $h'_{out}(t)$
(a: β = .1; b: β = .5; c: β = 1)

Figure 4.3. Equalized output pulse shapes with their spectra

4.4. Shot noise variance functions

We assumed the received optical pulse shape $h'_p(t)$ to be rectangular or Gaussian, and the equalized output pulse shape $h'_{out}(t)$ to be raised cosine or "optimum". Hence four combinations of $h'_p(t)$ with $h'_{out}(t)$ are possible, each giving a particular shape to the shot noise variance function $z'(t)$ according to (3.11). Appendix 1 shows a number of plots of $z'(t)/z'(o)$ versus t for each combination, calculated with the aid of Fast Fourier Transform algorithms. Parameters are the rolloff factor β of $h'_{out}(t)$ and the normalized r.m.s. optical pulse width σ/T of $h'_p(t)$ ($\sigma/T = \alpha_g$ for Gaussian pulses, and for rectangular pulses $\sigma/T = .144$ and $= .260$ correspond with $\alpha_r = .5$ and $= .9$ respectively, according to (4.11)).

These plots show a nearly identical behavior of $z'(t)/z'(o)$ for rectangular and Gaussian received optical pulses, provided that they have the same normalized r.m.s. pulse width σ/T. Furthermore $z'(t)$ is time-unlimited and decays faster for larger β and smaller σ/T; it decays slightly faster for "optimum" than for raised cosine equalized output pulses.

These plots show $z'(t) \geqslant 0$ for every t (see (3.24)) and $z'(k) > 0$ for every integer k. Thus even in the absence of timing errors (i.e. for $t_s = 0$) intersymbol interference arises in the shot noise contribution to the output variance (see (3.19) and (4.4)):

$$\mathrm{Var}[v_{out}(t_s=0)\,|\,B] = \frac{h\nu}{\eta}.F_e.b_{max} \sum_{k=-\infty}^{+\infty} b'_k.z'(-k) + Z_o + Z_{th}/G^2 \qquad (4.14)$$

Using a fairly large rolloff factor β and a not to large normalized r.m.s. optical pulse width σ/T (e.g. $\beta = 1$ and $\sigma/T = .144$), $z'(t)$ decays so fast, that this intersymbol interference is nearly negligible.

5. Calculating the error probability

5.1. Gaussian approximation of the output signal statistics

The equalizer output signal $v_{out}(t)$ is formed by the sum of a non-uniform filtered Poisson process and a stationary Gaussian process. Hence the statistics of $v_{out}(t_s)$, needed to carry out error probability calculations, are very complicated. To obtain mathematical simplifications we approximate these statistics by a Gaussian probability density function (p.d.f.), conditioned on the transmitted data sequence $B = \{b_k\}$. This Gaussian p.d.f. is completely defined by its conditional expectation $E[v_{out}(t_s)|B]$, and its conditional variance $\mathrm{Var}\,[v_{out}(t_s)|B]$, calculated in (3.18) and (3.19) respectively. It is a good approximation of the real p.d.f. of $v_{out}(t_s)$ if the intensity $\lambda(t)$ given by (3.3) is large compared with the bandwidth of the equalizer [5], in other words if the average number of primary electrons, generated during a time slot T, is much larger than 1. Thus we define the p.d.f. of $v_{out}(t_s)$, conditioned on the transmitted data sequence B, by

$$p_{v_{out}(t_s)}(\alpha|B) = \frac{1}{\sigma\sqrt{2\pi}} \cdot e^{-(\alpha-\mu)^2/2\sigma^2} \tag{5.1}$$

where

$$\mu = E[v_{out}(t_s)|B]$$

$$\sigma^2 = \mathrm{Var}\,[v_{out}(t_s)|B] \quad .$$

5.2. Average bit error probability

If we denote the decision threshold by D, the decision rule of the threshold detector is given by (bit-by-bit detection):

$$\begin{aligned} v_{out}(t_s) < D &\rightarrow \hat{b}_o = b_{min} \\ v_{out}(t_s) \geq D &\rightarrow \hat{b}_o = b_{max} \quad . \end{aligned} \tag{5.2}$$

Hence, with (5.1) the probability of an erroneous decision $\hat{b}_o$ for a given pattern of neighboring symbols $B' = \{b_{k,k \neq 0}\}$ becomes:

$$P_e(B') = P[b_o = b_{min}|B'] \cdot P[\hat{b}_o = b_{max}|B', b_o = b_{min}]$$

$$+ P[b_o = b_{max}|B'] \cdot P[\hat{b}_o = b_{min}|B', b_o = b_{max}]$$

$$= P[b_o = b_{min}|B'] \cdot Q\left(\frac{D - \mu_A}{\sigma_A}\right) \qquad (5.3)$$

$$+ P[b_o = b_{max}|B'] \cdot Q\left(\frac{\mu_B - D}{\sigma_B}\right)$$

where

$$Q(x) \triangleq \frac{1}{\sqrt{2\pi}} \int_x^\infty e^{-\alpha^2/2}\, d\alpha$$

$$\sigma_A^2 \triangleq \text{Var}\,[v_{out}(t_s)|B', b_o = b_{min}]$$

$$\sigma_B^2 \triangleq \text{Var}\,[v_{out}(t_s)|B', b_o = b_{max}]$$

$$\mu_A \triangleq E[v_{out}(t_s)|B', b_o = b_{min}]$$

$$\mu_B \triangleq E[v_{out}(t_s)|B', b_o = b_{max}] \quad .$$

If the conditional probabilities $P[b_o = b_{min}|B']$ and $P[b_o = b_{max}|B']$ are equal, the error probability $P_e(B')$ is minimized by taking D equal to the maximum likelihood threshold $D_{ML}(B')$ [9]. This threshold is situated on the intersection of the conditional p.d.f.'s $p_{v_{out}(t_s)}(\alpha|B', b_o = b_{min})$ and $p_{v_{out}(t_s)}(\alpha|B', b_o = b_{max})$, and is different for each pattern of neighboring symbols.

(N.B. because the variances of these p.d.f.-'s differ, there are in principle two intersections; for practical reasons, however, we only consider the intersection between both conditional expectations). Figure 5.1 shows all this and will be further discussed in section 6.1.

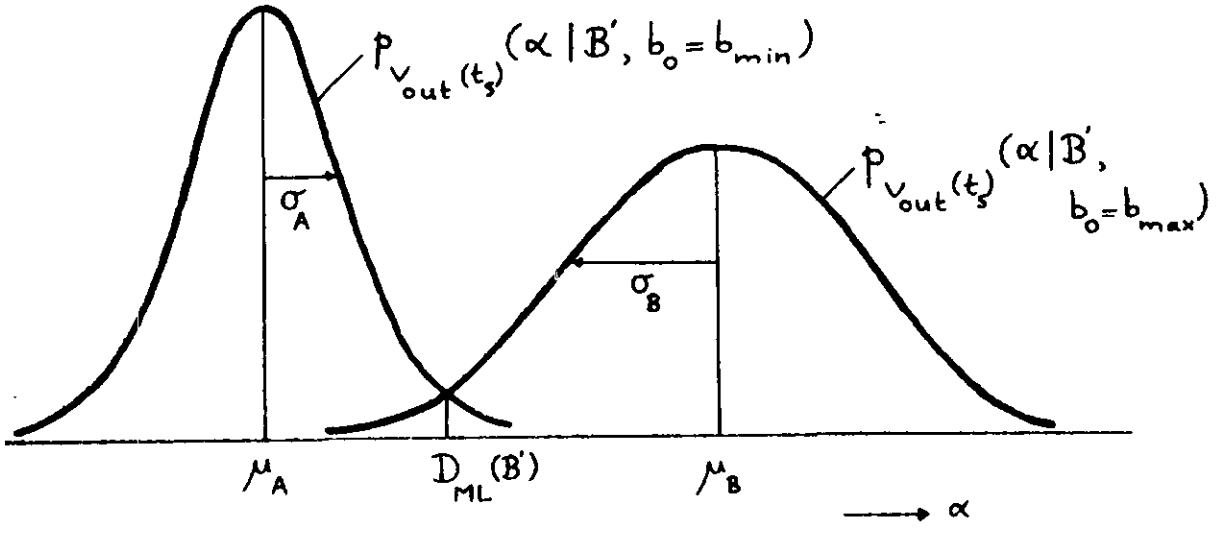

Figure 5.1. The conditional probability density functions of the equalizer output signal $v_{out}(t)$ at the sampling time t_s.

We calculate the average bit error probability P_e by averaging the error probabilities $P_e(B')$ over all possible patterns of neighboring symbols B':

$$P_e = \sum_{B'} P(B') \cdot P_e(B') \quad . \tag{5.4}$$

As for every pattern B' there is an optimum threshold minimizing $P_e(B')$, so there is an optimum threshold D_{opt} minimizing P_e.

5.3. Exhaustive method

A procedure to calculate the average bit error probability P_e according to (5.4) is the following [6]:

1. calculate the error probability $P_e(B')$ for a given pattern of neighboring symbols B' according to (5.3).
2. multiply $P_e(B')$ by the probability $P(B')$ of B'.
3. carry out 1 and 2 for all possible patterns B' and add the results $P(B') \cdot P_e(B')$.

In practice, this so-called exhaustive method requires that the expectation $E[v_{out}(t_s)|B]$ and the variance $Var[v_{out}(t_s)|B]$ only depend on a finite number of symbols b_k, say

$$B(k_1,k_2) \triangleq \{b_{k_1}, \ldots, b_{-1}, b_o, b_1, \ldots, b_{k_2}\} \quad . \tag{5.5}$$

This is necessary because the computational complexity exponentially increases with the number of interfering symbols.
According to (3.18) and (3.19), (5.5) implies

$$\left.\begin{aligned} h'_{out}\left(\frac{t_s}{T} - k\right) &= 0 \\ z'\left(\frac{t_s}{T} - k\right) &= 0 \end{aligned}\right\} \quad \text{for } k < k_1 \text{ and } k > k_2 \quad . \tag{5.6}$$

If there are no (acceptable) k_1 and k_2 satisfying (5.6) exactly, we must use an appropriate truncation criterion. We determine k_1 and k_2 such, that (5.6) holds with good accuracy. This will be discussed further in section 8.1.
To simplify the implementation on a digital computer, we modify (5.4) using (5.3) for data patterns $B_1 = B_1(k_1,k_2) = \{b^{(1)}_{k_1}, \ldots, b^{(1)}_{-1}, b^{(1)}_o, b^{(1)}_1, \ldots, b^{(1)}_{k_2}\}$ as follows:

$$P_e = \sum_1 P(B_1) \cdot P_e(B_1) \quad . \tag{5.7}$$

where

$$P_e(B_1) = Q\left(\frac{\mu_1 - D}{\sigma_1} \cdot \text{sign } (1)\right)$$

$$\mu_1 = E[v_{out}(t_s)|B_1]$$

$$\sigma_1^2 = \text{Var}[v_{out}(t_s)|B_1]$$

$$\text{sign } (1) = +1 \qquad \text{if } b^{(1)}_o = b_{max}$$

$$= -1 \qquad \text{if } b^{(1)}_o = b_{min}$$

and where the summation must be carried out over the indices 1 of all possible data patterns B_1.
In the case of binary mutually independent symbols b_k (straight binary transmission), the summation includes $2^{k_2-k_1+1}$ patterns B_1; if the alphabet

symbols b_{min} and b_{max} are equiprobable, the B_l-'s also are equiprobable. In the case of encoded data patterns a correlation between the data symbols exists, which decreases the number of possible patterns B_l.

5.4. Worst case analysis

To calculate the average bit error probability P_e we need the statistics of the data sequence B being transmitted. In practice this information is not known, hence we must use another criterion.
For simplicity we assume no timing errors at the sampler, so $t_s = 0$. We therefore have no intersymbol interference in $E[v_{out}(t_s)|B]$ according to (3.18) and (4.1), but in $Var[v_{out}(t_s)|B]$ according to (3.19) we have (see also section 4.4).
The maximum error probability is attained by the pattern of neighboring symbols maximizing this variance, hence according to (3.25) by the worst case pattern of neighboring symbols $B'_{WC} = \{b_{k,k\neq 0} \equiv b_{max}\}$. The worst case noise power at the equalizer output at $t_s = 0$ given b_o follows from (3.26) and (4.4):

$$NW(b_o) = Var[v_{out}(t_s = 0)|B'_{WC}, b_o]$$

$$= \frac{h\nu}{\eta} \cdot F_e \cdot \{b_o I_1 + b_{max}(\Sigma_1 - I_1)\} + Z_o + Z_{th}/G^2 \qquad (5.8)$$

where we have defined weighting factors I_1 and Σ_1 in agreement with [3] using (3.12) by

$$I_1 \triangleq z'(o) = h'_p(t) * h'^2_1(t) \Big|_{t=0} = \int_{-\infty}^{+\infty} h'_p(\tau) \cdot h'^2_1(-\tau)\, d\tau$$

$$= \int_{-\infty}^{+\infty} H'_p(f) \cdot (H'_1(f) * H'_1(f))df \quad . \qquad (5.9)$$

and

$$\Sigma_1 \triangleq \sum_{k=-\infty}^{+\infty} z'(-k) = \sum_{k=-\infty}^{+\infty} h'_p(t) * h'^2_1(t)\Big|_{t=-k}$$

$$= \sum_{k=-\infty}^{+\infty} \int_{-\infty}^{+\infty} h'_p(\tau-k) \cdot h'^2_1(-\tau)\, d\tau$$

$$= \sum_{k=-\infty}^{+\infty} \int_{-\infty}^{+\infty} e^{-j.2\pi f.k} \cdot H'_p(f) \cdot (H'_1(f) * H'_1(f))df$$

$$= \int_{-\infty}^{+\infty} \left[\sum_{k=-\infty}^{+\infty} \delta(f-k)\right] \cdot H'_p(f) \cdot (H'_1(f) * H'_1(f))df$$

$$= \sum_{k=-\infty}^{+\infty} H'_p(k) \cdot (H'_1(f) * H'_1(f))\Big|_{f=k} \qquad (5.10)$$

According to (5.8) I_1 is proportional to the shot noise power of the symbol under decision b_o, and $\Sigma_1 - I_1$ is proportional (with the same proportionality constant if $b_o = b_{max}$) to the shot noise power of the worst case pattern of neighboring symbols $B'_{WC} = \{b_{k,k\neq 0} \equiv b_{max}\}$.

5.4.1. Weighting factors

Substituting (3.21) and (4.4) into (5.8) we find

$$NW(b_o) = \frac{h\nu}{\eta} \cdot F_e \cdot \{b_o I_1 + b_{max}(\Sigma_1 - I_1)\}$$

$$+ \left(\frac{h\nu}{\eta}\right)^2 \cdot F_e.\lambda_o T.I_2 + \left(\frac{hf}{e\eta G}\right)^2 \left\{\left[\frac{2k\theta}{R_b}\right.\right.$$

$$\left.\left. + \frac{S_E}{R_T^2} + S_I\right] \cdot TI_2 + S_E \cdot (2\pi C_T)^2 \cdot \frac{I_3}{T}\right\} \quad . \qquad (5.11)$$

Note that the terms containing I_2 are inversely proportional to the signalling rate 1/T and that the term containing I_3 is proportional to 1/T. The terms containing I_1 and Σ_1, which account for the signal shot noise, are independent of 1/T.

Appendix 2 shows plots of the weighting factors I_1, Σ_1, $\Sigma_1 - I_1$, I_2 and I_3 for the four possible combinations of received optical pulse shapes (rectangular

or Gaussian) and equalized output pulse shapes (raised cosine or "optimum"). These factors are plotted versus the normalized r.m.s. optical pulse width σ/T, with the rolloff factor β of the equalized output pulses as a parameter ($\beta = .1$, $= .5$ and $= 1$).

These plots show a nearly identical behavior of the weighting factors as functions of σ/T for rectangular and Gaussian received optical pulses. The mutual differences are small for small σ/T, because of both pulse shapes approaching a Dirac impulse $\delta(t)$ according to (3.10); a larger σ/T increases the differences. For small σ/T the weighting factors generally are smaller for "optimum" equalized output pulses than for raised cosine pulses; however, this relation is inverted with increasing σ/T. The mutual differences are small for small rolloff factor β (e.g. $\beta = .1$), because of both spectra approaching an ideal low-pass characteristic; a larger β increases the differences. All the weighting factors always are increasing functions of σ/T, because a larger σ/T necessitates greater equalization. The plots of I_1 and $\Sigma_1 - I_1$ show clearly that a larger β and a smaller σ/T considerably reduce the shot noise power of the neighboring symbols as compared with that of the symbol under decision. If the received optical pulses become very narrow ($\sigma/T \to 0$, hence $h_p'(t) \to \delta(t)$ according to (3.10)), the shot noise of the neighboring pulses even disappears [3], whereas the shot noise power of the symbol under decision remains nearly constant. Practical values of σ/T and β usually yield $\Sigma_1 - I_1 \ll I_1$, thus making the shot noise power of the neighboring symbols much smaller than that of the symbol under decision. For instance, rectangular received optical pulses with duty cycle $\alpha_r = .5$ ($\sigma/T \approx .144$) and raised cosine equalized output pulses with $\beta = 1$ yield $\Sigma_1 - I_1 \approx 5.12.10^{-3}$ and $I_1 \approx 1.003$.

The weighting factors I_1 and $\Sigma_1 - I_1$ are related to the shot noise variance function $z'(t)$ by (see (5.9) and (5.10)) $I_1 = z'(0)$ and

$$\Sigma_1 = I_1 = \sum_{\substack{k=-\infty \\ k\neq 0}}^{+\infty} z'(-k) = \sum_{\substack{k=-\infty \\ k\neq 0}}^{+\infty} z'(k) \quad . \tag{5.12}$$

The behavior of $z'(t)$ as discussed in section 4.4, such as the faster decay for large β and smaller σ/T, agrees with the behavior of $\Sigma_1 - I_1$ according to (5.12).

6. Receiver optimization

This chapter is dealing with the receiver optimization, namely with setting the decision threshold and the average avalanche gain so that the average bit error probability is minimized. The relation between the average received optical power and the average bit error probability is also discussed. Throughout this chapter timing errors are not considered: $t_s = 0$. Hence using (3.18) and (4.1) we find for the expectation of the equalizer output signal

$$E[v_{out}(t_s = 0)|B] = b_o + V_o \tag{6.1}$$

while the variance is given by (4.14).

6.1. Choosing the decision threshold

The average bit error probability P_e is a function of the decision threshold D according to (5.3) and (5.4).

6.1.1. Minimizing the error probability for a fixed data pattern

As discussed in section 5.2, if $P[b_o = b_{min}|B'] = P[b_o = b_{max}|B']$ the error probability $P_e(B')$ for a pattern of neighboring symbols B' is minimized by taking D equal to the maximum likelihood threshold $D_{ML}(B')$, situated on the intersection of $p_{v_{out}(t_s)}(\alpha|B', b_o = b_{min})$ and $p_{v_{out}(t_s)}(\alpha|B', b_o = b_{max})$ (see figure 5.1).
The use of (5.1) and (6.1) yields

$$D_{ML}(B') = V_o + \frac{\left(\frac{\sigma_B}{\sigma_A}\right)^2 \cdot b_{min} - b_{max} + \left(\frac{\sigma_B}{\sigma_A}\right)\sqrt{(b_{max}-b_{min})^2+2(\sigma_B^2-\sigma_A^2)\ln\left(\frac{\sigma_B}{\sigma_A}\right)}}{\left(\frac{\sigma_B}{\sigma_A}\right)^2 - 1} \tag{6.2}$$

where

$$\sigma_A^2 = Var[\, v_{out}(t_s=0)|B', b_o = b_{min}\,]$$

$$\sigma_B^2 = Var[\, v_{out}(t_s=0)|B', b_o = b_{max}\,]$$

and where $Var[v_{out}(t_s=0)|B]$ is given by (4.14).

Normalizing this threshold on the maximum energy b_{max} in a received optical pulse using (3.14) yields

$$\frac{D_{ML}(B')}{b_{max}} = \frac{V_o}{b_{max}} + \frac{\left(\frac{\sigma_B}{\sigma_A}\right)^2 \cdot EXT - 1 + \left(\frac{\sigma_B}{\sigma_A}\right) \sqrt{(1 - EXT)^2 + \frac{2(\sigma_B^2 - \sigma_A^2)}{b_{max}^2} \cdot \ln\left(\frac{\sigma_B}{\sigma_A}\right)}}{\left(\frac{\sigma_B}{\sigma_A}\right)^2 - 1} \qquad (6.3)$$

As discussed in section 5.4, $P_e(B')$ is maximized (using $D = D_{ML}(B')$ by the worst case pattern of neighboring symbols B'_{WC}. In [3], Personick uses a threshold $D_p(B'_{WC})$, implicitly defined for B'_{WC} by

$$P_e(B'_{WC}, b_o = b_{min}) = P_e(B'_{WC}, b_o = b_{max}) = Q(\delta) \qquad (6.4)$$

where according to (5.3) and (6.1)

$$\delta = \frac{b_{max} + V_o - D_p(B'_{WC})}{\sigma_B} = \frac{D_p(B'_{WC}) - b_{min} - V_o}{\sigma_A} \quad . \qquad (6.5)$$

By eliminating δ we find with (3.14)

$$\frac{D_p(B'_{WC})}{b_{max}} = \frac{V_o}{b_{max}} + \frac{\sigma_A + \sigma_B \cdot EXT}{\sigma_A + \sigma_B} \qquad (6.6)$$

(according to (5.8) and (6.2) σ_A^2 and σ_B^2 are calculated with (5.11)). This threshold achieves a worst case error probability $P_e(B'_{WC})$, which is independent of the message statistics $P[b_o = b_{min}|B'_{WC}]$ and $P[b_o = b_{max}|B'_{WC}]$ according to (5.3):

$$P_e(B'_{WC}|D = D_p(B'_{WC})) \equiv Q(\delta) \quad . \qquad (6.7)$$

Hence one can prove that $D_p(B'_{WC})$ is the threshold of a MINIMAX-receiver [9].

6.1.2. Minimizing the average bit error probability

For a given pattern of neighboring symbols B' and if $P[b_o = b_{min}|B'] = P[b_o = b_{max}|B']$ the optimum decision threshold is $D_{ML}(B')$, given by (6.2). A not-worst case pattern B' leads to noise powers σ_A^2 and $\sigma_{B_2}^2$ at the equalizer output, which are the same amount smaller than σ_A^2 and σ_B^2 respectively for a worst case pattern B'_{WC}. Because $\sigma_A < \sigma_B$ σ_B/σ_A is larger

than for B'_{WC}, hence with (6.2) it follows that

$$D_{ML}(B') < D_{ML}(B'_{WC}) \quad . \tag{6.8}$$

In the same way we find with respect to the best case pattern of neighboring symbols B'_{BC}

$$D_{ML}(B') > D_{ML}(B'_{BC}) \quad . \tag{6.9}$$

Using equiprobable alphabet symbols b_{min} and b_{max}, we derive by averaging over all the possible B' (see (5.4)) for the optimum threshold D_{opt}, which minimizes the average bit error probability P_e

$$D_{ML}(B'_{BC}) < D_{opt} < D_{ML}(B'_{WC}) \quad . \tag{6.10}$$

The on b_{max} normalized optimum threshold D_{opt}/b_{max} satisfies

$$\frac{D_{ML}(B'_{BC})}{b_{max}} < \frac{D_{opt}}{b_{max}} < \frac{D_{ML}(B'_{WC})}{b_{max}} \quad . \tag{6.11}$$

We wish to analyze the influence of parameter variations on D_{opt}/b_{max}. Increasing the thermal noise parameter Z_{th_2} or the dark current λ_o yields an increase in the noise powers σ_A^2 and σ_B^2 at the equalizer output, both with the same amount according to (4.14); increasing the extinction EXT yields a larger increase in σ_A^2 than in σ_B^2 according to (3.16) and (4.14). Because of $\sigma_A < \sigma_B$ increasing Z_{th}, λ_o or EXT therefore means a smaller σ_B/σ_A, hence with (6.3) and (6.11) a larger D_{opt}/b_{max}. At sufficiently high signalling rates 1/T, Z_{th} is nearly proportional to 1/T according to (4.5), causing D_{opt}/b_{max} to increase if 1/T increases. Increasing the maximum energy b_{max} in a received optical pulse, or increasing the average avalanche gain G, yields according to (4.14) an increase in σ_B/σ_A because of $\sigma_A < \sigma_B$, hence with (6.3) and (6.11) a decrease in D_{opt}/b_{max}.

6.2. Choosing the average avalanche gain

The average bit error probability P_e is a function of the average avalanche

gain G according to (4.14), (5.3) and (5.4).

6.2.1. Minimizing the error probability for a fixed data pattern

The error probability $P_e(B_1)$ for a data pattern $B_1(k_1,k_2)$ (see (5.7)) is minimized by minimizing its noise power σ_1^2 at the equalizer output. Substituting (3.21) into (4.14) we have

$$\sigma_1^2 = \mathrm{Var}[v_{out}(t_s = 0)|B_1] = F_e \cdot A_1 + Z_{th}/G^2 \qquad (6.12)$$

where

$$A_1 \triangleq \frac{h\nu}{\eta} \cdot b_{max} \cdot \sum_{k=k_1}^{k_2} b_k'(1) \cdot z'(-k) + \left(\frac{hf}{\eta}\right)^2 \cdot \lambda_o T \cdot I_2 \qquad (6.13)$$

Because of F_e being an increasing function of G and $1/G^2$ a decreasing function of G, every B_1 has its optimum average avalanche gain $G_{opt}(B_1)$, which minimizes σ_1^2 and therefore $P_e(B_1)$. By putting

$$\delta\sigma_1^2/\delta G \Big|_{G = G_{opt}(B_1)} = 0$$

we derive using (3.30)

$$G_{opt}(B_1) = \left[\frac{Z_{th}}{A_1 \cdot k} + \sqrt{\left(\frac{1-k}{3k}\right)^3 + \left(\frac{Z_{th}}{A_1 \cdot k}\right)^2}\right]^{1/3} + \left[\frac{Z_{th}}{A_1 \cdot k} - \sqrt{\left(\frac{1-k}{3k}\right)^3 + \left(\frac{Z_{th}}{A_1 \cdot k}\right)^2}\right]^{1/3} . \qquad (6.14)$$

In practice we usually have $(Z_{th}/A_1) >> 1/k$, giving a good approximation of (6.14) by

$$G_{opt}(B_1) \approx \sqrt[3]{\frac{2 \cdot Z_{th}}{A_1 \cdot k}} \quad \text{if } (Z_{th}/A_1) >> 1/k \quad . \qquad (6.15)$$

6.2.2. Minimizing the average bit error probability

Every data pattern $B_1(k_1,k_2)$ has its optimum avalanche gain $G_{opt}(B_1)$, given by (6.14); each $G_{opt}(B_1)$ satisfies

$$G_{opt}(B_1 = \{b_k^{(1)} \equiv b_{max}\}) \leq G_{opt}(B_1) \leq G_{opt}(B_1 = \{b_k^{(1)} \equiv b_{min}\}). \quad (6.16)$$

By averaging over all possible B_1 (see (5.7)), we derive for the optimum average avalanche gain G_{opt}, which minimizes the average bit error probability P_e

$$G_{opt}(B = \{b_k \equiv b_{max}\}) < G_{opt} < G_{opt}(B = \{b_k \equiv b_{min}\}) \quad . \quad (6.17)$$

And in an analogous way

$$G_{opt}(B'_{WC} = \{b_{k,k\neq 0} \equiv b_{max}\}) < G_{opt} < G_{opt}(B'_{BC} = \{b_{k,k\neq 0} \equiv b_{min}\}) \quad (6.18)$$

We wish to analyze the influence of parameter variations on G_{opt}. Increasing the thermal noise parameter Z_{th}, decreasing the extinction EXT or decreasing the dark current λ_o yields an increase in G_{opt} according to (6.13), (6.14) and (6.17). Combining (6.15) en (6.17) we have the approximation

$$G_{opt} \sim \left[\frac{Z_{th}}{k \cdot b_{max}} \right]^{1/3} \quad (6.19)$$

where $\sim$ denotes proportionality. $G_{opt} \sim b_{max}^{-1/3}$ is a better approximation as the dark current contribution to the shot noise power decreases, for instance as the signalling rate 1/T increases (see (6.13)). At sufficiently large 1/T, Z_{th} is nearly proportional to 1/T according to (4.5), yielding the approximation

$$G_{opt} \sim \left[\frac{I_3}{k \cdot b_{max} \cdot T} \right]^{1/3} \quad \text{for large } 1/T \quad (6.20)$$

and using (3.17) the approximation

$$G_{opt} \sim \left[\frac{I_3 \cdot (1+EXT)}{k \cdot 10^{P_o/10} \cdot T^2} \right]^{1/3} \quad \text{for large } 1/T \quad . \tag{6.21}$$

G_{opt} also depends in some degree on the decision threshold D. A decrease in D emphasizes the minimizing over G of $\sigma_A^2 = \text{Var}\,[v_{out}(t_s=0) \mid B', b_o = b_{min}]$ more than that of $\sigma_B^2 = \text{Var}[\, v_{out}(t_s=0) \mid B', b_o = b_{max}]$. Thus with (6.16) G_{opt} increases if D decreases.

6.3. Average received optical power

The average bit error probability P_e strongly decreases if the average received optical power P_o increases, as we shall see in Chapters 8 and 9. The P_o needed to achieve a given P_e is minimized by using the optimum decision threshold D_{opt} in combination with the optimum average avalanche gain G_{opt}.
It is very difficult to express analytically how P_o affects P_e when using D_{opt} and G_{opt}. By introducing a number of simplifications however, it is possible to analyze the influence of P_o on the worst case error probability $P_e(B'_{WC})$. Personick [3, part II, formula (2)] calculates the average received optical power, required for a $P_e(B'_{WC}) = Q(\delta)$ using straight binary transmission with equiprobable symbols:

$$P_{o,req} = \frac{1}{2T} \cdot (\delta.\gamma_2)^{(2+x)/(1+x)} \cdot (Z.\gamma_1)^{x/(2+2x)} \tag{6.22}$$

for an optimum average avalanche gain

$$G_{opt}(B'_{WC}) = (\delta.\gamma_2)^{-1/(1+x)} \cdot (Z.\gamma_1)^{1/(2+2x)} \tag{6.23}$$

where

$$\gamma_1 \triangleq \frac{-(2\Sigma_1 - I_1) + \sqrt{(2\Sigma_1 - I_1)^2 + \frac{16(1+x)}{x^2} \cdot \Sigma_1 \cdot (\Sigma_1 - I_1)}}{2\Sigma_1 \cdot (\Sigma_1 - I_1)} \tag{6.24}$$

$$\gamma_2 \triangleq \sqrt{\Sigma_1 - I_1 + 1/\gamma_1} + \sqrt{\Sigma_1 + 1/\gamma_1} \quad . \tag{6.25}$$

In deriving these formulas the following simplifications have been made: dark current $\lambda_o = 0$, extinction EXT = 0, excess noise factor $F_e = G^x$ (see (3.32)) and decision threshold $D_P(B'_{WC})$ (see (6.6)). According to (4.5) and (4.6) we have

$$Z = \left(\frac{\eta}{h\nu}\right)^2 \cdot Z_{th} \simeq \left(\frac{2\pi}{e} \cdot C_T\right)^2 \cdot S_E \cdot \frac{I_3}{T} \quad \text{for large } 1/T \quad . \tag{6.26}$$

Substitution into (6.22) yields ($\sim$ denotes proportionality)

$$P_{o,req} \sim (1/T)^{(3x+2)/(2x+2)} \quad \text{for large } 1/T \tag{6.27}$$

hence the increase in $P_{o,req}$ with the signalling rate 1/T is given by

$$10 \cdot \frac{3x + 2}{2x + 2} \cdot {}^{10}\log 2 \quad \text{dB/octave of signalling rate} \quad . \tag{6.28}$$

In the same way we obtain from (6.23)

$$G_{opt}(B'_{WC}) \Big|_{P_e(B'_{WC}) = \text{constant}} \sim (1/T)^{1/(2+2x)} \quad \text{for large } 1/T \quad . \tag{6.29}$$

7. Line coding

By means of line coding we introduce correlation between the line symbols, thus getting a certain amount of redundancy. This can be used for error detection (and possibly correction), suppression of DC-wander, extra timing information, etcetera [11].
Because of the non-linear modulation characteristic of the optical transmitter (i.e. laser diode), we confine ourselves to binary code alphabets.
We consider the so-called mBnB-block codes: words of m binary digits are encoded into words of n binary digits ($m < n$). The advantages of coding mentioned above are achievable at the cost of bandwidth expansion (in other words: increase in the signalling rate) with a factor n/m. A large conversion ratio n/m leads to a small code efficiency, and to a large optical power penalty to achieve the same bit error rate as without coding. Thus a low redundancy (small n/m) mBnB code is attractive; its large blocksize m however increases the coder and decoder complexity.
The correlation between the line symbols, achieved with line coding, generally suppresses the most unfavorable (but also the most favorable) combinations of symbols neighboring the symbol under decision. This effect however may be neglected if the interference of the neighboring symbols is negligible.
The efficiency of an mBnB code is m/n; thus the information rate R of the coder output stream (with signalling rate 1/T), using equiprobable mutually independent input symbols, is given by

$$R = \frac{m}{n} \cdot \frac{1}{T} \quad \text{bits/sec} \tag{7.1}$$

As examples of mBnB codes we will consider the 1B2B split phase code and the 5B6B code.

7.1. 1B2B split phase code

Table 7.1 shows the very simple coding rule of the 1B2B split phase code.

Table 7.1. The 1B2B split phase code

input (1B)	output (2B)
0	0 1
1	1 0

Let the disparity of a binary code word be: the number of ones reduced by the number of zeros in it; and the running digital sum (RDS) of a binary data stream at a given time: the number of ones reduced by the number of zeros till that time, divided by 2. A minimum RDS variation implies a minimum DC-wander.

Advantages of the 1B2B split phase code as compared with straight binary transmission are:

- much timing information (maximum number of successive zeros or ones in the coder output stream is 2)
- balanced code (disparity of each code word equals 0, thus minimizing RDS-variations: $|RDS|_{max} = .5$)
- possibility of error detection (00 and 11 are not used as code words)

and disadvantages are:

- small efficiency (= m/n = 50% only)
- doubling the signalling rate 1/T, required for the same information rate R (see (7.1)).

Because of the very simple coding rule, the realization of coder and decoder is quite simple.

7.2. 5B6B code

Table 7.2 shows the more complicated coding rule of the 5B6B code. For the 6-bits code words only words with disparity -2,0 and +2 are selected, in order to minimize RDS variations. The encoder has two states:

- mode 1: the disparity of the next code word is 0 or +2
- mode 2: the disparity of the next code word is 0 or -2

The 0-disparity code words are identical in both modes; the +2 disparity code words in mode 1 are converted into the -2 disparity code words in mode 2 by bit inversion.Figure 7.1. shows the state diagram of the 5B6B code.

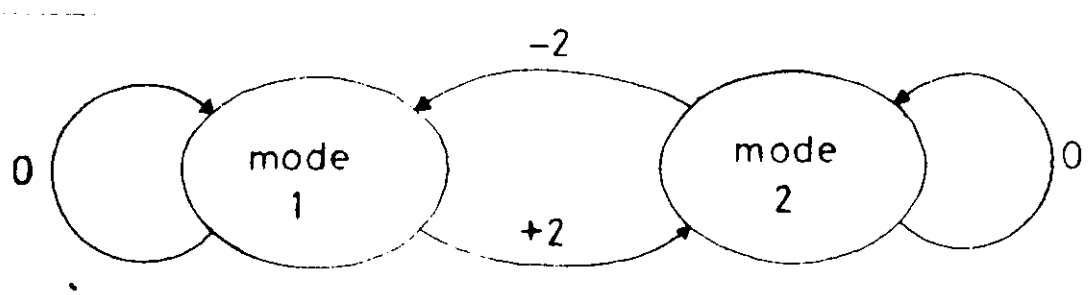

Figure 7.1. The state diagram of the 5B6B code

Table 7.2. The 5B6B code

input (5B)	output (6B)		input (5B)	output (6B)	
	mode 1	mode 2		mode 1	mode 2
00000	010111	101000	10000	011101	100010
00001	100111	011000	10001	100011	100011
00010	011011	100100	10010	100101	100101
00011	001111	110000	10011	100110	100110
00100	101011	010100	10100	101001	101001
00101	001011	001011	10101	101010	101010
00110	001101	001101	10110	101100	101100
00111	001110	001110	10111	110101	001010
01000	110011	001100	11000	110001	110001
01001	010011	010011	11001	110010	110010
01010	010101	010101	11010	110100	110100
01011	010110	010110	11011	111001	000110
01100	011001	011001	11100	111100	000011
01101	011010	011010	11101	101110	010001
01110	011100	011100	11110	110110	001001
01111	101101	010010	11111	111010	000101

The transmission of a code word coincides with a state transition. At each transition the disparity of the code word being transmitted is indicated.
Advantages of the 5B6B code as compared with straight binary transmission are:

- fairly much timing information (maximum number of successive zeros or ones is 6)
- balanced code (the first not-0-disparity word succeeding a +2 disparity word is a -2 disparity word, and vice versa; hence a limited RDS variation: $|RDS|_{max} = 2$)
- possibility of error detection (18 6-bits words are not used as code words; and the disparities of succeeding code words have to obey the rule mentioned before)

and disadvantages are:

- smaller efficiency (= $m/n \simeq 83\%$)
- increasing the signalling rate $1/T$, required for the same information rate R, by a factor $n/m = 1.2$ (see (7.1)).

These disadvantages are considerably smaller than those of the 1B2B split phase code; the coder and decoder however are much more complicated.

8. Numerical results of calculating the average bit error probability

In this chapter the average bit error probability P_e is numerically calculated as a function of a number of system parameters following the exhaustive method (5.7). We use the data for a typical optical receiver, enumerated by Personick in [3, part II, chapter III]. We leave timing errors out of consideration by putting $t_s = 0$. The influence of the received optical pulse shape is analyzed and also the influence of the dark current, of the extinction , of the decision threshold, of the average avalanche gain, and of the average received optical power. These calculations are carried out using straight binary transmission with equiprobable symbols. Finally we analyze the influence of line coding.

8.1. Receiver data

We use the data for a typical optical receiver, enumerated by Personick in [3, part II, chapter III]:

- information rate R = 25 Mbit/sec
- received optical pulse shape: rectangular, duty cycle $\alpha_r = .5$
- equalized output pulse shape: raised cosine, rolloff factor $\beta = 1$
- APD: - excess noise exponent x = .5
  - primary dark current $\lambda_o e = 100$ pA
  - quantum efficiency $\eta = .75$
- operating wavelength $\lambda_1 = 850$ nm
- APD biasing resistance: $R_b = 1$ MΩ
- amplifier input resistance: $R_A = 1$ MΩ
- APD junction capacitance C_d in parallel with amplifier input capacitance C_A: $C_T = C_d + C_A = 10$ pF
- temperature $\theta = 300$ K
- two-sided spectral noise densities:
  - of the amplifier input voltage noise source $e_a(t)$:
    $S_E = 2k\theta/(5.10^{-3}\ \Omega^{-1})$ (V^2/Hz)
  - of the amplifier input current noise source $i_a(t)$:
    $S_I = 2k\theta/(1M\Omega)$ (A^2/Hz) (8.1)

Hence

$$\frac{h\nu}{\eta} = \frac{hc_o}{\eta\lambda_1} \simeq 3.117.10^{-19}\ J \qquad (c_o\text{: light velocity in vacuum})$$

$$\lambda_o \simeq 6.25.10^{8}\ \text{primary electrons/sec}$$

$$R_T = R_b \,//\, R_A = .5\ M\Omega \tag{8.2}$$

and

$$I_1 \simeq 1.003 \qquad \Sigma_1 - I_1 \simeq 5.12.10^{-3}$$

$$I_2 \simeq .805 \qquad I_3 \simeq .072 \tag{8.3}$$

Because of $\Sigma_1 - I_1 \ll I_1$, the shot noise power of the neighboring signals is generally considerably smaller than that of the symbol under decision (see section 5.4).
By the assumption of straight binary transmission with equiprobable symbols, the signalling rate 1/T equals the information rate R:

$$1/T = 25\ \text{MBaud} \tag{8.4}$$

The excess noise exponent x = .5 corresponds fairly well with an APD ionisation constant

$$k = .1 \tag{8.5}$$

for average avalanche gains about 60 (see section 3.6).
From (4.4) we have for the thermal noise parameter

$$Z_{th} \simeq 4.6733\ .10^{-32}\ V^2 \tag{8.6}$$

according to (4.7) corresponding with a thermal noise of

$$n_{therm} \simeq 694\ \text{secondary electrons} \tag{8.7}$$

For the average number of primary electrons, generated by the dark current λ_o in the time slot T

$$n_d \triangleq \lambda_o T \tag{8.8}$$

we have

$$n_d = 25 \text{ primary electrons} \tag{8.9}$$

The dark current contribution to the expectation of the output signal $v_{out}(t)$ is according to (3.20)

$$V_o \simeq 7.7925 \cdot 10^{-18} \text{ V} \tag{8.10}$$

As discussed in section 5.3, the exhaustive method requires truncated data patterns $B(k_1,k_2) = \{b_{k1},\ldots,b_{-1},b_o,b_1,\ldots b_{k2}\}$, k_1 and k_2 being determined by (5.6). With $t_s = 0$ and (4.1), (5.6) is reduced to

$$z'(-k) = 0 \quad \text{for } k < k_1 \text{ and } k > k_2 \tag{8.11}$$

Because of $z'(t)$ being time-unlimited, we need an appropriate truncation criterion. For instance, according to (5.12) k_1 and k_2 can be determined by requiring

$$\sum_{\substack{k=k_1 \\ k\neq 0}}^{k_2} z'(-k)/(\Sigma_1-I_1) = 1-\varepsilon \quad \text{where } 0 \leq \varepsilon << 1 \tag{8.12}$$

If (8.12) is satisfied, all the neighboring symbols contributing noticeably to the worst case shot noise power are taken into the calculations. Here $z'(t)$ is an even function of t, since the received optical pulse shape $h'_p(t)$ and the equalized output pulse shape $h'_{out}(t)$ are even (see (3.12)). Hence we put $k_1 = -k_2$; $k_1 = -3$ and $k_2 = 3$ yield

$$\sum_{\substack{k=k_1 \\ k\neq 0}}^{k_2} z'(-k)/(\Sigma_1-I_1) \simeq .9997 \tag{8.13}$$

making this k_1 and k_2 acceptable.

8.2. Influence of the received optical pulse shape

In the first instance, we assume rectangular received optical pulses. As discussed in section 4.2, Gaussian pulses are more plausible when fiber

dispersion is no longer negligible.
The shot noise variance function $z'(t)$ and the weighting factors I_1, Σ_1, $\Sigma_1 - I_1$, I_2 and I_3 are for rectangular and Gaussian received optical pulses nearly identical, provided that both pulses have the same normalized r.m.s. width σ/T (see section 4.4 and subsection 5.4.1). Particularly for small σ/T (e.g. $\sigma/T < .15$) the mutual differences are negligible. Hence these pulse types are nearly equivalent in error probability calculations, if their normalized widths α_r and α_g are related to each other by $\alpha_g = \sigma/T = \alpha_r/\sqrt{12}$ (see (4.11)). The results of error probability calculations for rectangular received optical pulses with $\alpha_r = .5$, described in this chapter, are therefore nearly equal to those for Gaussian pulses with $\alpha_g \simeq .144$. This will be verified in section 8.6.

8.3. Influence of dark current and extinction

In this section the influence of the dark current λ_o and the extinction EXT on the decision threshold D and the average bit error probability P_e is analyzed.
As a starting point we take $\lambda_o = 0$, EXT = 0 and $D = D_p(B'_{WC})$ (see (6.6)). Using (6.22) through (6.25) we calculate the average received optical power, required for a $P_e(B'_{WC}) = Q(6) \simeq 10^{-9}$, at the optimum average avalanche gain $G_{opt}(B'_{WC})$:

$$P_{o,req} = -57.80 \text{ dBm} \tag{8.14}$$

$$G_{opt}(B'_{WC}) = 56.89 \tag{8.15}$$

hence with (3.17)

$$b_{max} = 1.3289 \cdot 10^{-16} \text{ J} \tag{8.16}$$

Throughout this section we will put $b_{max} = 1.3289 \cdot 10^{-16}$ J ($P_o = -57.80$ dBm) and $G = 56.89$.
For the average number of primary electrons, generated by a received optical pulse with the maximum energy b_{max}

$$n_p \triangleq \frac{\eta}{h\nu} \cdot b_{max} \tag{8.17}$$

we have

$$n_p \simeq 426 \text{ primary electrons} \tag{8.18}$$

From (6.1), (8.10) and (8.16) it follows, that the dark current contribution V_o to $E[v_{out}(t_s=0)|B]$ is much smaller that the maximum signal contribution. Moreover, V_o is inversely proportional to the signalling rate 1/T. According to (3.21) the dark current contribution to $Var[v_{out}(t_s=0)|B]$ is

$$Z_o \simeq 1.4616 \ .10^{-35} \ V^2 \tag{8.19}$$

and the thermal noise contribution according to (4.4) and (8.6) is

$$E[n_{th}^2(t)] = Z_{th}/G^2 \simeq 1.4440 \ .10^{-35} \ V^2 \tag{8.20}$$

(and the maximum signal contribution according to (5.8) is $F_e.b_{max}.\Sigma_1.h\nu/\eta \simeq 3.1207 \ .10^{-34} \ V^2$). Here the contribution of the dark current and of the thermal noise are nearly equal; for larger 1/T or smaller G however the latter dominates.

Table 8.1. The influence of the dark current λ_o and the extinction EXT on various normalized decision thresholds and on the average bit error probability P_e.
(straight binary transmission with equiprobable symbols; $t_s = 0$; $b_{max} = 1.3289.10^{-16}$ J; G = 56.89; further receiver data: section 8.1)

λ_o (sec^{-1})	0	$6.25 \ .10^8$	$6.25 \ .10^8$
EXT	0	0	.01
$D_p(B'_{WC})/b_{max}$	.1814	.2893	.3055
P_e	$6.17.10^{-10}$	$1.27 \ .10^{-8}$	$2.52 \ .10^{-8}$
$D_{ML}(B'_{WC})/b_{max}$	.1875	.2962	.3126
P_e		$1.18 \ .10^{-8}$	$2.34 \ .10^{-8}$
$D_{ML}(B'_{BC})/b_{max}$	.1801	.2918	.3087
P_e			

Table 8.1 shows the influence of λ_o and EXT on the various normalized decision thresholds; in some cases the average bit error probability P_e is also calculated. We always have $D_p(B'_{WC}) < D_{ML}(B'_{WC})$ (see subsection 6.1.1). The difference between $D_{ML}(B'_{BC})$ and $D_{ML}(B'_{WC})$ is very small, because of the shot noise of the neighboring symbols being very small as compared with that of the symbol under decision ($\Sigma_1 - I_1 \ll I_1$, see (8.3)). Using (6.10) we find that the optimum threshold D_{opt} increases if λ_o or EXT increases. This agrees with subsection 6.1.2. P_e increases with increasing λ_o or EXT due to the increasing noise power at the equalizer output.

8.4. Influence of the decision threshold

In the remaining sections of this chapter we consider the average bit error probability P_e as a function of the maximum energy b_{max} in a received optical pulse, the average avalanche gain G, and the decision threshold D:

$$P_e = P_e(b_{max}, G, D) \tag{8.21}$$

We put $\lambda_o = 6.25.10^8$ primary electrons/sec (see (8.2)), and EXT = .01. The relation between b_{max} and the average received optical power P_o is given by (3.17).

Figure 8.1 shows a plot of P_e versus the normalized decision threshold D/b_{max}, calculated for $b_{max} = 1.3289 .10^{-16}$ J ($P_o \simeq -57.75$ dBm) and G = 56.89. Also plotted are the maximum and the minimum error probability, $P_{emax} = P_e(B'_{WC})$ and $P_{emin} = P_e(B'_{BC})$ respectively. These bounds on P_e are tight, because the shot noise of the neighboring symbols is very small as compared with that of the symbol under decision ($\Sigma_1 - I_1 \ll I_1$, see (8.3)). There is a sharp minimum in P_e at the normalized optimum threshold D_{opt}/b_{max}, in P_{emax} at $D_{ML}(B'_{WC})/b_{max}$ and in P_{emin} at $D_{ML}(B'_{BC})/b_{max}$. In agreement with (6.10) we have $D_{ML}(B'_{BC}) < D_{opt} < D_{ML}(B'_{WC})$. Note that the setting of D_{opt} must be very accurate.

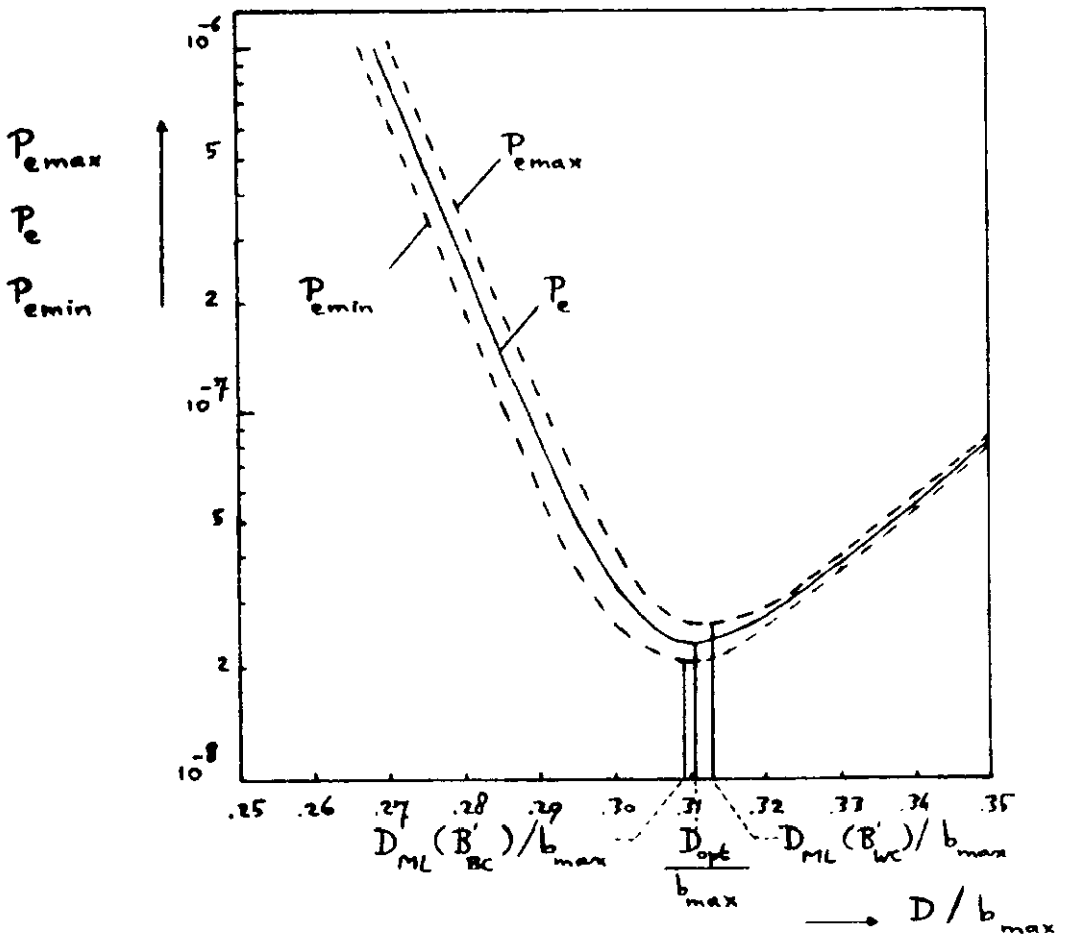

Figure 8.1. The average bit error probability P_e versus the normalized decision threshold D/b_{max} (straight binary transmission with equiprobable symbols; $t_s = 0$; $1/T = 25$ MBaud; $b_{max} = 1.3289.10^{-16}$ J ($P_o \simeq -57.75$ dBm); $G = 56.89$; EXT = .01; received optical pulses: rectangular, duty cycle $\alpha_r = .5$ (Gaussian, $\alpha_g \simeq .144$); equalized output pulses: raised cosine, rolloff factor $\beta = 1$; further receiver data: section 8.1)

8.5. Influence of the average avalanche gain

Figure 8.2 shows a plot of P_e versus G, calculated using D_{opt}/b_{max} and putting $b_{max} = 1.3289.10^{-16}$ J ($P_o \simeq -57.75$ dBm). Also plotted are D_{opt}/b_{max}, $P_{emax} = P_e(B'_{WC})$ and $P_{emin} = P_e(B'_{BC})$. D_{opt}/b_{max} is calculated by minimizing $P_e = P_e(b_{max},G,D)$ over D, with b_{max} and G fixed.
In agreement with subsection 6.1.2., D_{opt}/b_{max} decreases if G increases.
P_e is again tightly bounded by P_{emax} and P_{emin}, as discussed in section 8.4.

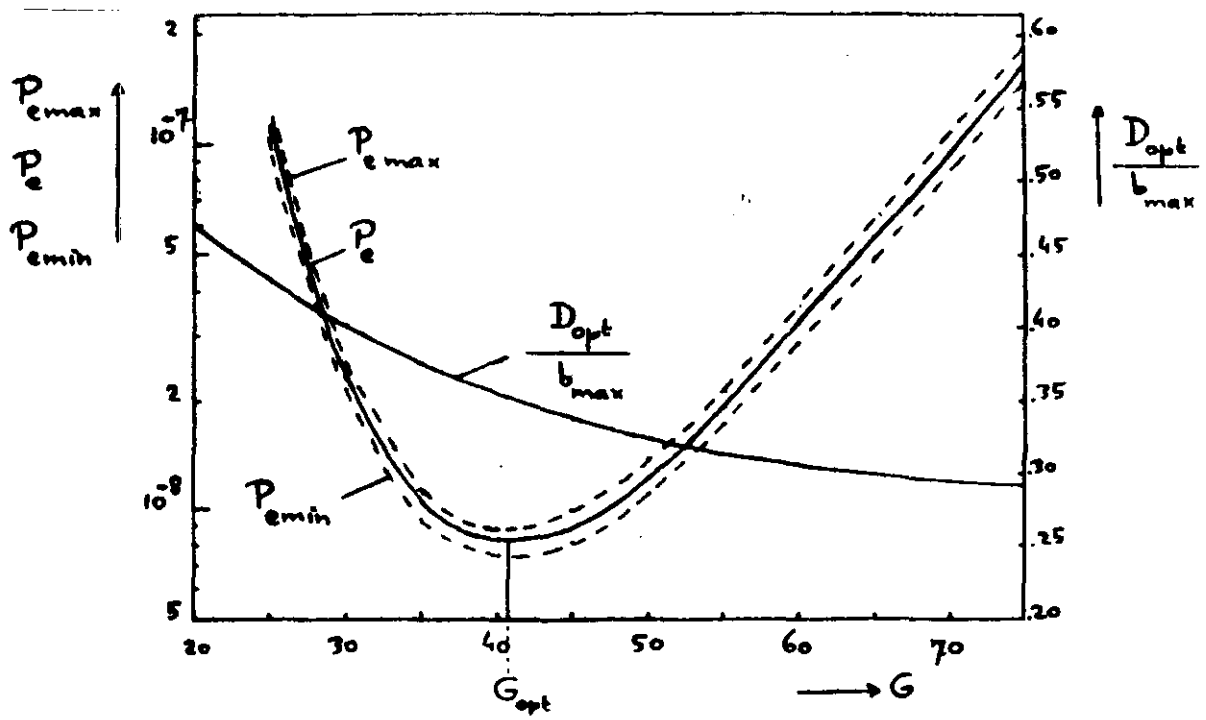

Figure 8.2. The average bit error probability P_e versus the average avalanche gain G, using the normalized optimum decision threshold D_{opt}/b_{max}. (straight binary transmission with equiprobable symbols; $t_s = 0$; $1/T = 25$ MBaud; $b_{max} = 1.3289.10^{-16}$ J ($P_o \simeq -57.75$ dBm); EXT = .01; received optical pulses: rectangular, duty cycle $\alpha_r = .5$ (Gaussian, $\alpha_g \simeq .144$); equalized output pulses: raised cosine, rolloff factor $\beta = 1$; further receiver data: section 8.1)

There is a minimum in P_e at the optimum average avalanche gain G_{opt}, in P_{emax} at $G_{opt}(B'_{WC})$, and in P_{emin} at $G_{opt}(B'_{BC})$. In agreement with (6.18) we have $G_{opt}(B'_{WC}) < G_{opt} < G_{opt}(B'_{BC})$. Since the minimum in P_e at G_{opt} is not very sharp small deviations of G from G_{opt} cause no serious degradation in the error performance.

8.6. Influence of the average received optical power, and of line coding

In this section the influence of the average received optical power P_o on the average bit error probability P_e is analyzed and also the influence of mBnB line coding.

Figure 8.3.a shows plots of P_e versus P_o, calculated using the optimum average avalanche gain G_{opt} and the normalized optimum threshold D_{opt}/b_{max}.

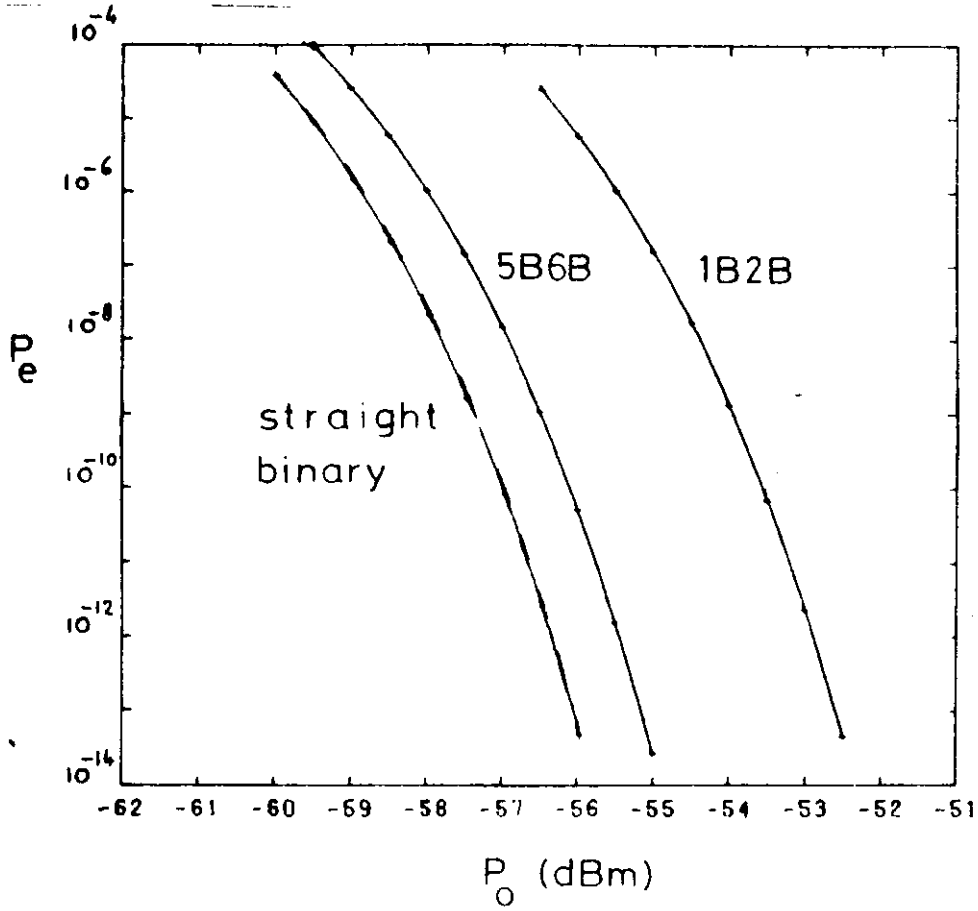

Figure 8.3.a. The average bit error probability P_e

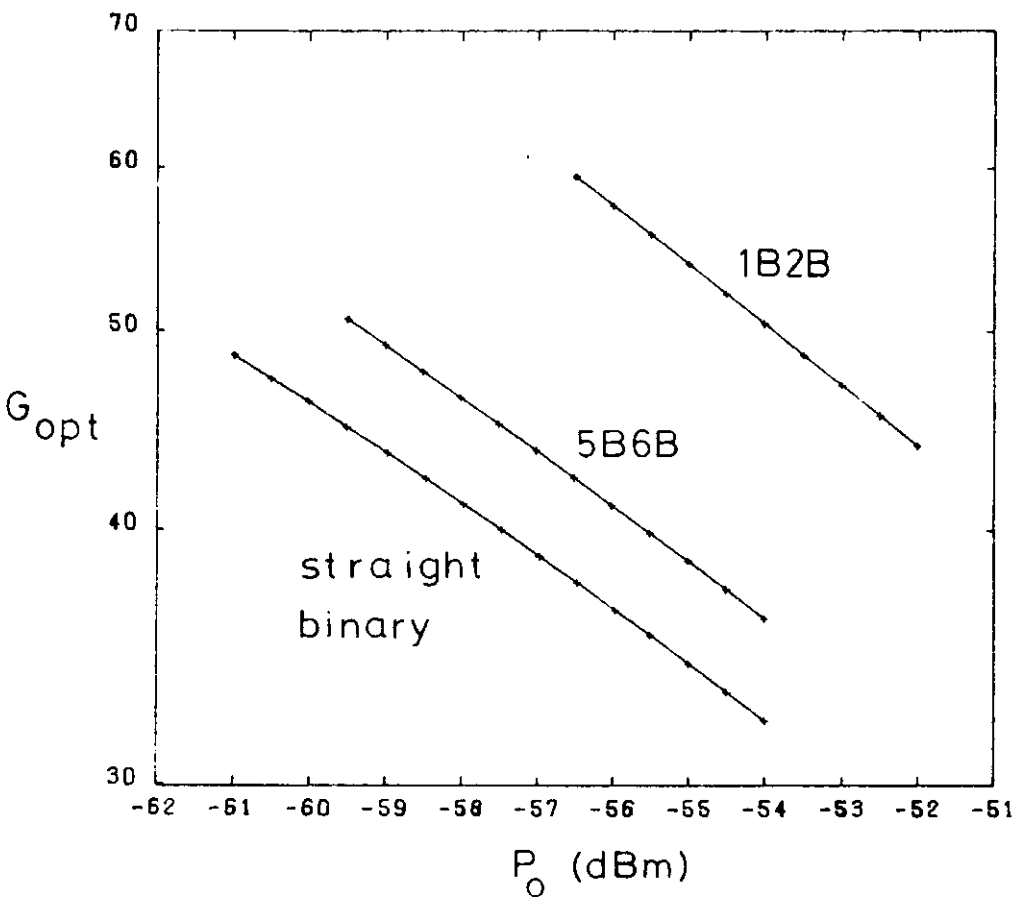

Figure 8.3.b. The optimum average avalanche gain G_{opt}

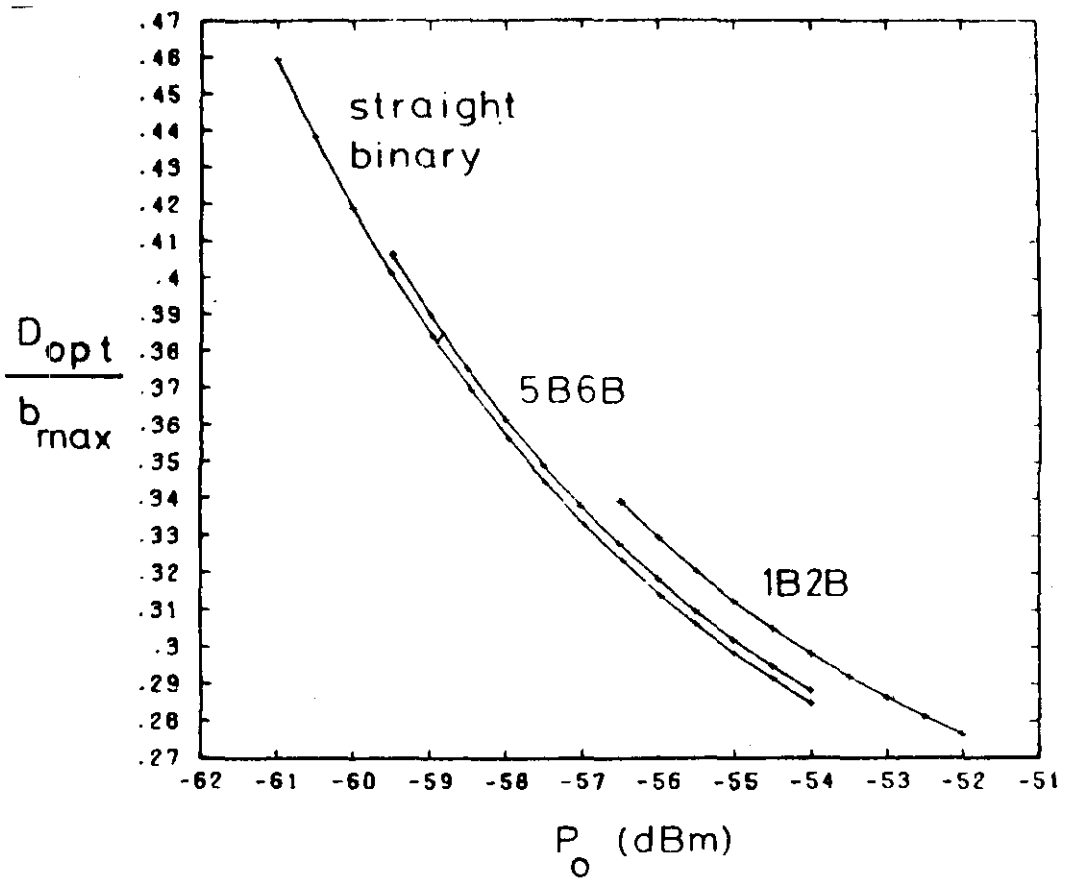

Figure 8.3.c. The normalized optimum decision threshold D_{opt}/b_{max}

Figure 8.3. The average bit error probability P_e versus the average received optical power P_o, using the optimum average avalanche gain G_{opt} and the normalized optimum decision threshold D_{opt}/b_{max}; calculated for straight binary transmission with equiprobable symbols, 5B6B coding and 1B2B split phase coding. (t_s = 0; R = 25 Mbit/sec; EXT = .01; received optical pulses: rectangular, duty cycle α_r = .5 (Gaussian, $\alpha_g \simeq .144$); equalized output pulses: raised cosine, rolloff factor β = 1; further receiver data: section 8.1)

Plots of G_{opt} and of D_{opt}/b_{max} versus P_o are shown by figure 8.3.b and 8.3.c respectively. These plots are calculated for straight binary transmission with equiprobable symbols, for 5B6B coding, and for 1B2B split phase coding. G_{opt} and D_{opt}/b_{max} are calculated by minimizing $P_e = P_e(b_{max},G,D)$ over G and D, with b_{max} fixed. The relation between P_o and b_{max} is given by (3.17). P_o can also be related to n_p, i.e. the average number of primary electrons generated by a received optical pulse having the maximum energy b_{max};

according to (3.17) and (8.17) we obtain

$$n_p = \frac{\eta}{h\nu} \cdot \frac{2.10^{-3}}{(1 + EXT)} \cdot T \cdot 10^{P_o/10} \tag{8.22}$$

where P_o is expressed in dBm.
For an information rate R = 25 Mbit/sec (see section 8.1), straight binary transmission with equiprobable symbols requires a signalling rate 1/T = 25 MBaud; 5B6B coding requires according to (7.1)

$$\frac{1}{T} = \frac{n}{m} \cdot R = 30 \text{ MBaud} \tag{8.23}$$

and 1B2B split phase coding

$$\frac{1}{T} = 50 \text{ MBaud} \tag{8.24}$$

Hence for straight binary transmission with equiprobable symbols P_o = -60 dBm corresponds with $n_p \simeq 254$ primary electrons, and for 1B2B split phase coding P_o = -56.5 dBm corresponds with $n_p \simeq 284$ primary electrons.
The plots in figure 8.3, obtained for rectangular received optical pulses with duty cycle $\alpha_r = .5$, are according to section 8.2 nearly identical with those obtained for Gaussian pulses with $\alpha_g = \alpha_r/\sqrt{12} \simeq .144$. This can be verified from table 8.2 in the case of straight binary transmission with equiprobable symbols. The differences are too small to notice in figure 8.3.
By assuming no timing errors ($t_s = 0$), the neighboring symbols do not affect $E[v_{out}(t_s = 0)|B]$ (see (6.1)). Moreover, as compared with the symbol under decision, the neighboring symbols hardly contribute to the shot noise power at the equalizer output ($\Sigma_1 - I_1 \ll I_1$, see (8.3)), and therefore hardly to $Var[v_{out}(t_s = 0)|B]$. Hence, the interference of the neighboring symbols is nearly negligible. This is illustrated in figure 8.3.a, where in the case of straight binary transmission with equiprobable symbols in addition to P_e (solid curve) also $P_{emax} = P_e(B'_{WC})$ and $P_{emin} = P_e(B'_{BC})$ (both broken curves) are plotted. These three curves nearly coincide with each other.
If P_o increases, P_e decreases strongly, as shown by figure 8.3.a. In the case of straight binary transmission with equiprobable symbols $P_e = 10^{-9}$ requires $P_o \simeq$ -57.35 dBm (corresponding with 1.84 nW) at $G_{opt} \simeq 39.7$ and $D_{opt}/b_{max} \simeq .342$.
As compared with straight binary transmission with equiprobable symbols, mBnB

Table 8.2. The average bit error probability P_e as a function of the average received optical power P_o, using the optimum average avalanche gain G_{opt} and the normalized optimum decision threshold D_{opt}/b_{max}; calculated for rectangular and Gaussian received optical pulses with the same r.m.s. width σ/T ($\sigma/T = \alpha_g = \alpha_r/\sqrt{12} \simeq .144$; straight binary transmission with equiprobable symbols; $t_s = 0$; $1/T = 25$ MBaud; EXT = .01; equalized output pulses: raised cosine, rolloff factor $\beta = 1$; further receiver data: section 8.1)

P_o (dBm)	P_e*	G_{opt}*	D_{opt}/b_{max}*
-59	$1.73 \cdot 10^{-6}$	43.76	.3855
	$1.79 \cdot 10^{-6}$	43.57	.3861
-57.5	$2.11 \cdot 10^{-9}$	40.14	.3454
	$2.24 \cdot 10^{-9}$	39.94	.3462
-56	$6.72 \cdot 10^{-14}$	36.66	.3147
	$7.50 \cdot 10^{-14}$	36.43	.3159

* The first numbers apply to rectangular, the second to Gaussian received optical pulses.

coding requires for the same information rate R an increase in the signalling rate 1/T by a factor n/m (see (7.1)). We have seen that the interference of the neighboring symbols is nearly negligible here. Hence the suppression of the most unfavourable (but also of the most favourable) combinations of these symbols, as achieved by mBnB coding (see chapter 7), hardly plays a part. The increase in 1/T is therefore (and because a balanced code is assumed) the most important aspect of mBnB coding as far as error probability calculations are concerned.

As compared with straight binary transmission with equiprobable symbols, the power penalty for using the 5B6B code is according to figure 8.3.a .85 to .9 dB to achieve the same P_e, and for using the 1B2B split phase code 3.4 to 3.5 dB. Because of $P_e \simeq P_e(B'_{WC})$ and the increase in 1/T being the most important influence of mBnB coding on P_e, the penalty for using mBnB coding can be approximated here according to (6.28) by

$$10 \cdot \frac{3x + 2}{2x + 2} \cdot {}^{10}\log \left(\frac{m}{n}\right) \quad \text{dB} \tag{8.25}$$

The receiver in question has an APD excess noise exponent x = .5 (see section 8.1), leading to a penalty of .924 dB for using the 5B6B code and of 3.51 dB for using the 1B2B split phase code. Thus (8.25) is a good approximation here. Figure 8.3.b shows, that at a given P_o the use of 5B6B coding instead of straight binary transmission with equiprobable symbols requires an increase in G_{opt} by approximately a factor 1.12, and the use of 1B2B split phase coding an increase by approximately a factor 1.57 (both at P_o = -55 dBm). If we take into account mBnB coding only by its increase in 1/T again, this increase in G_{opt} at a given P_o is according to (6.21) by approximately a factor

$$(n/m)^{2/3} \tag{8.26}$$

which is $(1.2)^{2/3} \approx 1.13$ for 5B6B coding and $(2)^{2/3} \approx 1.59$ for 1B2B split phase coding. Thus (8.26) is a good approximation here.
From the figures 8.3.a and 8.3.b it follows that, as compared with straight binary transmission with equiprobable symbols, 5B6B coding requires for $P_e = 10^{-9}$ an increase in G_{opt} by approximately a factor 1.07, and 1B2B split phase coding by approximately a factor 1.26. Because of $P_e \approx P_e(B'_{WC})$ and the increase in 1/T being the most important influence of mBnB coding on P_e, this increase in G_{opt} at a fixed P_e is according to (6.29) by approximately a factor

$$(n/m)^{1/(2+2x)} \tag{8.27}$$

The receiver in question has an APD excess noise exponent x = .5 (see section 8.1), leading to a factor $(1.2)^{1/3} \approx 1.063$ for 5B6B coding and a factor $(2)^{1/3} \approx 1.260$ for 1B2B split phase coding. Thus (8.27) is a good approximation here. Plotting G_{opt} logarithmically here as a function of P_o at a fixed 1/T (and fixed I_3, k and EXT), we get according to (6.21) approximately a straight line. The approximation errors decrease as 1/T increases, as discussed in subsection 6.2.2. Figure 8.3.b confirms this. The slopes of the curves satisfy (6.21) pretty well: starting from G_{opt} = 53.87 at P_o = -55 dBm for 1B2B split phase coding, we calculate with the aid of (6.21) the approximation G_{opt} = 49.89 at P_o = -54 dBm, whereas minimization of P_e at P_o = -54 dBm yields G_{opt} = 50.41. The approximation value is slightly smaller than the

value found by minimization because of the decrease in D_{opt}/b_{max} at increasing P_o (see figure 8.3.c), which increases G_{opt} slightly (see subsection 6.2.2). Figure 8.3.c shows a decrease in D_{opt}/b_{max} if P_o increases at fixed 1/T (in other words: if b_{max} increases; see (3.17)). This agrees with subsection 6.1.2. Figure 8.3.c shows also an increase in D_{opt}/b_{max} at fixed P_o if we use mBnB coding instead of straight binary transmission with equiprobable symbols; this increase becomes larger as the conversion ratio n/m grows. Due to mBnB coding 1/T increases by a factor n/m, implying at fixed P_o a decrease in b_{max} (see (3.17)). Both effects increase D_{opt}/b_{max} according to subsection 6.1.2. Hence figure 8.3.c agrees with subsection 6.1.2.

9. A modified receiver model

In the preceding chapters we have assumed DC coupling in the amplifier and the equalizer. The decision threshold of the threshold detector may therefore be a DC voltage, which has to be very stable. This makes high demands on the technical realization.

Let us now consider another receiver model with AC coupling in the amplifier and the equalizer. The AC coupled amplifier and equalizer can be represented by a DC coupled amplifier and equalizer followed by a coupling capacitor, as shown in figure 9.1. The threshold detector can be realized by a comparator with one input grounded.

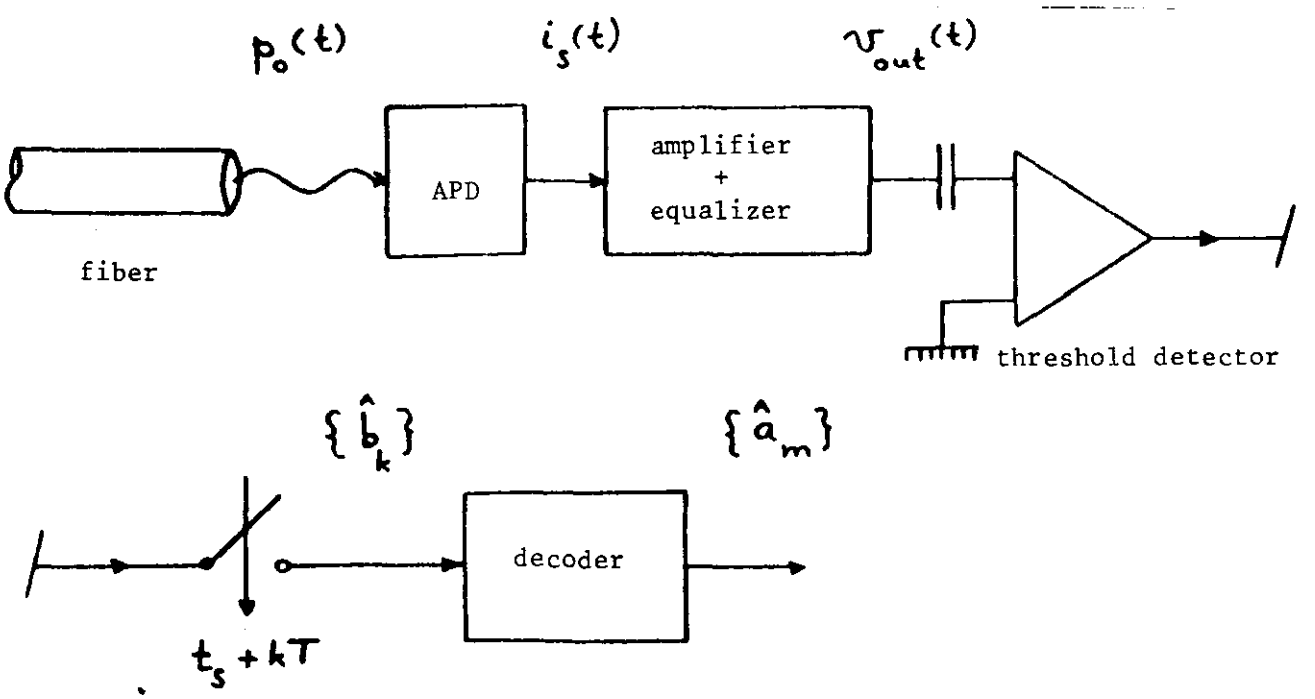

Figure 9.1. A modified receiver model

9.1. Threshold setting

By the way in which the threshold detector is realized, we may assume an equivalent decision threshold D_{eq} operating on the signal $v_{out}(t)$ at the equalizer output:

$$D_{eq} = \text{DC level of } v_{out}(t) \tag{9.1}$$

From the linearity of the receiver we have

$$\text{DC level of } v_{out}(t) = (\text{DC level of } p_o(t)) \cdot \frac{H_{out}(o)}{H_p(o)} + V_o \tag{9.2}$$

From (2.2) it follows that

$$\text{DC level of } p_o(t) = \frac{1}{T} \int_{-T/2}^{T/2} E[p_o(t)]\, dt$$

$$= \frac{1}{T} \int_{-T/2}^{T/2} \sum_{k=-\infty}^{+\infty} E[b_k] \cdot h_p(t-kT)dt \tag{9.3}$$

Using a balanced line code, or straight binary transmission with equiprobable symbols, we have with (3.14)

$$E[b_k] = \frac{b_{max} + b_{min}}{2} = \frac{b_{max}}{2} \cdot (1+EXT) \tag{9.4}$$

Hence

$$\text{DC level of } p_o(t) = \frac{b_{max}(1+EXT)}{2T} \int_{-T/2}^{T/2} \sum_{k=-\infty}^{+\infty} h_p(t-kT)dt$$

$$= \frac{b_{max}\,(1+EXT)}{2T} \int_{-\infty}^{+\infty} h_p(t)dt$$

$$= \frac{b_{max}\,(1+EXT)}{2T} \cdot H_p(o) \tag{9.5}$$

which yields with (3.9), (9.1) and (9.2)

$$D_{eq} = \frac{b_{max}\,(1+EXT)}{2} \cdot H'_{out}(o) + V_o \tag{9.6}$$

and with (3.20)

$$D_{eq} = \{\frac{b_{max}\,(1+EXT)}{2} + \lambda_o T \cdot \frac{h\nu}{\eta}\} . H'_{out}(o) \tag{9.7}$$

Thus using this receiver model, we can vary D_{eq} by varying $H'_{out}(o)$. For instance, let us assume a raised cosine equalized spectrum $H'_{out}(f)$ with a rolloff factor $\beta > 1$ (see also (4.12)):

$$H'_{out}(f) = \sin(\frac{\pi}{2\beta}) \cdot \cos(\frac{\pi f}{\beta}) \qquad \text{for } |f| < (\beta-1)/2$$

$$= \tfrac{1}{2}.[1-\sin(\frac{\pi}{\beta}(|f| - \tfrac{1}{2}))] \qquad \text{for } (\beta-1)/2 \leq |f| < (\beta+1)/2$$

$$= 0 \qquad \text{otherwise}$$

$$h'_{out}(t) = \frac{\sin(\pi t).\cos(\beta\pi t)}{\pi t.[1-(2\beta t)^2]} \tag{9.8}$$

Figure 9.2.a shows this spectrum (see also figure 4.3.a), and figure 9.2.b the time functions (see also figure 4.3.c). These time functions decay very fast; the larger β is, the faster the decay. The worst case eye patterns, shown by figure 9.3, are therefore wide open. Rolloff factors $\beta > 1.5$ introduce small irregularities in the eye pattern, because of $h'_{out}(t)$ having zero crossings for $|t| < 1$.
From (4.12) and (9.8) we have

$$H'_{out}(o) = 1 \qquad \text{for } \beta \leq 1$$

$$= \sin(\frac{\pi}{2\beta}) \qquad \text{for } \beta > 1 \tag{9.9}$$

Hence, by varying $\beta > 1$ we can vary the normalized equivalent decision threshold:

$$\frac{D_{eq}}{b_{max}} = \{\frac{1+EXT}{2} + \frac{\lambda_o T}{b_{max}} \cdot \frac{h\nu}{\eta}\}.\sin(\frac{\pi}{2\beta}) \text{ for } \beta > 1 \tag{9.10}$$

Figure 9.4 illustrates this for a dark current $\lambda_o = 0$ and an extinction EXT = 0; for instance, $\beta = 2.4$ yields $D_{eq}/b_{max} \simeq .3$. As using the previous receiver model we calculated a normalized optimum decision threshold D_{opt}/b_{max}, so using this receiver model we may calculate an optimum rolloff factor β_{opt}.
Appendix 3 shows plots of the weighting factors I_1, Σ_1, Σ_1-I_1, I_2 and I_3 versus β, with the normalized r.m.s. optical pulse width σ/T as a parameter. We have assumed raised cosine equalized output pulses $h'_{out}(t)$, and rectangular or Gaussian received optical pulses $h'_p(t)$.
According to (4.11) we have $\alpha_g = \sigma/T$; $\sigma/T = .029$, $= .087$ and $= .144$ correspond with $\alpha_r = .1$, $= .3$ and $= .5$ respectively.
Appendix 2 shows plots of the same weighting factors versus σ/T, with β as a

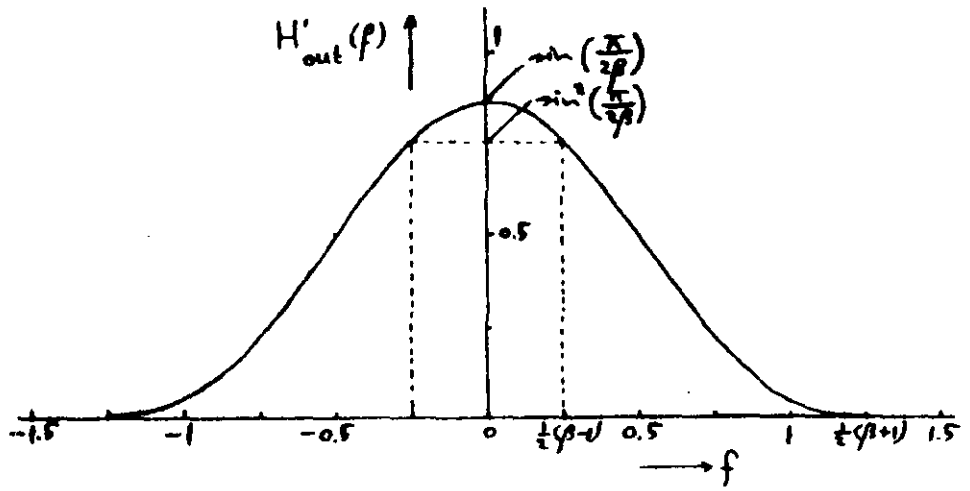

9.2.a. Raised cosine spectrum $H'_{out}(f)$

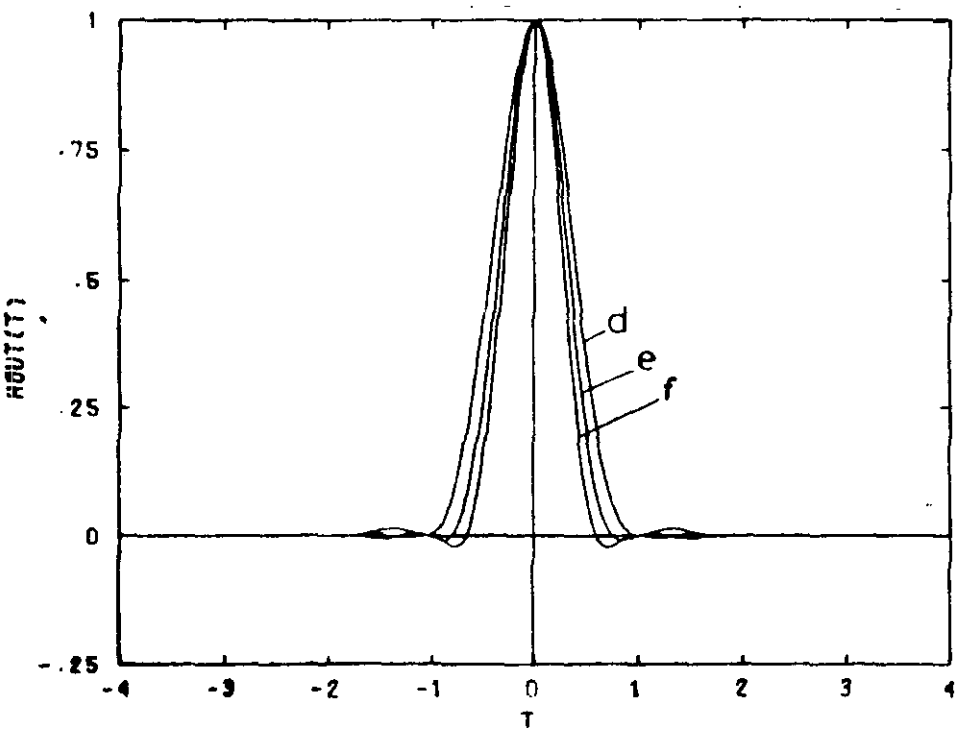

9.2.b. Raised cosine time function $h'_{out}(t)$
(d: $\beta = 1.5$; e: $\beta = 2$; f: $\beta = 2.5$)

Figure 9.2. Raised cosine equalized output spectrum with corresponding time functions for rolloff factor $\beta > 1$

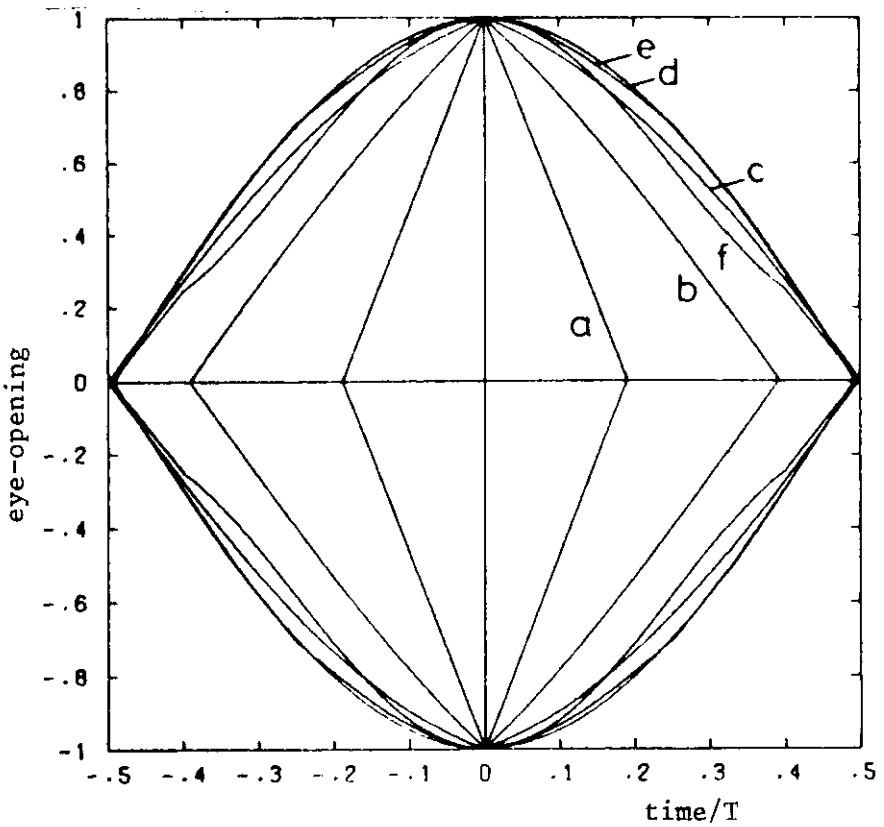

Figure 9.3. Worst case eye patterns for raised cosine pulses with rolloff factor β (a: β = .1; b: β = .5; c: β = 1; d: β = 1.5; e: β = 2; f: β = 2.5)

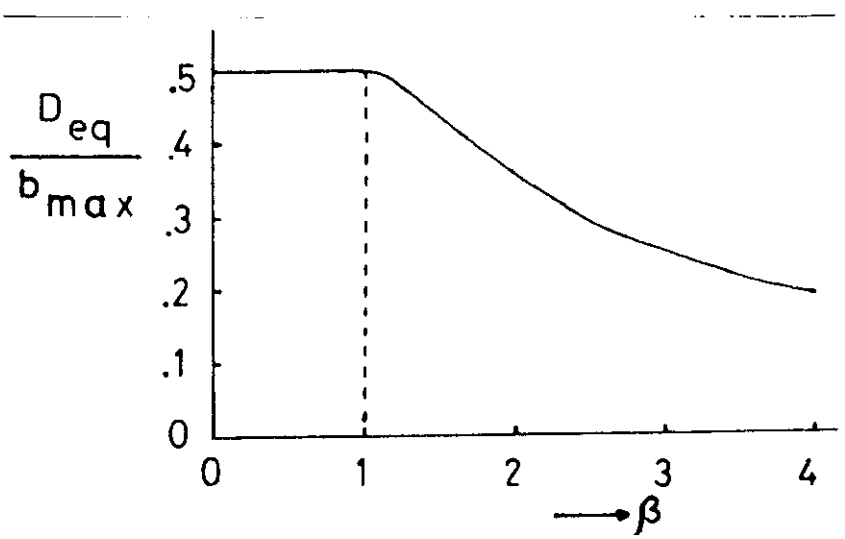

Figure 9.4. The normalized equivalent decision threshold D_{eq}/b_{max} versus the rolloff factor β of the raised cosine equalized output pulses (λ_o = 0; EXT = 0)

parameter. These were discussed in subsection 5.4.1; the same discussion holds for the plots in appendix 3. Generally, we have $\Sigma_1 - I_1 \ll I_1$: the shot noise power of the neighboring symbols is nearly negligible as compared with that of the symbol under decision. Moreover, $\Sigma_1 - I_1$ exhibits as a function of β local minima for $\beta \simeq 1.5$ and $\beta \simeq 2.5$, which become smaller and sharper as σ/T decreases. So if we use a rolloff factor $\beta \simeq 2.5$, the shot noise power of the neighboring symbols is even smaller.

9.2. Received optical pulses

In the preceding chapters we have assumed, that narrowing the received optical pulses leads to a proportional increase in pulse height, thus leaving the pulse energy unchanged (see figure 4.2). The peak power of a practical optical transmitter (laser diode or LED) however is limited. Hence there is an upper bound on the pulse height, and therefore a lower bound on the pulse width. Let us now assume for the received optical pulses having the maximum energy b_{max} (the so-called ON pulses) a fixed height P_{max} such, that the peak power limit of the optical transmitter is not exceeded. Hence the pulse energy is proportional to the pulse width. Figure 9.5 shows rectangular and Gaussian ON pulses. We have for the pulse power p(t)

$$p(t) = P_{max} \cdot \frac{h_p(t)}{h_p(o)} \tag{9.11}$$

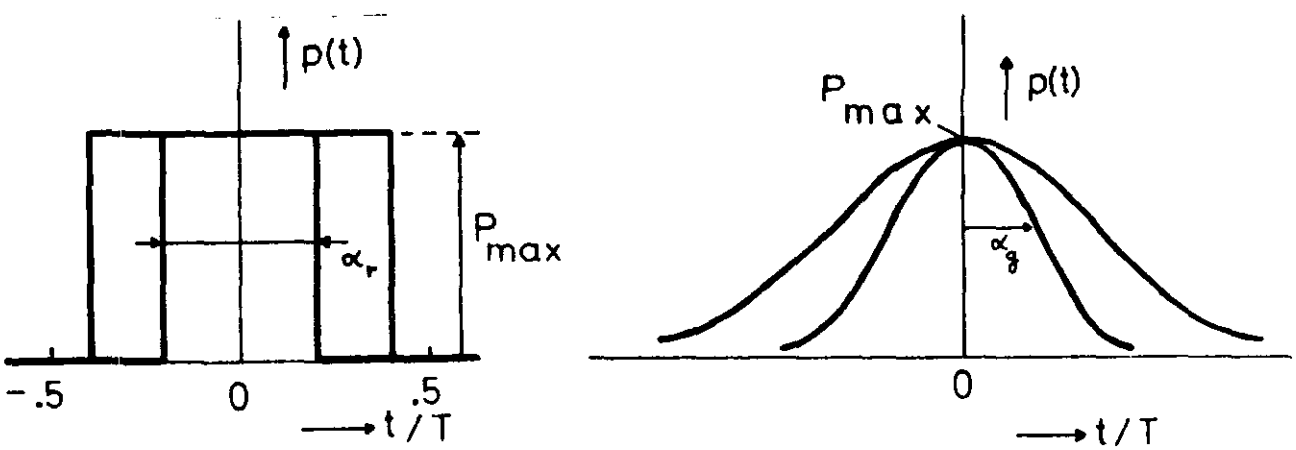

9.5.a. rectangular ($\alpha_r < 1$) 9.5.b. Gaussian

Figure 9.5. The received optical pulses (ON pulses)

yielding with (2.3)

$$b_{max} = \int_{-\infty}^{+\infty} p(t)dt = P_{max}/h_p(o) \qquad (9.12)$$

From (3.9) and (4.8) we have for rectangular pulses

$$b_{max} = T.P_{max}/h_p'(o) = \alpha_r.T.P_{max} \qquad (9.13)$$

and in the same way from (4.9) for Gaussian pulses

$$b_{max} = \alpha_g.\sqrt{2\pi}.T.P_{max} \qquad (9.14)$$

If we use straight binary transmission with equiprobable symbols, or a balanced line code, the average received optical power P_o according to (3.17) for rectangular pulses is

$$P_o = 10.^{10}\log\left[\frac{\alpha_r.P_{max}.(1+EXT)}{2\ mW}\right] \quad (dBm) \qquad (9.15)$$

and for Gaussian pulses

$$P_o = 10.^{10}\log\left[\frac{\alpha_g.\sqrt{2\pi}.P_{max}.(1+EXT)}{2\ mW}\right] \quad (dBm) \qquad (9.16)$$

9.3. Numerical results of calculating the average bit error probability

In this section the average bit error probability P_e is calculated as a function of a number of system parameters following the exhaustive method (5.7). We use the data for a typical optical receiver, enumerated by Personick in [3, part II, chapter III]. We leave timing errors out of consideration by putting $t_s = 0$. The influence of the received optical pulse shape is analyzed, and also the influence of the rolloff factor of the raised cosine equalized output spectrum, of the average received optical power, and of line coding.

9.3.1. Receiver data

We use the data for a typical optical receiver again, enumerated by Personick in [3, part II, chapter III] (see (8.1) and (8.2)). The following additions and

modifications are made:

- information rate R = 70 Mbit/sec
- received optical pulses:
  - rectangular, duty cycle α_r
  - maximum height P_{max} = 100 nW
- equalized output pulses: raised cosine, rolloff factor β
- extinction EXT = .01
- APD ionisation constant k = .1 (see (8.5)). (9.17)

The data pattern truncation parameters k_1 and k_2 are determined in the same way as in section 8.1. With the α_r (< .5) and the β used in this chapter, $k_1 = -2$ and $k_2 = 2$ are acceptable.

9.3.2. Influence of the received optical pulse shape

In the first instance, we assume rectangular received optical pulses. As discussed in section 4.2, Gaussian pulses are more plausible when fiber dispersion is no longer negligible.

Using the same arguments as in section 8.2, we state here also that rectangular and Gaussian received optical pulses are nearly equivalent in error probability calculations, if their normalized widths α_r and α_g are related to each other by $\alpha_g = \sigma/T = \alpha_r/\sqrt{12}$. Furthermore, let the maximum heights $P_{max,r}$ and $P_{max,g}$ of a rectangular and a Gaussian pulse respectively be related to each other by

$$P_{max,g} = \sqrt{\frac{6}{\pi}} \cdot P_{max,r} \tag{9.18}$$

Then from (9.15) and (9.16) we have the same average received optical power P_o for both pulse types, if we have the same r.m.s. pulse width σ/T. Hence, the results of error probability calculations using rectangular received optical pulses with duty cycle α_r and maximum height $P_{max,r}$ = 100 nW, described in the following sections, are nearly equal to those using Gaussian pulses with $\alpha_g = \alpha_r/\sqrt{12}$ and $P_{max,g} \simeq 138.20$ nW. This will be verified in subsection 9.3.4.

9.3.3. Influence of the rolloff factor of the raised cosine equalized output spectrum

Figure 9.6 shows a plot of the average bit error probability P_e versus the roll-off factor β of the raised cosine equalized output spectrum. It is calculated

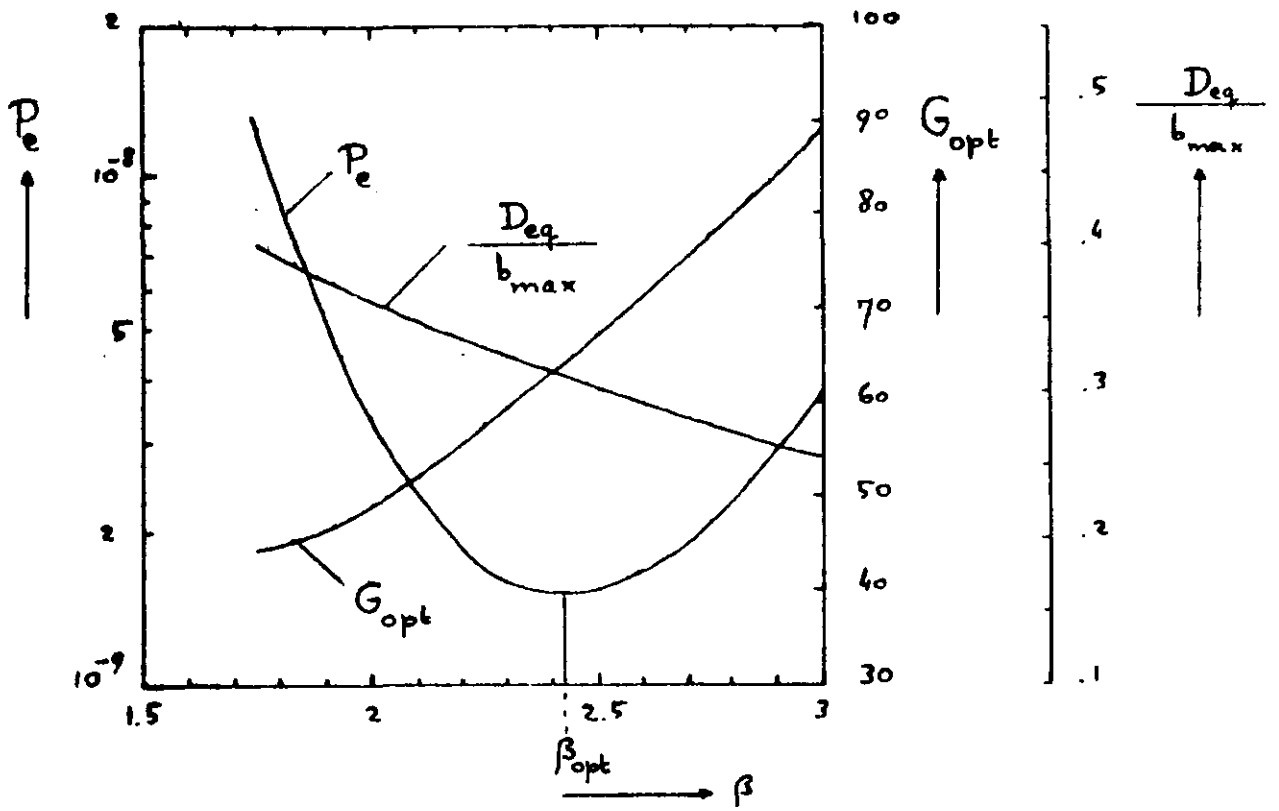

Figure 9.6. The average bit error probability P_e versus the rolloff factor β of the raised cosine equalized output spectrum, using the optimum average avalanche gain G_{opt} (normalized equivalent decision threshold D_{eq}/b_{max}).
(1B2B split phase coding; $t_s = 0$; $1/T = 140$ MBaud; EXT = .01; received optical pulses: rectangular, duty cycle $\alpha_r = .3$; maximum height $P_{max,r} = 100$ nW (Gaussian, $\alpha_g = \alpha_r/\sqrt{12} \simeq .087$, $P_{max,g} = P_{max,r} \cdot \sqrt{6/\pi} \simeq 138.20$ nW) ($P_o \simeq -48.20$ dBm); further receiver data: subsection 9.3.1)

using the optimum average avalanche gain G_{opt}, and rectangular received optical pulses with $\alpha_r = .3$ (yielding $P_o \simeq -48.20$ dBm according to (9.15) and (9.17)). We have assumed 1B2B split phase coding; thus the signalling rate is given with (7.1) and (9.17) by

$$\frac{1}{T} = \frac{n}{m} \cdot R = 140 \text{ MBaud} \tag{9.19}$$

Figure 9.6 shows also plots of G_{opt}, and of the normalized equivalent decision threshold D_{eq}/b_{max} (see (9.10)).

There is a minimum in P_e at the optimum rolloff factor β_{opt}. Since this minimum is not very sharp, small deviations of β from β_{opt} cause no serious degradation in the error performance. G_{opt} increases if β increases. According to (6.21) this is due to the increase in the weighting factor I_3 for larger β (see appendix 3).

9.3.4. Influence of the average received optical power, and of line coding

In this subsection the influence of the average received optical power P_o on the average bit error probability P_e is analyzed, and also the influence of mBnB line coding.

Figure 9.7.a shows plots of P_e versus P_o, calculated using the optimum average avalanche gain G_{opt} and the optimum rolloff factor β_{opt} of the

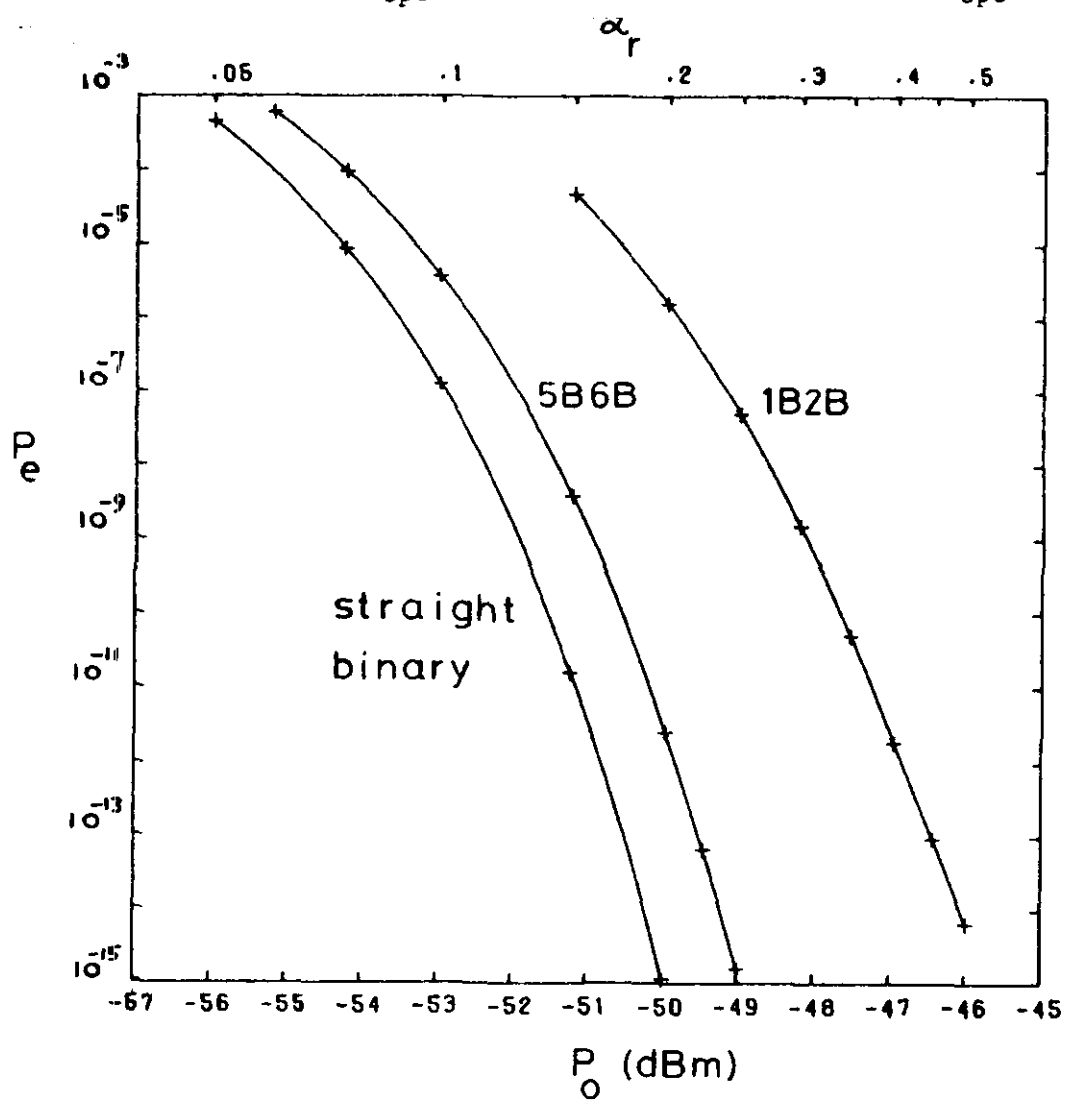

9.7.a. The average bit error probability P_e

raised cosine equalized output spectrum. Plots of G_{opt} and β_{opt} are shown by figure 9.7.b and 9.7.c respectively. These plots are calculated for straight binary transmission with equiprobable symbols, for 5B6B coding, and for 1B2B split phase coding. G_{opt} and βopt are found by minimizing $P_e = P_e(P_o,G,\beta)$ over G and β, with P_o fixed. In the first instance, the received optical pulses are assumed to be rectangular with a duty cycle α_r and a maximum height $P_{max,r}$ = 100 nW. The relation between P_o and α_r is given by (9.15).

For an information rate R = 70 Mbit/sec (see subsection 9.3.1), straight binary transmission with equiprobable symbols requires a signalling rate

$$\frac{1}{T} = R = 70 \text{ MBaud} \tag{9.20}$$

and according to (7.1) 5B6B coding requires

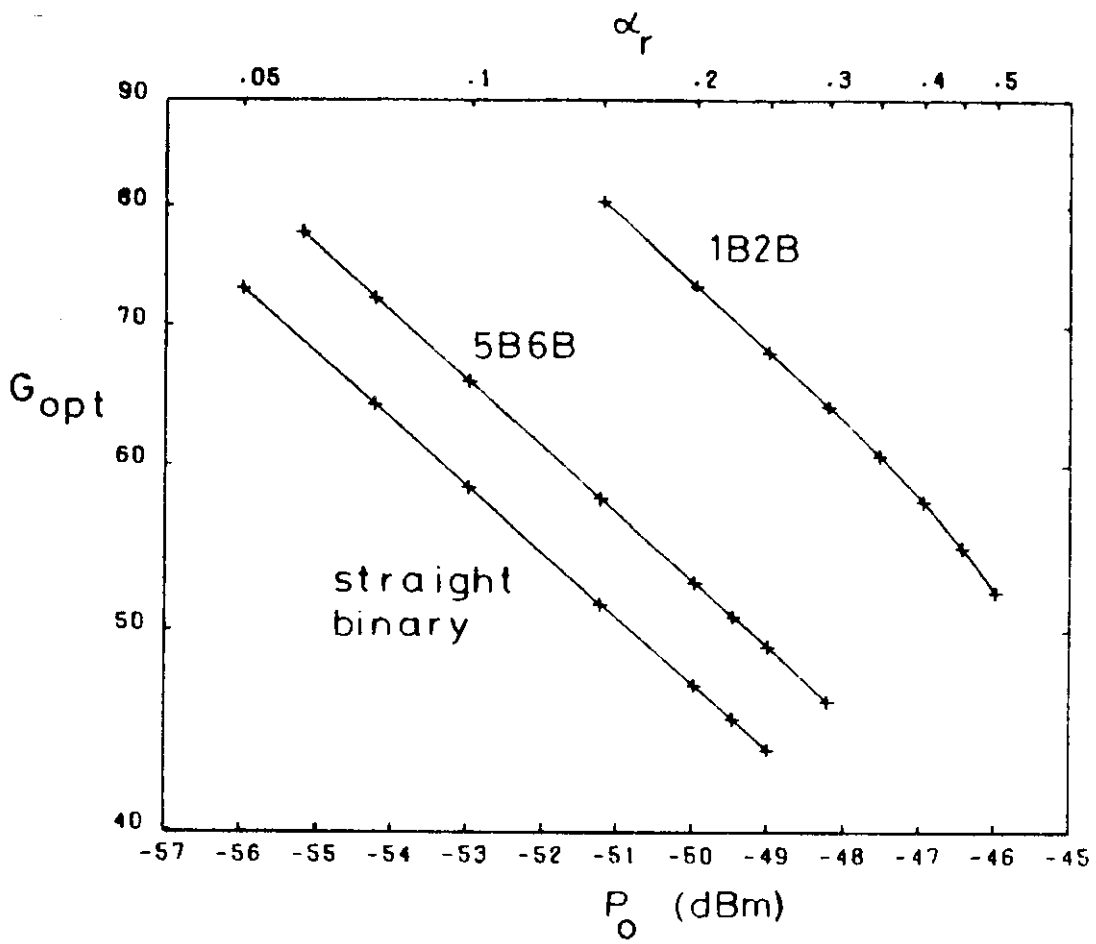

9.7.b. The optimum average avalanche gain G_{opt}

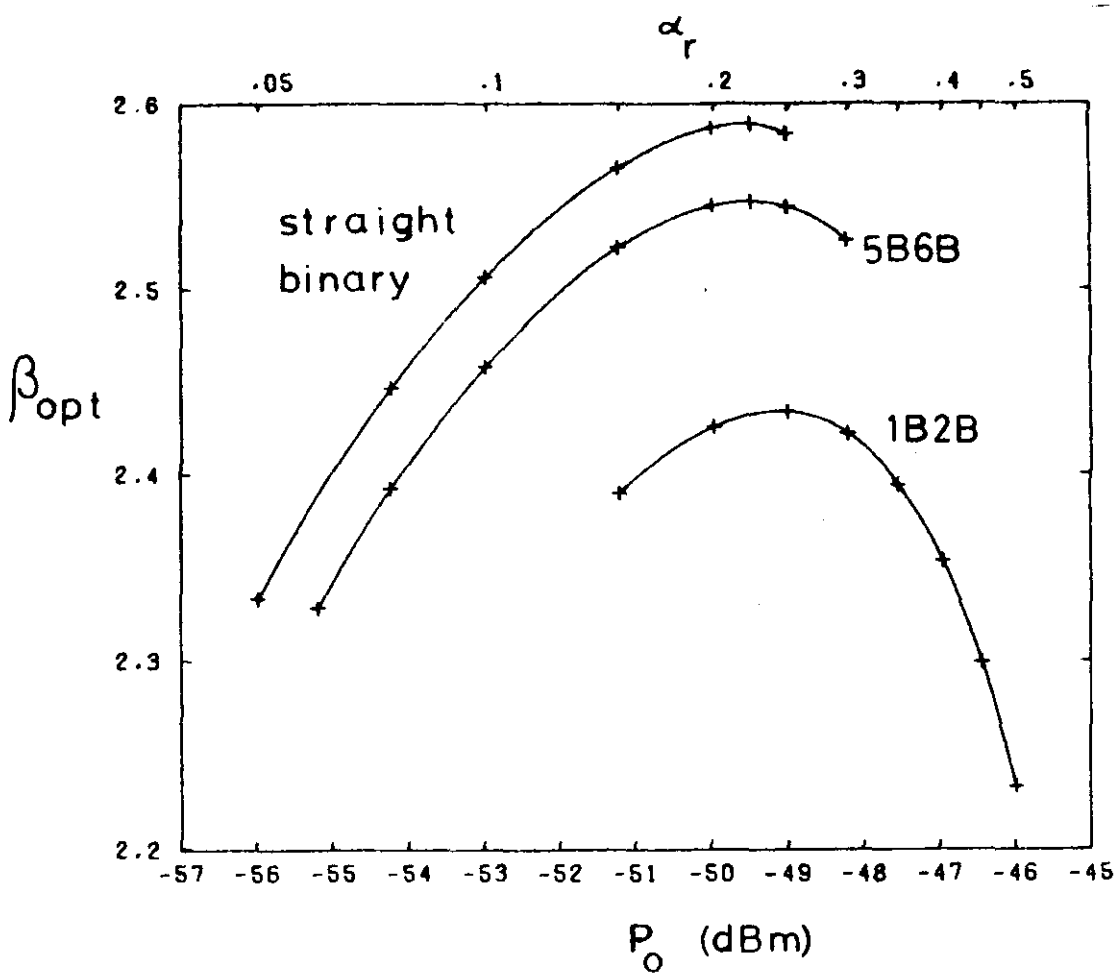

9.7.c. The optimum rolloff factor β_{opt}

Figure 9.7. The average bit error probability P_e versus the average received optical power P_o, using the optimum average avalanche gain G_{opt} and the optimum rolloff factor β_{opt} of the raised cosine equalized output spectrum; calculated for straight binary transmission with equiprobable symbols, 5B6B coding and 1B2B split phase coding. (t_s = 0; R = 70 Mbit/sec; EXT = .01; received optical pulses: rectangular, duty cycle α_r, maximum height $P_{max,r}$ = 100 nW (Gaussian, $\alpha_g = \alpha_r/\sqrt{12}$, $P_{max,g} = P_{max,r}.\sqrt{6/\pi} \simeq 138.20$ nW); further receiver data: subsection 9.3.1)

$$\frac{1}{T} = \frac{n}{m}.R = 84 \text{ MBaud} \qquad (9.21)$$

and 1B2B split phase coding 1/T = 140 MBaud (see (9.19)).

The plots in figure 9.7, obtained for rectangular received optical pulses with duty cycle α_r and maximum height $P_{max,r}$ = 100 nW, are according to subsection

9.3.2 nearly identical with those for Gaussian pulses with $\alpha_g = \alpha_r/\sqrt{12}$ and $P_{max,g} = P_{max,r}.\sqrt{6/\pi} \simeq 138.20$ nW. This can be verified from table 9.1 in the case of straight binary transmission with equiprobable symbols. The differences are too small to notice in figure 9.7.

Table 9.1. The average bit error probability P_e as a function of the average received optical power P_o, using the optimum average avalanche gain G_{opt} and the optimum rolloff factor β_{opt} of the raised cosine equalized output spectrum; calculated for rectangular and Gaussian received optical pulses with the same r.m.s. width σ/T and with maximum height $P_{max,r} = 100$ nW and $P_{max,g} = P_{max,r}.\sqrt{6/\pi} \simeq 138.20$ nW respectively ($\sigma/T = \alpha_g = \alpha_r/\sqrt{12}$; straight binary transmission with equiprobable symbols; $t_s = 0$; $1/T = 70$ MBaud; EXT = .01; further receiver data: subsection 9.3.1)

P_o(dBm)	P_e^*	G_{opt}^*	β_{opt}^*
-55.98	$4.512\ .10^{-4}$	72.95	2.333
	$4.512\ .10^{-4}$	72.95	2.333
-52.97	$1.289\ .10^{-7}$	58.57	2.507
	$1.290\ .10^{-7}$	58.56	2.507
-49.96	$1.125\ .10^{-15}$	47.04	2.587
	$1.135\ .10^{-15}$	46.99	2.587

* The first numbers apply to rectangular, the second to Gaussian received optical pulses

With the same arguments as used in section 8.6, here also the interference of the neighboring symbols is nearly negligible. Thus the increase in 1/T is the most important aspect of mBnB coding as far as error probability calculations are concerned.

As compared with straight binary transmission with equiprobable symbols, the power penalty for using the 5B6B code is according to figure 9.7.a approximately 1 (1) dB, and for using the 1B2B split phase code approximately 3.8 (4) dB to achieve a $P_e = 10^{-9}$ (10^{-12}). According to (8.25) these penalties are .924 dB and 3.51 dB respectively. For the previous receiver model (8.25) was quite

accurate (see section (8.6), but here it underestimates the power penalties. This can be explained as follows. As compared with the previous receiver model, increasing P_o yields here a larger increase in the noise power at the equalizer output: the weighting factors I_1, $\Sigma_1 - I_1$, I_2 and I_3 do not remain constant, but increase with P_o because of the increasing optical pulse width (and the variations in β_{opt}: see figure 9.7.c). Thus P_e decreases less fast if P_o increases, particularly for larger P_o. Hence the power penalties for using mBnB coding increase as P_e decreases.

Figure 9.7.b shows an increase in G_{opt} at fixed P_o if the conversion ratio n/m of the mBnB code increases. As compared with straight binary transmission with equiprobable symbols, G_{opt} increases at P_o = -50 dBm using 5B6B coding by approximately a factor 1.12, and using 1B2B split phase coding by approximately a factor 1.56. According to (8.26) these factors are $(1.2)^{2/3} \simeq 1.13$ and $(2)^{2/3} \simeq 1.59$ respectively. Thus (8.26) is a good approximation here. For the previous receiver model however it was slightly more accurate (see section 8.6), because there the weighting factor I_3 for instance, on which G_{opt} also depends (see (6.21)), did not vary.

The figures 9.7.a and 9.7.b show an increase in G_{opt} at fixed P_e if n/m increases. As compared with straight binary transmission with equiprobable symbols, G_{opt} increases at $P_e \simeq 10^{-9}$ using 5B6B coding by approximately a factor 1.05, and using 1B2B split phase coding by approximately a factor 1.17. According to (8.27) these factors are $(1.2)^{1/3} \simeq 1.063$ and $(2)^{1/3} \simeq 1.260$ respectively. Approximation (8.27) was more accurate for the previous receiver model, because there the weighting factors did not vary.

Plotting G_{opt} logarithmically as a function of P_o at a fixed 1/T (and fixed I_3, k and EXT), we get according to (6.21) approximately a straight line. This applies to sufficiently large 1/T, and is confirmed by figure 9.7.b. Here also approximation errors are caused by the variations in the weighting factors (e.g. in I_3) accompanying the increase in P_o. Particularly at a large pulse width (α_r or α_g) and at a strongly varying optimum rolloff factor β_{opt} these errors are noticeable, as shown by figure 9.7.b for 1B2B split phase coding.

Figure 9.7.c shows a plot of β_{opt} versus P_o. Using the previous receiver model, the normalized optimum decision threshold D_{opt}/b_{max} increased at fixed P_o if we used mBnB coding instead of straight binary transmission with equiprobable symbols; the larger n/m, the larger this increase was (see figure 8.3.c). According to (9.10) this corresponds with a decreasing β_{opt}

if n/m increases at fixed P_o, as shown by figure 9.7.c. Using the previous receiver model, D_{opt}/b_{max} decreased if P_o increased at fixed 1/T (see figure 8.3.c). This corresponds with the initial increase in β_{opt} if P_o increases at fixed 1/T, shown by figure 9.7.c. Increasing P_o (and thus α_r or α_g: see (9.15) and (9.16)) together with increasing β however yields an increase in the weighting factor I_3 according to appendix 3, and therefore in the thermal noise parameter Z_{th} according to (4.5). This increase in noise power with increasing β ultimately dominates the positive effect of decreasing the decision threshold with increasing β. Hence the plot of β_{opt} versus P_o exhibits a maximum at a certain P_o, beyond which β_{opt} decreases with increasing P_o.

10. Conclusions and final remarks

We numerically calculated the average bit error probability using two receiver models. The influence of a number of important system parameters and of mBnB line coding was analyzed. The decision threshold and the average avalanche gain were optimized to yield a minimum average bit error probability. Timing errors in the receiver were not considered, and the shape of the received optical pulses was assumed to be known (rectangular or Gaussian). The equalization in the receiver was of the raised cosine type. A Gaussian approximation of the statistics of the signal at the threshold detector input was introduced. Average bit error probabilities were calculated using the exhaustive method.

The Gaussian approximation of the statistics of the signal at the threshold detector input is allowed at the average received optical powers and signalling rates considered here, because of the average number of primary electrons generated in a time slot being very large. This approximation gives fairly accurate results, but tends to underestimate the optimum threshold setting and to overestimate the optimum average avalanche gain. This occurs because the Gaussian approximation depends only on the expectation and the variance of the avalanche gain distribution, and is insensitive to its skewness towards large values of the avalanche gain [1].

The assumption of rectangular received optical pulses makes sense only in the case of negligible fiber dispersion. A certain amount of fiber dispersion makes Gaussian pulses more plausible. Both pulse types appear to be nearly equivalent in error probability calculations, if they have the same normalized r.m.s. width.

Practical values of the received optical pulse width (for instance, a duty cycle not exceeding 50% for rectangular pulses) and of the rolloff factor of the pulses at the equalizer output (for instance, a rolloff factor 1 or larger for raised cosine pulses) yield a shot noise power of the neighboring symbols, which is nearly negligible as compared with that of the symbol under decision. In the absence of timing errors in the receiver, the interference of the neighboring symbols is therefore very small. Hence the exhaustive method, which can deal only with a finite (preferably small) number of neighboring symbols, is well suited to calculate average bit error probabilities. Moreover, this method facilitates the implementation of line coding in the calculations.

As compared with straight binary transmission with equiprobable symbols, mBnB line coding requires for the same information rate an increase in the signalling rate by a factor n/m. Since the interference of the neighboring symbols is very small here (and a balanced code is assumed), this increase is the most important aspect of mBnB coding as far as error probability calculations are concerned. The power penalty for using mBnB coding increases as n/m increases. The optimum average avalanche gain and the optimum decision threshold (normalized on the maximum energy in a received optical pulse) increase if n/m increases at a fixed average received optical power.
The approximations derived to point out the relations between various system parameters and the average bit error probability, the optimum average avalanche gain, the optimum decision threshold and the average received optical power, agree (fairly) well with the results of the numerical calculations.
The average bit error probability decreases strongly if the average received optical power increases. This error probability is very sensitive to deviations of the decision threshold from the optimum value, but less sensitive to deviations of the average avalanche gain from the optimum value. For the modified receiver model the threshold setting is achieved by varying the rolloff factor of the raised cosine equalized output spectrum. The average bit error probability is not very sensitive to deviations of the rolloff factor from the optimum value. The error performance of this receiver model appears to be nearly as good as that of the previous receiver model.
In treating a subject as extensive as error probability calculations in digital fiber optic communication systems, we have of course only discussed a limited number of system aspects. For instance, further investigation is possible into the influence of the optical fiber characteristics, and into the influence of timing errors in the receiver. These timing errors however will generally increase the number of interfering neighboring symbols, thus making the exhaustive method less attractive.

Acknowledgement

The author wishes to thank lecturer ir. J. van der Plaats and dr.ir. W.C. van Etten for many helpfull and stimulating discussions. He is also grateful to Mrs. T. van de Ven-Pellegrino and Mrs. L. de Jong-Vriens for typing this paper.

Eindhoven, May 11, 1979

A.M.J. Koonen.

References

[1] S.D. Personick, P. Balaban, J.H. Bobsin and P.R. Kumar: "A detailed comparison of four approaches to the calculation of the sensitivity of optical fiber system receivers", IEEE Tr. on Communications, Vol. COM-25, No. 5, May 1977, pp. 541-548.

[2] S.D. Personick: "Baseband linearity and equalization in fiber optic digital communication systems", BSTJ, Vol. 52, No. 7, Sept. 1973, pp. 1175-1194.

[3] S.D. Personick: "Receiver design for digital fiber optic communication systems, I and II", BSTJ, Vol. 52, No. 6, July-Aug. 1973, pp. 843-886.

[4] E. Parzen: Stochastic processes , San Francisco: Holden-Day, 1962.

[5] A. Papoulis: Probability, random variables and stochastic processes , New York: Mc Graw Hill, 1965.

[6] G. Cariolaro: "Error probability in digital fiber optic communication systems", IEEE Tr. on Information Theory, Vol. IT-24, No. 2, Mar. 1978, pp. 213-221.

[7] L.E. Franks: "Further results on Nyquist's problem in pulse transmission", IEEE Tr. on Communication Technology, Vol. COM-16, No. 2, Apr. 1968, pp. 337-340.

[8] R. Dogliotti, A. Luvison and G. Pirani: "Pulse shaping and timing errors in optical fibre systems", Proc. of the Fourth European Conference on Optical Communication, Genova, Italy, Sept. 12-15, 1978, pp. 510-516.

[9] J.M. Wozencraft and I.M. Jacobs: Principles of communication engineering , New York: Wiley, 1965.

[10] S.D. Personick: "Statistics of a general class of avalanche detectors with applications to optical communication", BSTJ, Vol. 50, No. 10, Dec. 1971, pp. 3075-3095.

[11] Y. Takasaki, M. Tanaka, N. Maeda, K. Yamashita and K. Nagano: "Optical pulse formats for fiber optic digital communications", IEEE Tr. on Communications, Vol. COM-24, No. 4, Apr. 1976, pp. 404-413.

BSTJ = Bell System Technical Journal

Appendix 1

Plots of the shot noise variance functions

Normalized shot noise variance function z'(t)/z'(o)

According to (3.12) we have $z'(t) = h'_p(t) * h'^2_1(t)$

where according to (3.11) $h'_1(t) = \mathcal{F}^{-1}[H'_{out}(f)/H'_p(f)]$

and $h'_{out}(t) = \mathcal{F}^{-1}[H'_{out}(f)]$

$h'_p(t) = \mathcal{F}^{-1}[H'_p(f)]$

Time-normalized received optical pulse shape $h'_p(t)$ (section 4.2): rectangular or Gaussian, normalized r.m.s. pulse width σ/T.

Time-normalized equalized output pulse shape $h'_{out}(t)$ (section 4.3): raised cosine or "optimum", rolloff factor β.

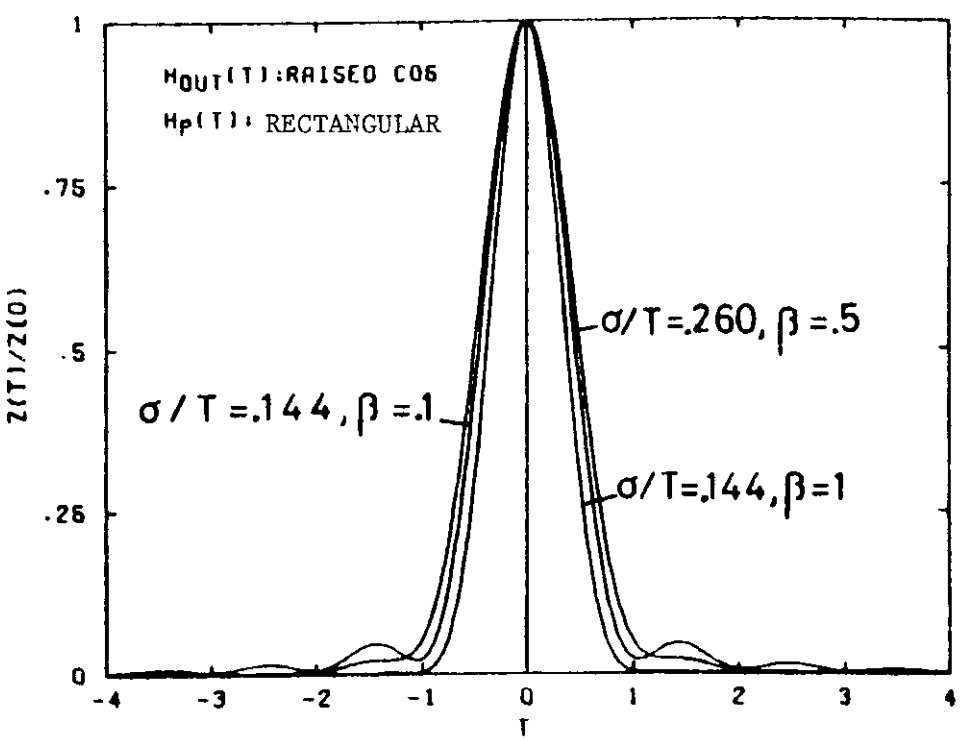

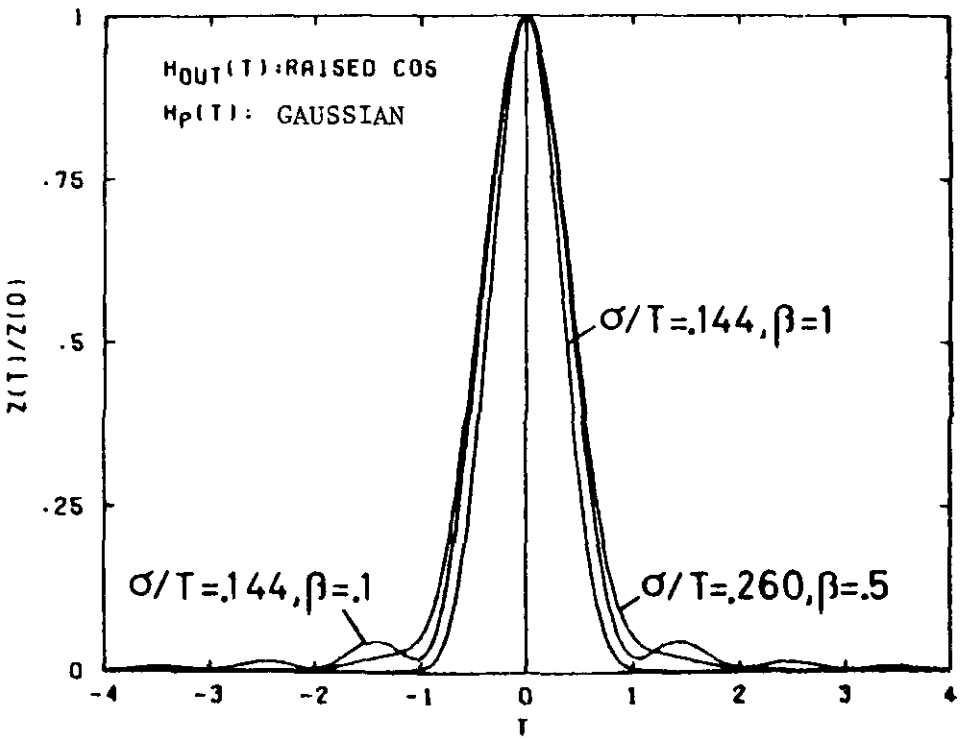
$H_{OUT}(T)$:RAISED COS
$H_P(T)$: GAUSSIAN
σ/T=.144,β=1
σ/T=.144,β=.1
σ/T=.260,β=.5
Z(T)/Z(0)
T
1
.75
.5
.25
0
-4
-3
-2
-1
0
1
2
3
4

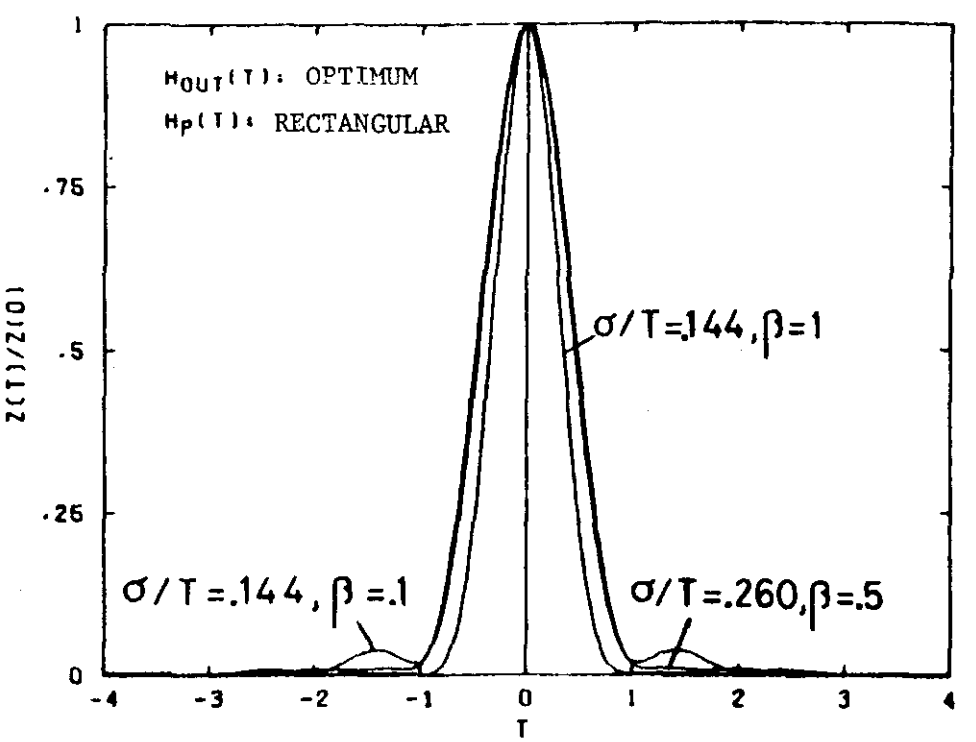
$H_{OUT}(T)$: OPTIMUM
$H_P(T)$: RECTANGULAR
σ/T=.144,β=1
σ/T=.144,β=.1
σ/T=.260,β=.5
Z(T)/Z(0)
T
1
.75
.5
.25
0
-4
-3
-2
-1
0
1
2
3
4

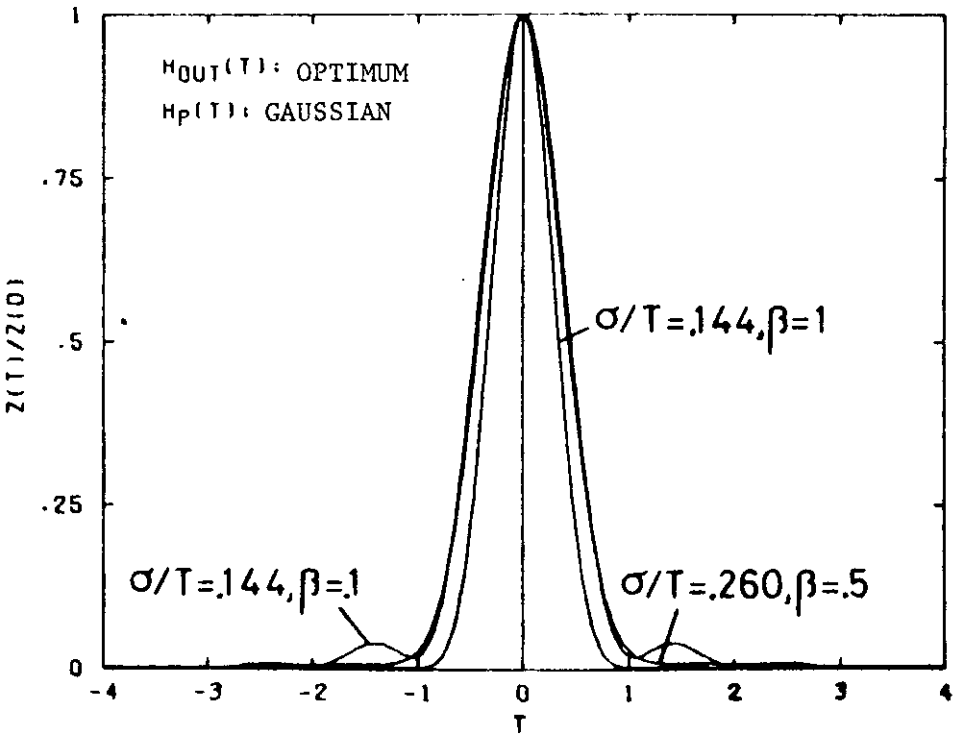
$H_{OUT}(T)$: OPTIMUM
$H_P(T)$: GAUSSIAN
σ/T=.144,β=1
σ/T=.144,β=.1
σ/T=.260,β=.5
Z(T)/Z(0)
T
1
.75
.5
.25
0
-4
-3
-2
-1
0
1
2
3
4

Appendix 2

Plots of the weighting factors versus the normalized r.m.s. optical pulse width, with the rolloff factor of the equalized output spectrum as a parameter

Weighting factors: I_1, Σ_1, $\Sigma_1 - I_1$, I_2 and I_3.

Received optical pulse shape (section 4.2): rectangular or Gaussian, normalized r.m.s. optical pulse width σ/T ($\leq .5$).

Equalized output pulse shape (section 4.3): raised cosine or "optimum", rolloff factor β (= .1, = .5 and =1).

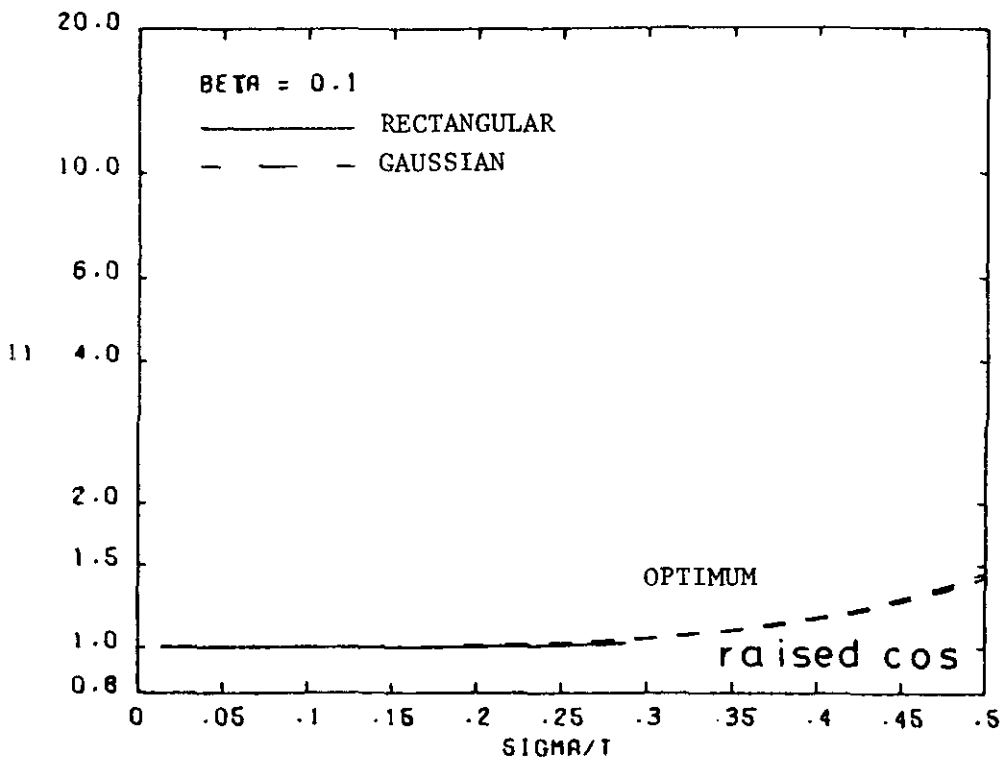

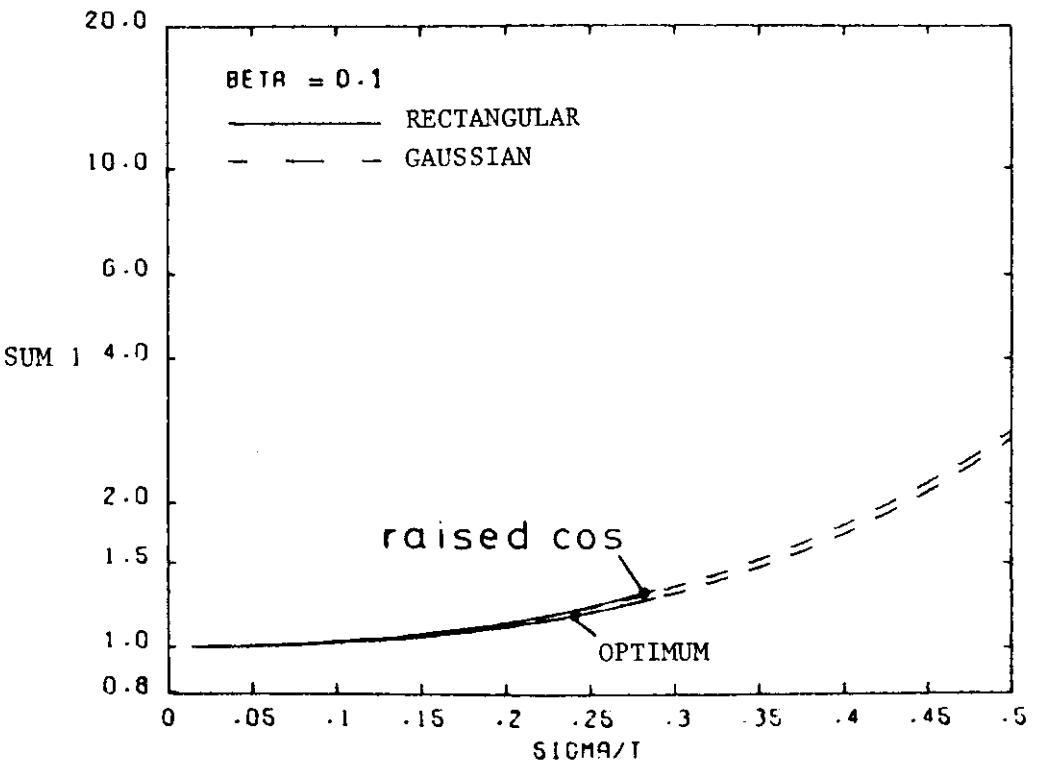
20.0
10.0
6.0
4.0
2.0
1.5
1.0
0.8
SUM 1
BETA = 0.1
RECTANGULAR
GAUSSIAN
raised cos
OPTIMUM
0
.05
.1
.15
.2
.25
.3
.35
.4
.45
.5
SIGMA/T

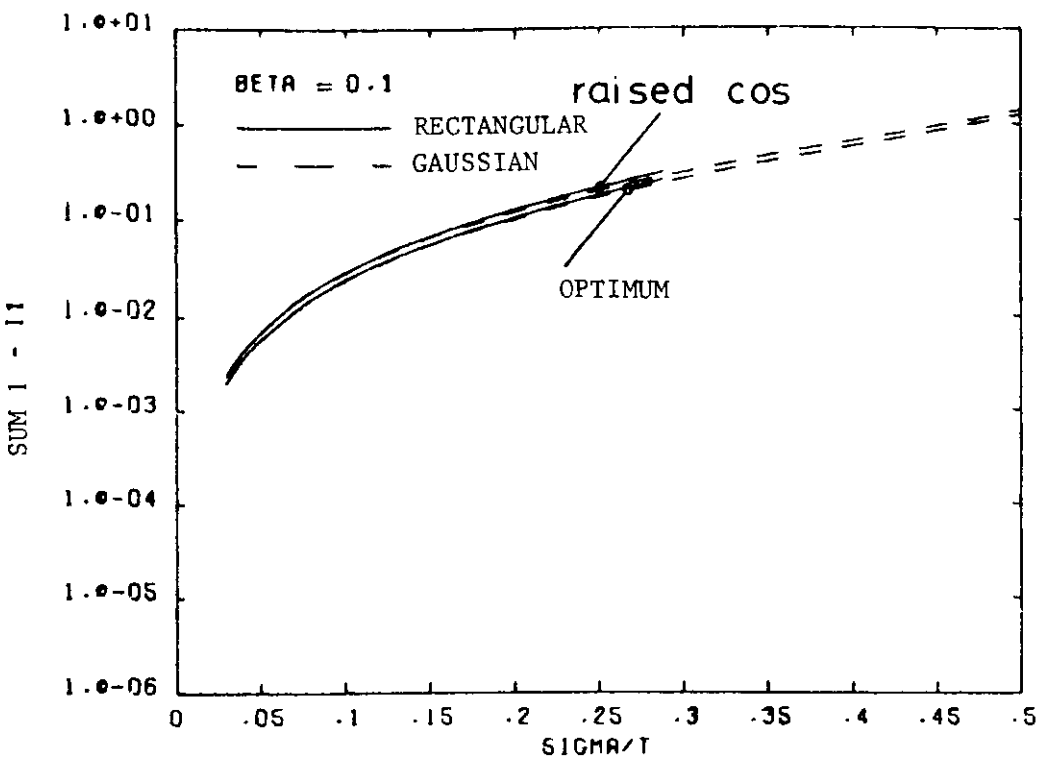
1.e+01
1.e+00
1.e-01
1.e-02
1.e-03
1.e-04
1.e-05
1.e-06
SUM 1 - I1
BETA = 0.1
RECTANGULAR
GAUSSIAN
raised cos
OPTIMUM
0
.05
.1
.15
.2
.25
.3
.35
.4
.45
.5
SIGMA/T

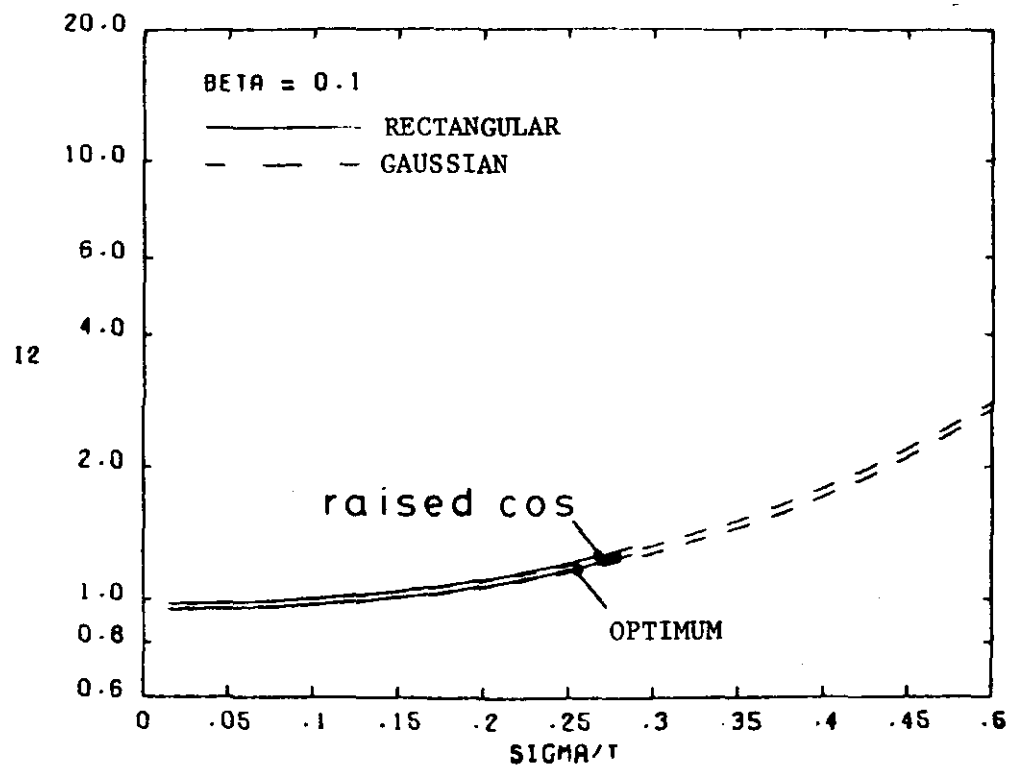
20.0
10.0
6.0
4.0
2.0
1.0
0.8
0.6
I2
BETA = 0.1
RECTANGULAR
GAUSSIAN
raised cos
OPTIMUM
0
.05
.1
.15
.2
.25
.3
.35
.4
.45
.5
SIGMA/T

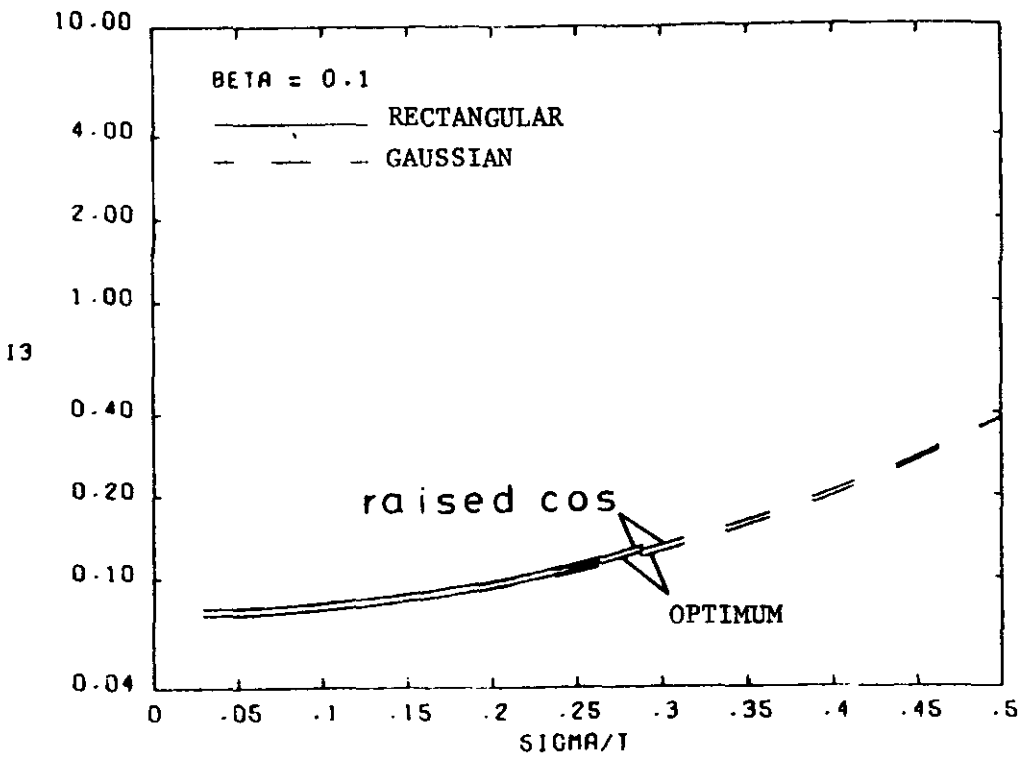
10.00
4.00
2.00
1.00
0.40
0.20
0.10
0.04
I3
BETA = 0.1
RECTANGULAR
GAUSSIAN
raised cos
OPTIMUM
0
.05
.1
.15
.2
.25
.3
.35
.4
.45
.5
SIGMA/T

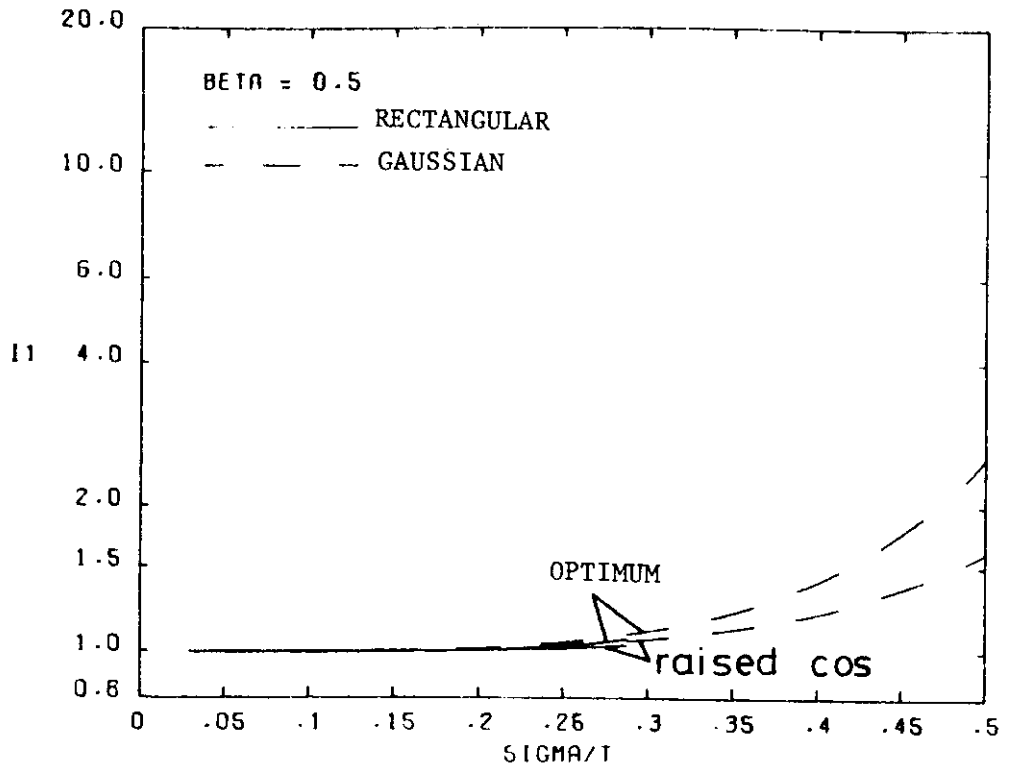
20.0
BETA = 0.5
RECTANGULAR
GAUSSIAN
10.0
6.0
I1
4.0
2.0
1.5
OPTIMUM
1.0
raised cos
0.8
0
.05
.1
.15
.2
.25
.3
.35
.4
.45
.5
SIGMA/T

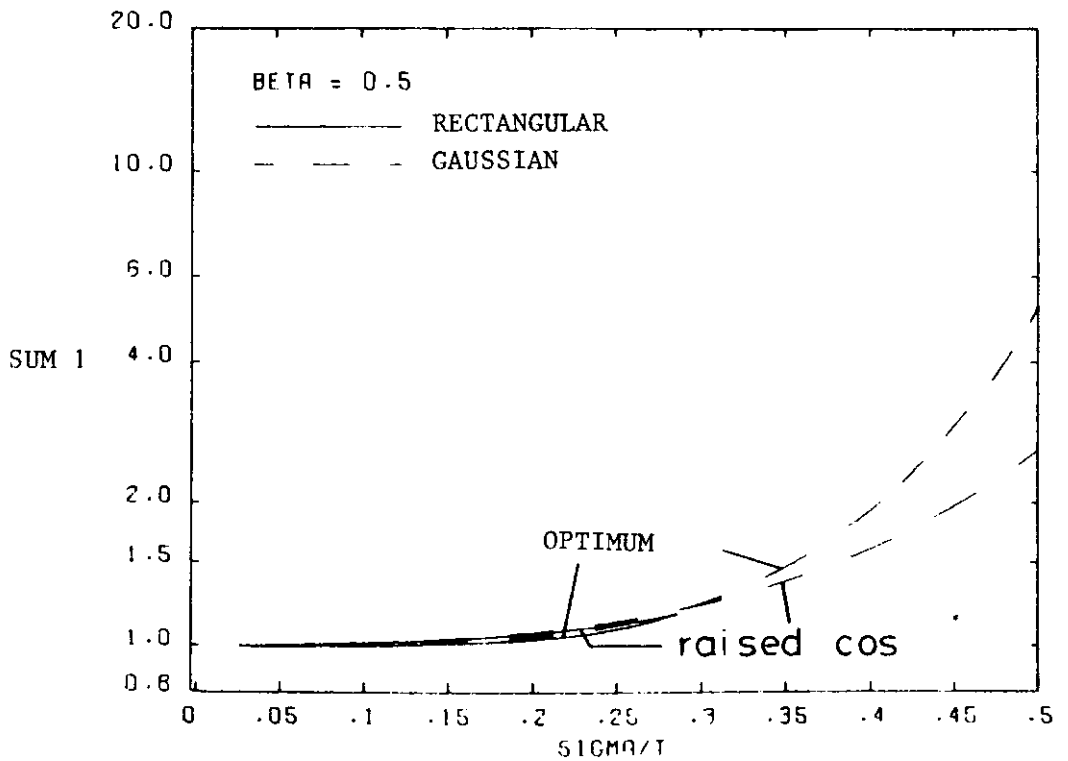
20.0
BETA = 0.5
RECTANGULAR
GAUSSIAN
10.0
6.0
SUM 1
4.0
2.0
1.5
OPTIMUM
1.0
raised cos
0.8
0
.05
.1
.15
.2
.25
.3
.35
.4
.45
.5
SIGMA/T

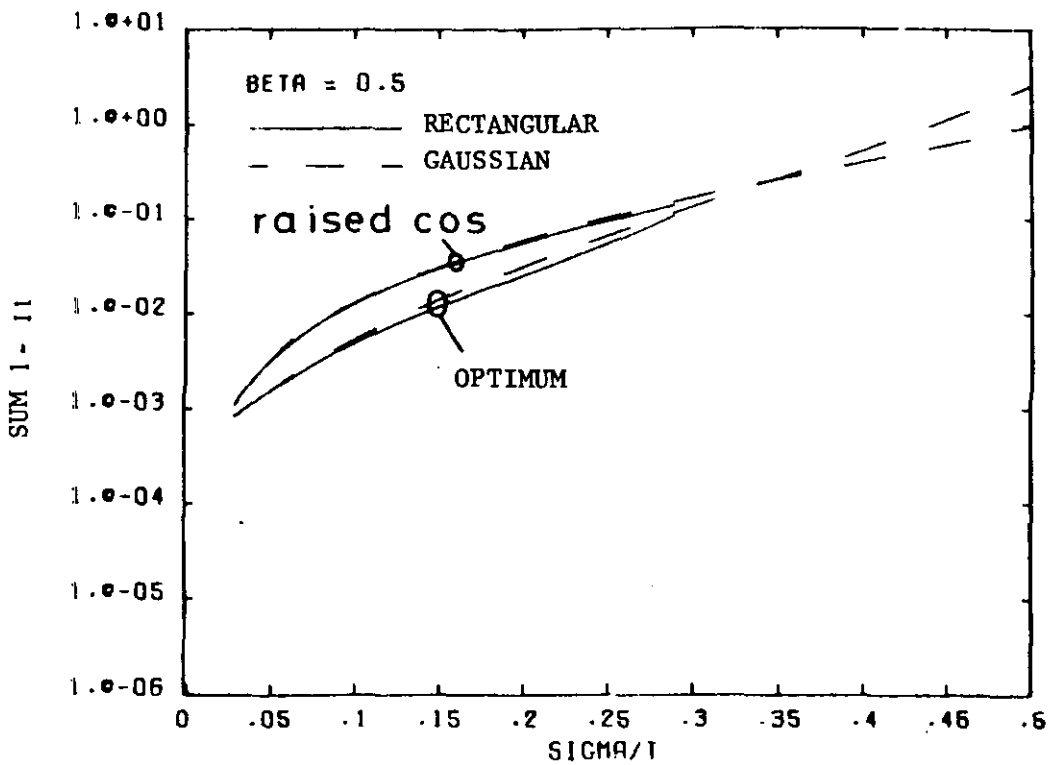
1.0+01
1.0+00
1.0-01
1.0-02
1.0-03
1.0-04
1.0-05
1.0-06
SUM I - II
BETA = 0.5
RECTANGULAR
GAUSSIAN
raised cos
OPTIMUM
0
.05
.1
.15
.2
.25
.3
.35
.4
.45
.5
SIGMA/T

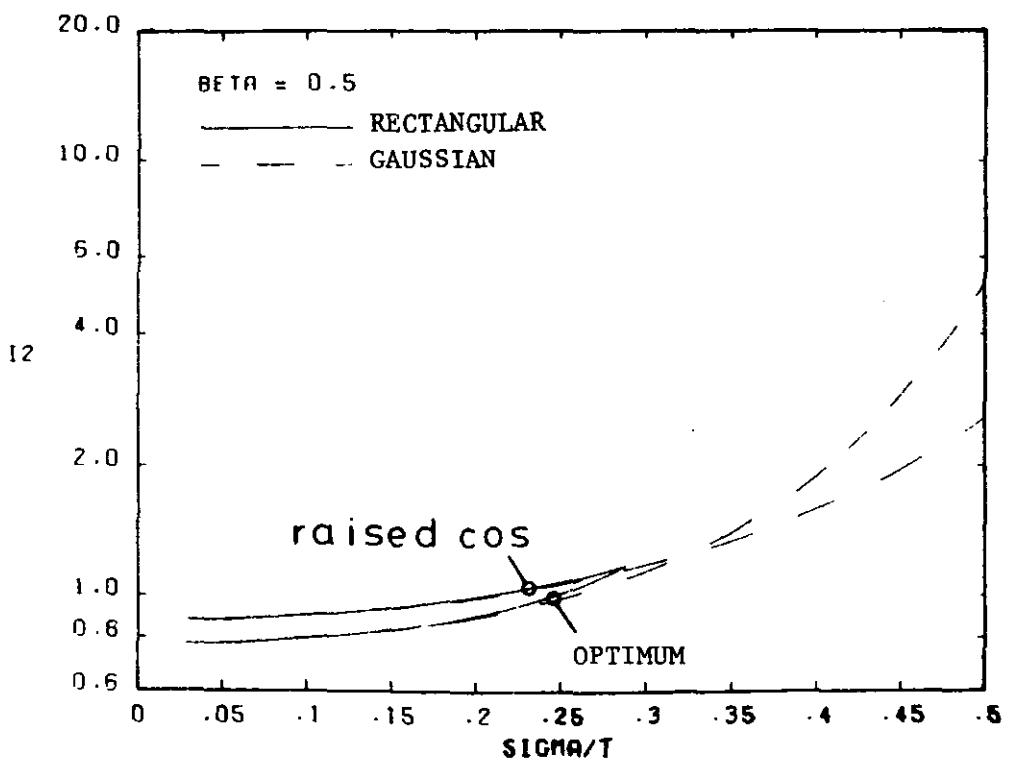
20.0
10.0
6.0
4.0
2.0
1.0
0.8
0.6
I2
BETA = 0.5
RECTANGULAR
GAUSSIAN
raised cos
OPTIMUM
0
.05
.1
.15
.2
.25
.3
.35
.4
.45
.5
SIGMA/T

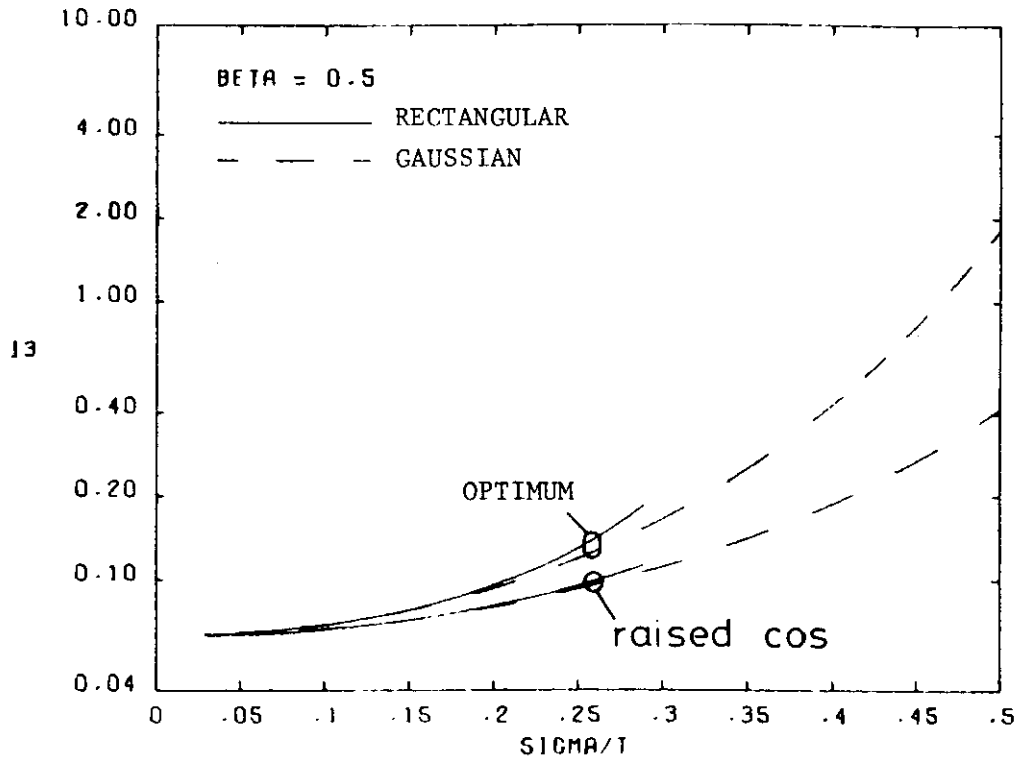
10.00
4.00
2.00
1.00
I3
0.40
0.20
0.10
0.04
BETA = 0.5
RECTANGULAR
GAUSSIAN
OPTIMUM
raised cos
0
.05
.1
.15
.2
.25
.3
.35
.4
.45
.5
SIGMA/T

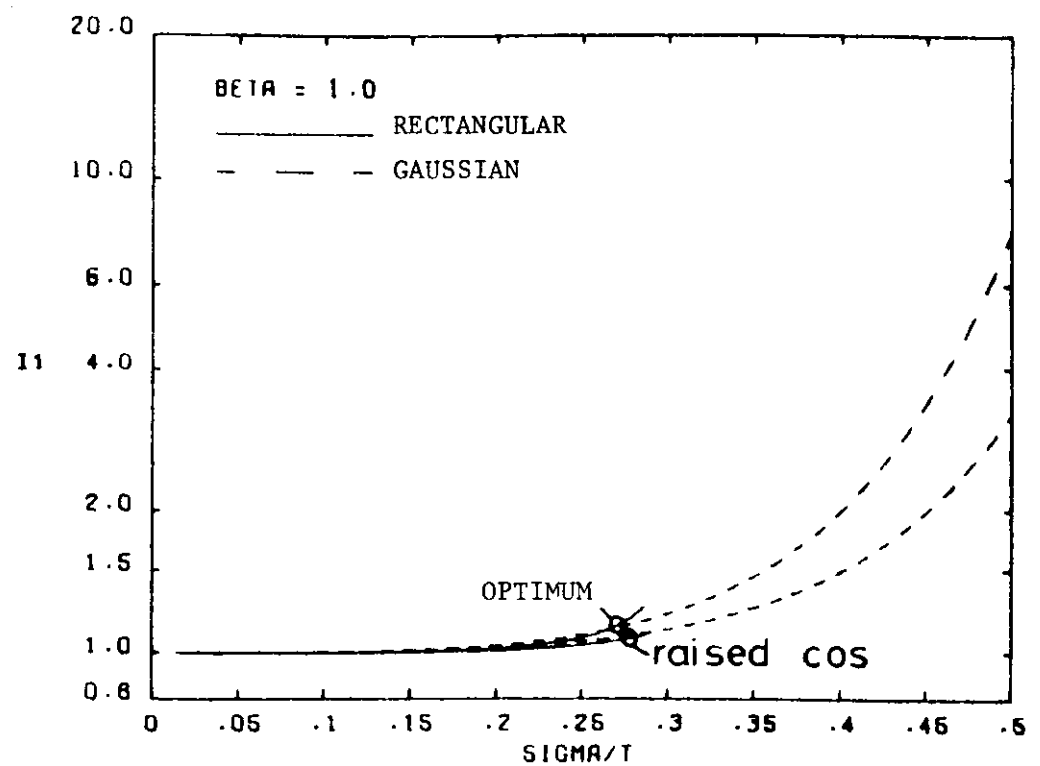
20.0
10.0
6.0
I1
4.0
2.0
1.5
1.0
0.8
BETA = 1.0
RECTANGULAR
GAUSSIAN
OPTIMUM
raised cos
0
.05
.1
.15
.2
.25
.3
.35
.4
.45
.5
SIGMA/T

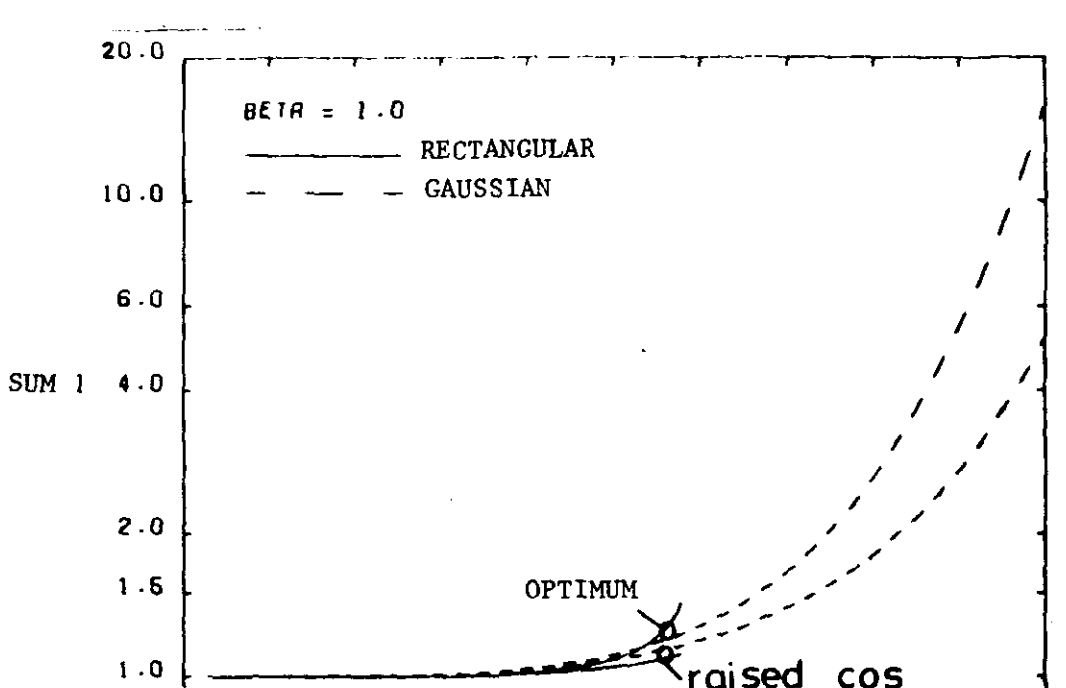
20.0
10.0
6.0
4.0
2.0
1.5
1.0
0.8
SUM 1
BETA = 1.0
RECTANGULAR
GAUSSIAN
OPTIMUM
raised cos
0
.05
.1
.15
.2
.25
.3
.35
.4
.45
.5
SIGMA/T

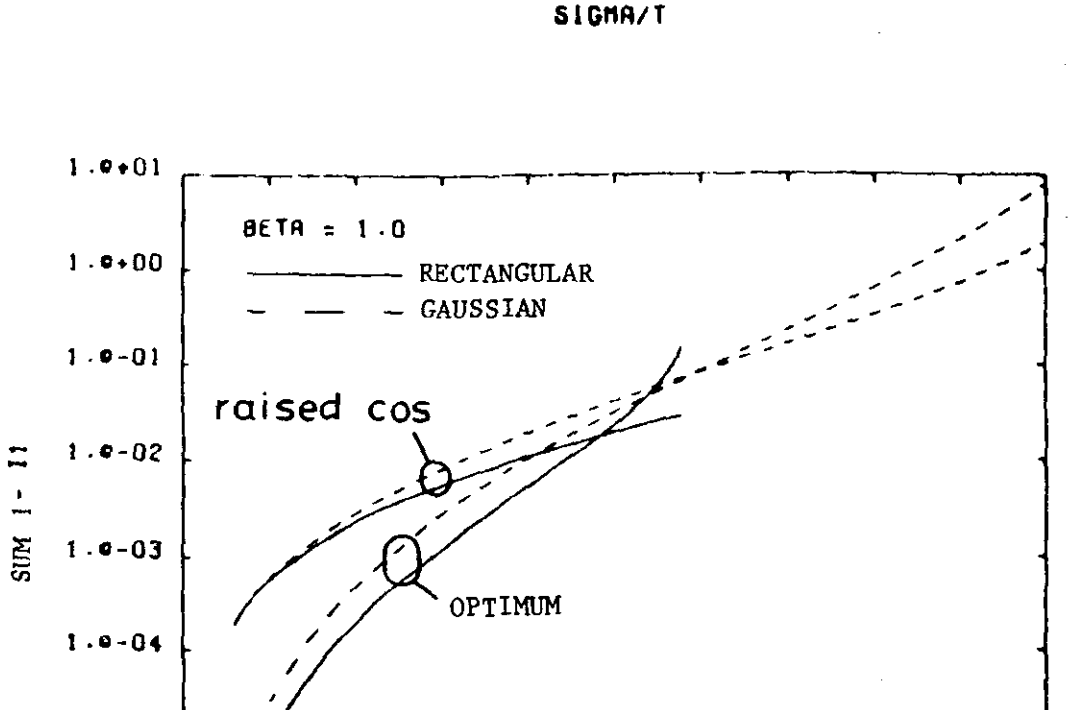
1.0+01
1.0+00
1.0-01
1.0-02
1.0-03
1.0-04
1.0-05
1.0-06
SUM 1 - I1
BETA = 1.0
RECTANGULAR
GAUSSIAN
raised cos
OPTIMUM
0
.05
.1
.15
.2
.25
.3
.35
.4
.45
.5
SIGMA/T

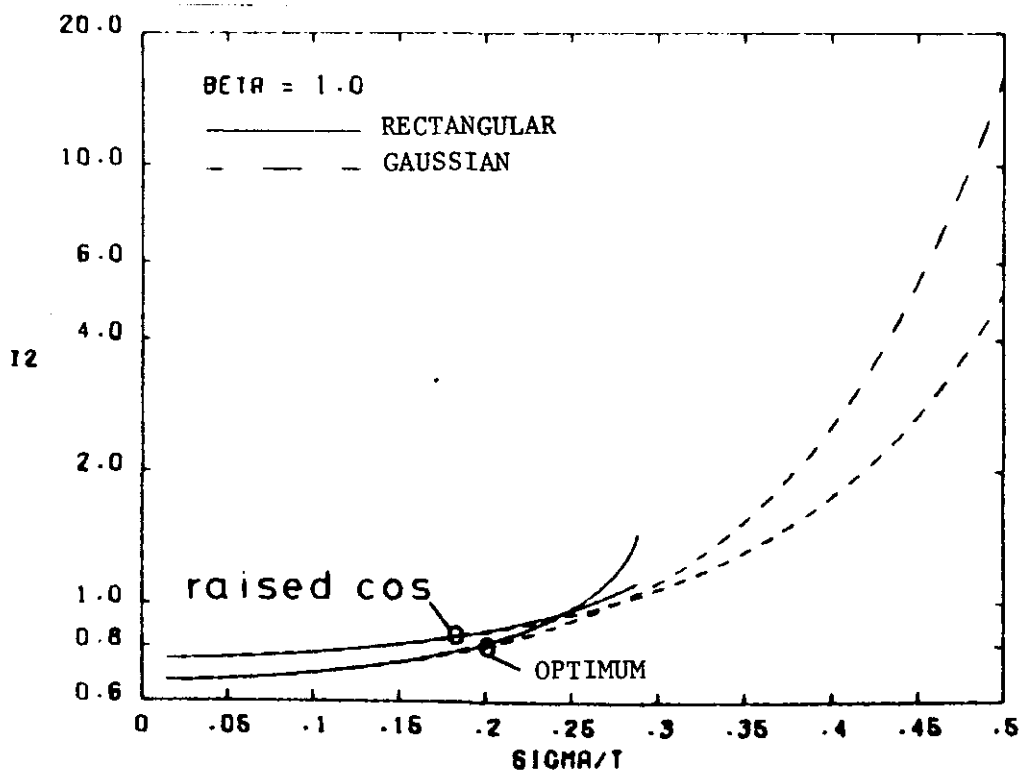
20.0
10.0
6.0
4.0
2.0
1.0
0.8
0.6
I2
BETA = 1.0
RECTANGULAR
GAUSSIAN
raised cos
OPTIMUM
0
.05
.1
.15
.2
.25
.3
.35
.4
.45
.5
SIGMA/T

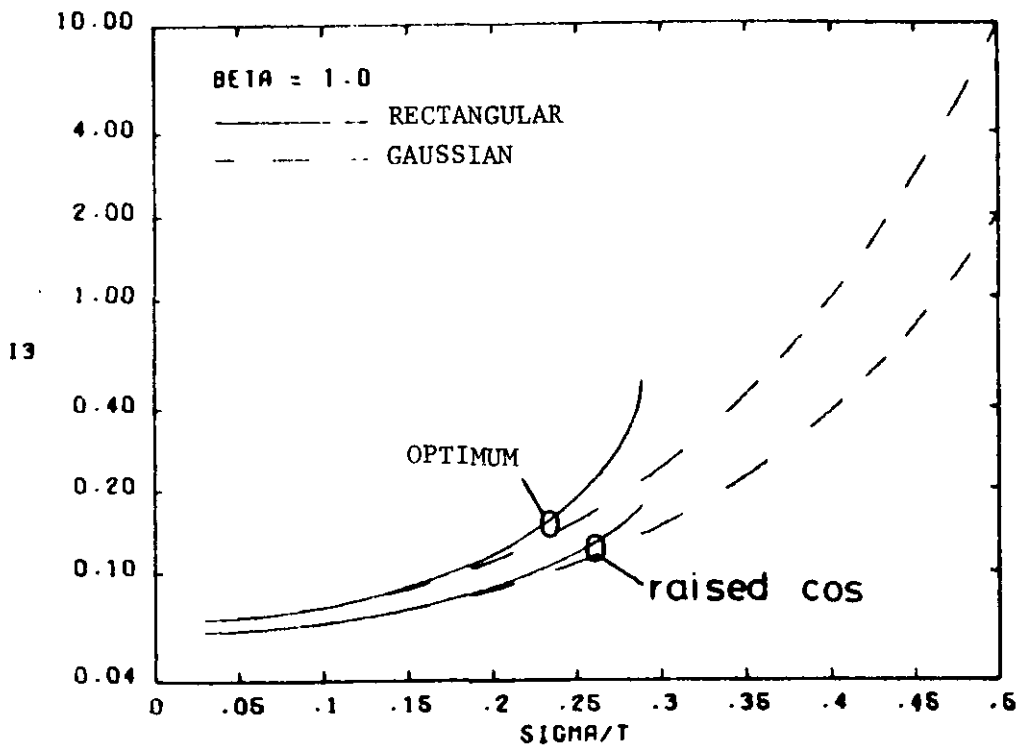
10.00
4.00
2.00
1.00
0.40
0.20
0.10
0.04
I3
BETA = 1.0
RECTANGULAR
GAUSSIAN
OPTIMUM
raised cos
0
.05
.1
.15
.2
.25
.3
.35
.4
.45
.5
SIGMA/T

Appendix 3

Plots of the weighting factors versus the rolloff factor of the raised cosine equalized output spectrum, with the normalized r.m.s. optical pulse width as a parameter

Weighting factors: I_1, Σ_1, $\Sigma_1 - I_1$, I_2 and I_3.

Received optical pulse shape (section 4.2): rectangular or Gaussian, normalized r.m.s. optical pulse width σ/T (= .029, = .087 and = .144).

Equalized output pulse shape (section 4.3): raised cosine, rolloff factor β ($\leq$ 3).

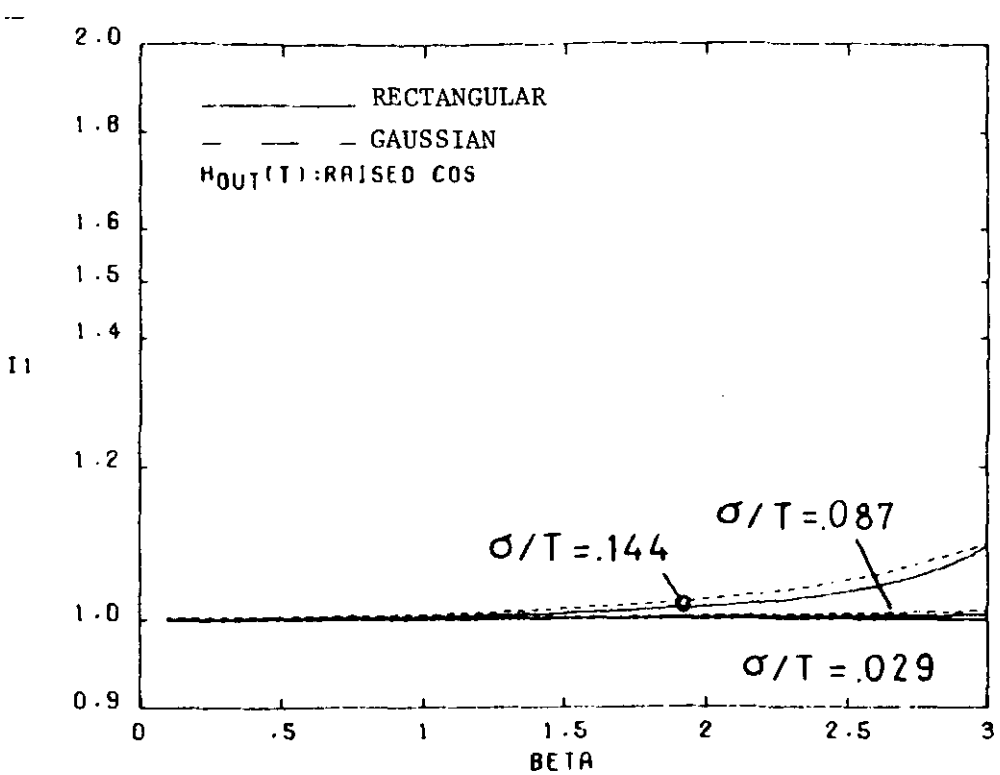

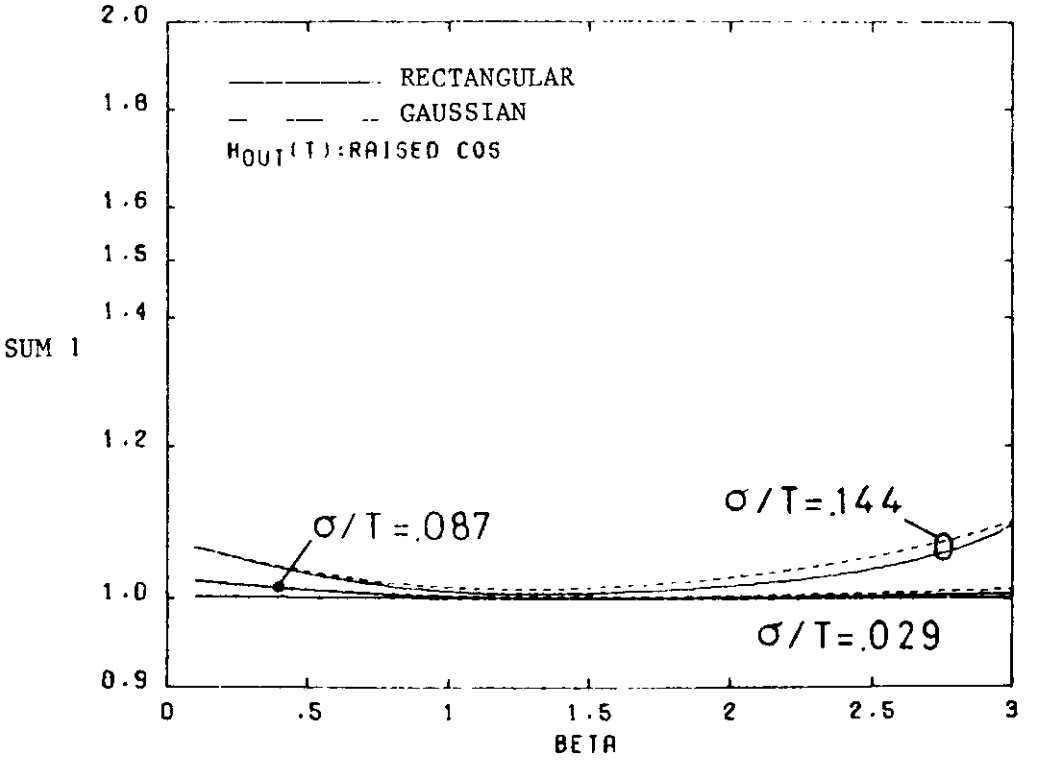
2.0
1.8
1.6
1.5
1.4
SUM 1
1.2
1.0
0.9
RECTANGULAR
GAUSSIAN
$H_{OUT}(f)$:RAISED COS
σ/T=.087
σ/T=.144
σ/T=.029
0
.5
1
1.5
2
2.5
3
BETA

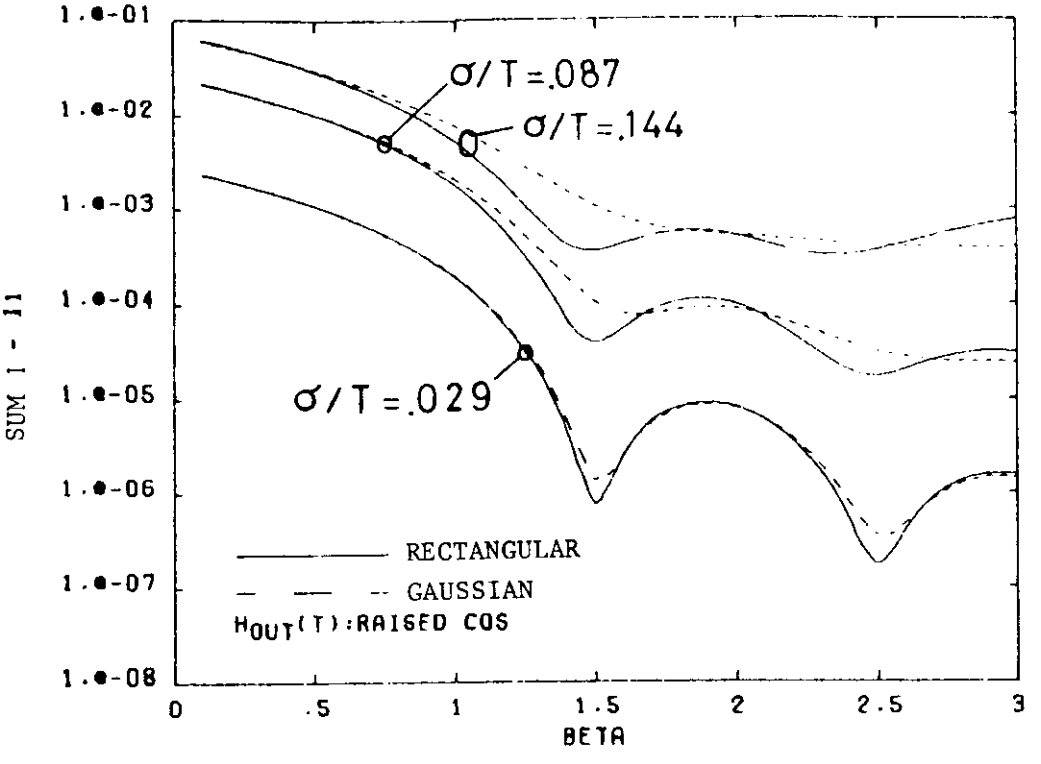
1.●-01
1.●-02
1.●-03
1.●-04
1.●-05
1.●-06
1.●-07
1.●-08
SUM 1 - I1
σ/T=.087
σ/T=.144
σ/T=.029
RECTANGULAR
GAUSSIAN
$H_{OUT}(f)$:RAISED COS
0
.5
1
1.5
2
2.5
3
BETA

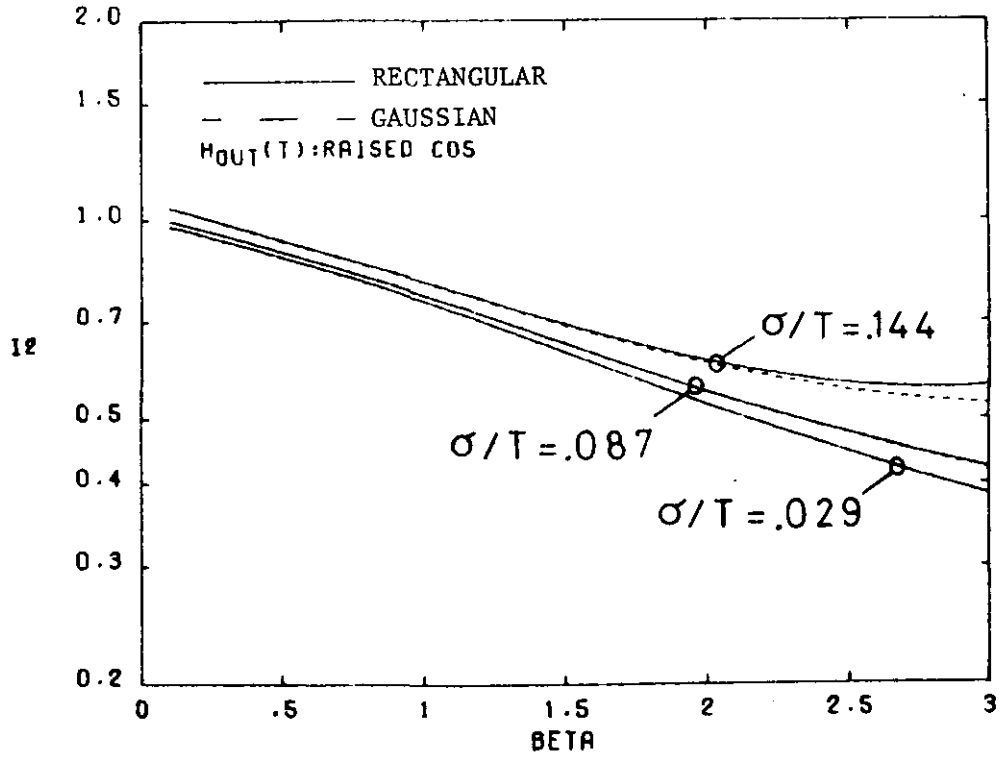
RECTANGULAR
GAUSSIAN
$H_{OUT}(T)$:RAISED COS
$\sigma/T = .144$
$\sigma/T = .087$
$\sigma/T = .029$
I2
BETA
2.0
1.5
1.0
0.7
0.5
0.4
0.3
0.2
0
.5
1
1.5
2
2.5
3

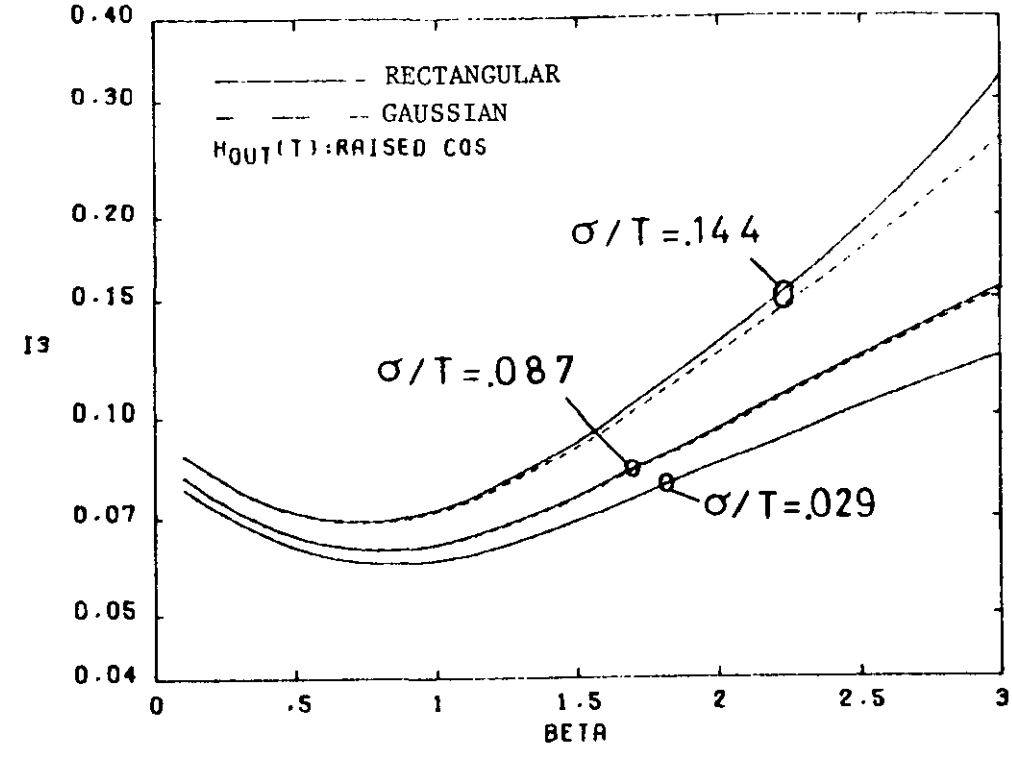
RECTANGULAR
GAUSSIAN
$H_{OUT}(T)$:RAISED COS
$\sigma/T = .144$
$\sigma/T = .087$
$\sigma/T = .029$
I3
BETA
0.40
0.30
0.20
0.15
0.10
0.07
0.05
0.04
0
.5
1
1.5
2
2.5
3

EINDHOVEN UNIVERSITY OF TECHNOLOGY
THE NETHERLANDS
DEPARTMENT OF ELECTRICAL ENGINEERING

Reports:

1) **Dijk, J., M. Jeuken and E.J. Maanders**
AN ANTENNA FOR A SATELLITE COMMUNICATION GROUND STATION (PROVISIONAL ELECTRICAL DESIGN).
TH-Report 68-E-01. 1968. ISBN 90-6144-001-7

2) **Veefkind, A., J.H. Blom and L.H.Th. Rietjens**
THEORETICAL AND EXPERIMENTAL INVESTIGATION OF A NON-EQUILIBRIUM PLASMA IN A MHD CHANNEL. Submitted to the Symposium on Magnetohydrodynamic Electrical Power Generation, Warsaw, Poland, 24-30 July, 1968.
TH-Report 68-E-02. 1968. ISBN 90-6144-002-5

3) **Boom, A.J.W. van den and J.H.A.M. Melis**
A COMPARISON OF SOME PROCESS PARAMETER ESTIMATING SCHEMES.
TH-Report 68-E-03. 1968. ISBN 90-6144-003-3

4) **Eykhoff, P., P.J.M. Ophey, J. Severs and J.O.M. Oome**
AN ELECTROLYTIC TANK FOR INSTRUCTIONAL PURPOSES REPRESENTING THE COMPLEX-FREQUENCY PLANE.
TH-Report 68-E-02. 1968. ISBN 90-6144-004-1

5) **Vermij, L. and J.E. Daalder**
ENERGY BALANCE OF FUSING SILVER WIRES SURROUNDED BY AIR.
TH-Report 68-E-05. 1968. ISBN 90-6144-005-X

6) **Houben, J.W.M.A. and P. Massee**
MHD POWER CONVERSION EMPLOYING LIQUID METALS.
TH-Report 69-E-06. 1969. ISBN 90-6144-006-8

7) **Heuvel, W.M.C. van den and W.F.J. Kersten**
VOLTAGE MEASUREMENT IN CURRENT ZERO INVESTIGATIONS.
TH-Report 69-E-07. 1969. ISBN 90-6144-007-6

8) **Vermij, L.**
SELECTED BIBLIOGRAPHY OF FUSES.
TH-Report 69-E-08. 1969. ISBN 90-6144-008-4

9) **Westenberg, J.Z.**
SOME IDENTIFICATION SCHEMES FOR NON-LINEAR NOISY PROCESSES.
TH-Report 69-E-09. 1969. ISBN 90-6144-009-2

10) **Koop, H.E.M., J. Dijk and E.J. Maanders**
ON CONICAL HORN ANTENNAS.
TH-Report 70-E-10. 1970. ISBN 90-6144-010-6

11) **Veefkind, A.**
NON-EQUILIBRIUM PHENOMENA IN A DISC-SHAPED MAGNETOHYDRODYNAMIC GENERATOR.
TH-Report 70-E-11. 1970. ISBN 90-6144-011-4

12) **Jansen, J.K.M., M.E.J. Jeuken and C.W. Lam. rechtse**
THE SCALAR FEED.
TH-Report 70-E-12. 1969. ISBN 90-6144-012-2

13) **Teuling, D.J.A.**
ELECTRONIC IMAGE MOTION COMPENSATION IN A PORTABLE TELEVISION CAMERA.
TH-Report 70-E-13. 1970. ISBN 90-6144-013-0

EINDHOVEN UNIVERSITY OF TECHNOLOGY
THE NETHERLANDS
DEPARTMENT OF ELECTRICAL ENGINEERING

Reports:

14) **Lorencin, M.**
AUTOMATIC METEOR REFLECTIONS RECORDING EQUIPMENT.
TH-Report 70-E-14. 1970. ISBN 90-6144-014-9

15) **Smets, A.S.**
THE INSTRUMENTAL VARIABLE METHOD AND RELATED IDENTIFICATION SCHEMES.
TH-Report 70-E-15. 1970. ISBN 90-6144-015-7

16) **White, Jr., R.C.**
A SURVEY OF RANDOM METHODS FOR PARAMETER OPTIMIZATION.
TH-Report 70-E-16. 1971. ISBN 90-6144-016-5

17) **Talmon, J.L.**
APPROXIMATED GAUSS-MARKOV ESTIMATORS AND RELATED SCHEMES.
TH-Report 71-E-17. 1971. ISBN 90-6144-017-3

18) **Kalášek, V.**
MEASUREMENT OF TIME CONSTANTS ON CASCADE D.C. ARC IN NITROGEN.
TH-Report 71-E-18. 1971. ISBN 90-6144-018-1

19) **Hosselet, L.M.L.F.**
OZONBILDUNG MITTELS ELEKTRISCHER ENTLADUNGEN.
TH-Report 71-E-19. 1971. ISBN 90-6144-019-X

20) **Arts, M.G.J.**
ON THE INSTANTANEOUS MEASUREMENT OF BLOODFLOW BY ULTRASONIC MEANS.
TH-Report 71-E-20. 1971. ISBN 90-6144-020-3

21) **Roer, Th.G. van de**
NON-ISO THERMAL ANALYSIS OF CARRIER WAVES IN A SEMICONDUCTOR.
TH-Report 71-E-21. 1971. ISBN 90-6144-021-1

22) **Jeuken, P.J., C. Huber and C.E. Mulders**
SENSING INERTIAL ROTATION WITH TUNING FORKS.
TH-Report 71-E-22. 1971. ISBN 90-6144-022-X

23) **Dijk, J., J.M. Berends and E.J. Maanders**
APERTURE BLOCKAGE IN DUAL REFLECTOR ANTENNA SYSTEMS - A REVIEW.
TH-Report 71-E-23. 1971. ISBN 90-6144-023-8

24) **Kregting, J. and R.C. White, Jr.**
ADAPTIVE RANDOM SEARCH.
TH-Report 71-E-24. 1971. ISBN 90-6144-024-6

25) **Damen, A.A.H. and H.A.L. Piceni**
THE MULTIPLE DIPOLE MODEL OF THE VENTRICULAR DEPOLARISATION.
TH-Report 71-E-25. 1971. ISBN 90-6144-025-4

26) **Bremmer, H.**
A MATHEMATICAL THEORY CONNECTING SCATTERING AND DIFFRACTION PHENOMENA, INCLUDING BRAGG-TYPE INTERFERENCES.
TH-Report 71-E-26. 1971. ISBN 90-6144-026-2

27) **Bokhoven, W.M.G. van**
METHODS AND ASPECTS OF ACTIVE RC-FILTERS SYNTHESIS.
TH-Report 71-E-27. 1970. ISBN 90-6144-027-0

28) **Boeschoten, F.**
TWO FLUIDS MODEL REEXAMINED FOR A COLLISIONLESS PLASMA IN THE STATIONARY STATE.
TH-Report 72-E-28. 1972. ISBN 90-6144-028-9

EINDHOVEN UNIVERSITY OF TECHNOLOGY
THE NETHERLANDS
DEPARTMENT OF ELECTRICAL ENGINEERING

Reports:

29) REPORT ON THE CLOSED CYCLE MHD SPECIALIST MEETING. Working group of the joint ENEA/IAEA International MHD Liaison Group.
Eindhoven, The Netherlands, September 20-22, 1971. Edited by **L.H.Th. Rietjens.**
TH-Report 72-E-29. 1972. ISBN 90-6144-029-7

30) **Kessel, C.G.M. van and J.W.M.A. Houben**
LOSS MECHANISMS IN AN MHD GENERATOR.
TH-Report 72-E-30. 1972. ISBN 90-6144-030-0

31) **Veefkind, A.**
CONDUCTION GRIDS TO STABILIZE MHD GENERATOR PLASMAS AGAINST IONIZATION INSTABILITIES.
TH Report 72-E-31. 1972. ISBN 90-6144-031-9

32) **Daalder, J.E., and C.W.M. Vos**
DISTRIBUTION FUNCTIONS OF THE SPOT DIAMETER FOR SINGLE- AND MULTI-CATHODE DISCHARGES IN VACUUM.
TH-Report 73-E-32. 1973. ISBN 90-6144-032-7

33) **Daalder, J.E.**
JOULE HEATING AND DIAMETER OF THE CATHODE SPOT IN A VACUUM ARC.
TH-Report 73-E-33. 1973. ISBN 90-6144-033-5

34) **Huber, C.**
BEHAVIOUR OF THE SPINNING GYRO ROTOR.
TH-Report 73-E-34. 1973. ISBN 90-6144-034-3

35) **Bastian, C. et al.**
THE VACUUM ARC AS A FACILITY FOR RELEVANT EXPERIMENTS IN FUSION RESEARCH. Annual Report 1972. EURATOM-T.H.E. Group 'Rotating Plasma'.
TH-Report 73-E-35. 1973. ISBN 90-6144-035-1

36) **Blom, J.A.**
ANALYSIS OF PHYSIOLOGICAL SYSTEMS BY PARAMETER ESTIMATION TECHNIQUES.
TH-Report 73-E-36. 1973. ISBN 90-6144-036-X

37) Cancelled

38) **Andriessen, F.J., W. Boerman and I.F.E.M. Holtz**
CALCULATION OF RADIATION LOSSES IN CYLINDER SYMMETRIC HIGH PRESSURE DISCHARGES BY MEANS OF A DIGITAL COMPUTER.
TH-Report 73-E-38. 1973. ISBN 90-6144-038-6

39) **Dijk, J., C.T.W. van Diepenbeek, E.J. Maanders and L.F.G. Thurlings**
THE POLARIZATION LOSSES OF OFFSET ANTENNAS.
TH-Report 73-E-39. 1973. ISBN 90-6144-039-4

40) **Goes, W.P.**
SEPARATION OF SIGNALS DUE TO ARTERIAL AND VENOUS BLOOD FLOW IN THE DOPPLER SYSTEM THAT USES CONTINUOUS ULTRASOUND.
TH-Report 73-E-40. 1973. ISBN 90-6144-040-8

41) **Damen, A.A.H.**
A COMPARATIVE ANALYSIS OF SEVERAL MODELS OF THE VENTRICULAR DEPOLARIZATION; INTRODUCTION OF A STRING-MODEL.
TH-Report 73-E-41. 1973. ISBN 90-6144-041-6

EINDHOVEN UNIVERSITY OF TECHNOLOGY
THE NETHERLANDS
DEPARTMENT OF ELECTRICAL ENGINEERING

Reports:

42) **Dijk, G.H.M. van**
THEORY OF GYRO WITH ROTATING GIMBAL AND FLEXURAL PIVOTS.
TH-Report 73-E-42. 1973. ISBN 90-6144-042-4

43) **Breimer, A.J.**
ON THE IDENTIFICATION OF CONTINOUS LINEAR PROCESSES.
TH-Report 74-E-43. 1974. ISBN 90-6144-043-2

44) **Lier, M.C. van and R.H.J.M. Otten**
CAD OF MASKS AND WIRING.
TH-Report 74-E-44. 1974. ISBN 90-6144-044-0

45) **Bastian, C. et al.**
EXPERIMENTS WITH A LARGE SIZED HOLLOW CATHODE DISCHARDE FED WITH ARGON. Annual Report 1973. EURATOM-T.H.E. Group 'Rotating Plasma'.
TH-Report 74-E-45. 1974. ISBN 90-6144-045-9

46) **Roer, Th.G. van de**
ANALYTICAL SMALL-SIGNAL THEORY OF BARITT DIODES.
TH-Report 74-E-46. 1974. ISBN 90-6144-046-7

47) **Leliveld, W.H.**
THE DESIGN OF A MOCK CIRCULATION SYSTEM.
TH-Report 74-E-47. 1974. ISBN 90-6144-047-5

48) **Damen, A.A.H.**
SOME NOTES ON THE INVERSE PROBLEM IN ELECTRO CARDIOGRAPHY.
TH-Report 74-E-48. 1974. ISBN 90-6144-048-3

49) **Meeberg, L. van de**
A VITERBI DECODER.
TH-Report 74-E-49. 1974. ISBN 90-6144-049-1

50) **Poel, A.P.M. van der**
A COMPUTER SEARCH FOR GOOD CONVOLUTIONAL CODES.
TH-Report 74-E-50. 1974. ISBN 90-6144-050-5

51) **Sampic, G.**
THE BIT ERROR PROBABILITY AS A FUNCTION PATH REGISTER LENGTH IN THE VITERBI DECODER.
TH-Report 74-E-51. 1974. ISBN 90-6144-051-3

52) **Schalkwijk, J.P.M.**
CODING FOR A COMPUTER NETWORK.
TH-Report 74-E-52. 1974. ISBN 90-6144-052-1

53) **Stapper, M.**
MEASUREMENT OF THE INTENSITY OF PROGRESSIVE ULTRASONIC WAVES BY MEANS OF RAMAN-NATH DIFFRACTION.
TH-Report 74-E-53. 1974. ISBN 90-6144-053-X

54) **Schalkwijk, J.P.M. and A.J. Vinck**
SYNDROME DECODING OF CONVOLUTIONAL CODES.
TH-Report 74-E-54. 1974. ISBN 90-6144-054-8

55) **Yakimov, A.**
FLUCTUATIONS IN IMPATT-DIODE OSCILLATORS WITH LOW Q-FACTORS.
TH-Report 74-E-55. 1974. ISBN 90-6144-055-6

EINDHOVEN UNIVERSITY OF TECHNOLOGY
THE NETHERLANDS
DEPARTMENT OF ELECTRICAL ENGINEERING

Reports:

56) **Plaats, J. van der**
ANALYSIS OF THREE CONDUCTOR COAXIAL SYSTEMS. Computer-aided determination of the frequency characteristics and the impulse and step response of a two-port consisting of a system of three coaxial conductors terminating in lumped impedances.
TH-Report 75-E-56. 1975. ISBN 90-6144-056-4

57) **Kalken, P.J.H. and C. Kooy**
RAY-OPTICAL ANALYSIS OF A TWO DIMENSIONAL APERTURE RADIATION PROBLEM.
TH-Report 75-E-57. 1975. ISBN 90-6144-057-2

58) **Schalkwijk, J.P.M., A.J. Vinck and L.J.A.E. Rust**
ANALYSIS AND SIMULATION OF A SYNDROME DECODER FOR A CONSTRAINT LENGTH k = 5, RATE R = ½ BINARY CONVOLUTIONAL CODE.
TH-Report 75-E-58. 1975. ISBN 90-6144-058-0.

59) **Boeschoten, F. et al.**
EXPERIMENTS WITH A LARGE SIZED HOLLOW CATHODE DISCHARGE FED WITH ARGON, II. Annual Report 1974. EURATOM-T.H.E. Group 'Rotating Plasma'.
TH-Report 75-E-59. 1975. ISBN 90-6144-059-9

60) **Maanders, E.J.**
SOME ASPECTS OF GROUND STATION ANTENNAS FOR SATELLITE COMMUNICATION.
TH-Report 75-E-60. 1975. ISBN 90-6144-060-2

61) **Mawira, A. and J. Dijk**
DEPOLARIZATION BY RAIN: Some Related Thermal Emission Considerations.
TH-Report 75-E-61. 1975. ISBN 90-6144-061-0

62) **Safak, M.**
CALCULATION OF RADIATION PATTERNS OF REFLECTOR ANTENNAS BY HIGH-FREQUENCY ASYMPTOTIC TECHNIQUES.
TH-Report 76-E-62. 1976. ISBN 90-6144-062-9

63) **Schalkwijk, J.P.M. and A.J. Vinck**
SOFT DECISION SYNDROME DECODING.
TH-Report 76-E-63. 1976. ISBN 90-6144-063-7

64) **Damen, A.A.H.**
EPICARDIAL POTENTIALS DERIVED FROM SKIN POTENTIAL MEASUREMENTS.
TH-Report 76-E-64. 1976. ISBN 90-6144-064-5

65) **Bakhuizen, A.J.C. and R. de Boer**
ON THE CALCULATION OF PERMEANCES AND FORCES BETWEEN DOUBLY SLOTTED STRUCTURES.
TH-Report 76-E-65. 1976. ISBN 90-6144-065-3

66) **Geutjes, A.J.**
A NUMERICAL MODEL TO EVALUATE THE BEHAVIOUR OF A REGENERATIVE HEAT EXCHANGER AT HIGH TEMPERATURE.
TH-Report 76-E-66. 1976. ISBN 90-6144-066-1

67) **Boeschoten, F. et al.**
EXPERIMENTS WITH A LARGE SIZED HOLLOW CATHODE DISCHARGE, III; concluding work Jan. 1975 to June 1976 of the EURATOM-THE Group 'Rotating Plasma'.
TH-Report 76-E-67. 1976. ISBN 90-6144-067-X

68) **Cancelled.**

EINDHOVEN UNIVERSITY OF TECHNOLOGY
THE NETHERLANDS
DEPARTMENT OF ELECTRICAL ENGINEERING

Reports:

69) **Merck, W.F.H. and A.F.C. Sens**
THOMSON SCATTERING MEASUREMENTS ON A HOLLOW CATHODE DISCHARGE.
TH-Report 76-E-69. 1976. ISBN 90-6144-069-6

70) **Jongbloed, A.A.**
STATISTICAL REGRESSION AND DISPERSION RATIOS IN NONLINEAR SYSTEM IDENTIFICATION.
TH-Report 77-E-70. 1977. ISBN 90-6144-070-X

71) **Barrett, J.F.**
BIBLIOGRAPHY ON VOLTERRA SERIES HERMITE FUNCTIONAL EXPANSIONS AND RELATED SUBJECTS.
TH-Report 77-E-71. 1977. ISBN 90-6144-071-8

72) **Boeschoten, F. and R. Komen**
ON THE POSSIBILITY TO SEPARATE ISOTOPES BY MEANS OF A ROTATING PLASMA COLUMN: Isotope separation with a hollow cathode discharge.
TH-Report 77-E-72. 1977. ISBN 90-6144-072-6

73) **Schalkwijk, J.P.M., A.J. Vinck and K.A. Post**
SYNDROME DECODING OF BINARY RATE-k/n CONVOLUTIONAL CODES.
TH-Report 77-E-73. 1977. ISBN 90-6144-073-4

74) **Dijk, J., E.J. Maanders and J.M.J. Oostvogels**
AN ANTENNA MOUNT FOR TRACKING GEOSTATIONARY SATELLITES.
TH-Report 77-E-74. 1977. ISBN 90-6144-074-2

75) **Vinck, A.J., J.G. van Wijk and A.J.P. de Paepe**
A NOTE ON THE FREE DISTANCE FOR CONVOLUTIONAL CODES.
TH-Report 77-E-75. 1977. ISBN 90-6144-075-0

76) **Daalder, J.E.**
RADIAL HEAT FLOW IN TWO COAXIAL CYLINDRICAL DISKS.
TH-Report 77-E-76. 1977. ISBN 90-6144-076-9

77) **Barrett, J.F.**
ON SYSTEMS DEFINED BY IMPLICIT ANALYTIC NONLINEAR FUNCTIONAL EQUATIONS.
TH-Report 77-E-77. 1977. ISBN 90-6144-077-7

78) **Jansen, J. and J.F. Barrett**
ON THE THEORY OF MAXIMUM LIKELIHOOD ESTIMATION OF STRUCTURAL RELATIONS. Part 1: One dimensional case.
TH-Report 78-E-78. 1977. ISBN 90-6144-078-5

79) **Borghi, C.A., A.F.C. Sens, A. Veefkind and L.H.Th. Rietjens**
EXPERIMENTAL INVESTIGATION ON THE DISCHARGE STRUCTURE IN A NOBLE GAS MHD GENERATOR.
TH-Report 78-E-79. 1978. ISBN 90-6144-079-3

80) **Bergmans, T.**
EQUALIZATION OF A COAXIAL CABLE FOR DIGITAL TRANSMISSION: Computer-optimized location of poles and zeros of a constant-resistance network to equalize a coaxial cable 1.2/4.4 for high-speed digital transmission (140 Mb/s).
TH-Report 78-E-80. 1978. ISBN 90-6144-080-7

EINDHOVEN UNIVERSITY OF TECHNOLOGY
THE NETHERLANDS
DEPARTMENT OF ELECTRICAL ENGINEERING

Reports:

81) **Kam, J.J. van der and A.A.H. Damen**
OBSERVABILITY OF ELECTRICAL HEART ACTIVITY STUDIES WITH THE SINGULAR VALUE DECOMPOSITION
TH-Report 78-E-81. 1978. ISBN 90-6144-081-5

82) **Jansen, J. and J.F. Barrett**
ON THE THEORY OF MAXIMUM LIKELIHOOD ESTIMATION OF STRUCTURAL RELATIONS. Part 2: Multi-dimensional case.
TH-Report 78-E-82. 1978. ISBN 90-6144-082-3

83) **Etten, W. van and E. de Jong**
OPTIMUM TAPPED DELAY LINES FOR THE EQUALIZATION OF MULTIPLE CHANNEL SYSTEMS.
TH-Report 78-E-83. 1978. ISBN 90-6144-083-1

83) **Vinck, A.J.**
MAXIMUM LIKELIHOOD SYNDROME DECODING OF LINEAR BLOCK CODES.
TH-Report 78-E-84. 1978. ISBN 90-6144-084-X

85) **Spruit, W.P.**
A DIGITAL LOW FREQUENCY SPECTRUM ANALYZER, USING A PROGRAMMABLE POCKET CALCULATOR.
TH-Report 78-E-85. 1978. ISBN 90-6144-085-8

86) **Beneken, J.E.W. et al**
TREND PREDICTION AS A BASIS FOR OPTIMAL THERAPY.
TH-Report 78-E-86. 1978. ISBN 90-6144-086-6

87) **Geus, C.A.M. and J. Dijk**
CALCULATION OF APERTURE AND FAR-FIELD DISTRIBUTION FROM MEASUREMENTS IN THE FRESNEL ZONE OF LARGE REFLECTOR ANTENNAS.
TH-Report 78-E-87. 1978. ISBN 90-6144-087-4

88) **Hajdasinski, A.K.**
THE GAUSS-MARKOV APPROXIMATED SCHEME FOR IDENTIFICATION OF MULTIVARIABELE DYNAMICAL SYSTEMS VIA THE REALIZATION THEORY.
An Explicit Approach.
TH-Report 78-E-88. 1978. ISBN 90-6144-088-2

89) **Niederlinski, A.**
THE GLOBAL ERROR APPROACH TO THE CONVERGENDE OF CLOSED-LOOP IDENTIFICATION, SELF-TUNING REGULATORS AND SELF-TUNING PREDICTORS.
TH-Report 78-E-89. 1978. ISBN 90-6144-089-0

90) **Vinck, A.J. and A.J.P. de Paepe**
REDUCING THE NUMBER OF COMPUTATIONS IN STACK DECODING OF CONVOLUTIONAL CODES BY EXPLOITING SYMMETRIES OF THE ENCODER.
TH-Report 78-E-90. 1978. ISBN 90-6144-090-4

91) **Geutjes, A.J. and D.J. Kleyn**
A PARAMETRIC STUDY OF 1000 MWe COMBINED CLOSED CYCLE MHD/STEAM ELECTRICAL POWER GENERATING PLANTS.
TH-Report 78-E-91. 1978. ISBN 90-6144-091-2

92) **Massee, P.**
THE DISPERSION RELATION OF ELECTROTHERMAL WAVES IN A NONEQUILIBRIUM MHD PLASMA.
TH-Report 78-E-92. 1978. ISBN 90-6144-092-0

EINDHOVEN UNIVERSITY OF TECHNOLOGY
THE NETHERLANDS
DEPARTMENT OF ELECTRICAL ENGINEERING

Reports:

93) Duin, C.A. van
DIPOLE SCATTERING OF ELECTROMAGNETIC WAVES PROPAGATION THROUGH A RAIN MEDIUM. TH-Report 79-E-93. 1979. ISBN 90-6144-093-9

94) Kuijper, A.H. de and L.K.J. Vandamme
CHARTS OF SPATIAL NOISE DISTRIBUTION IN PLANAR RESISTORS WITH FINITE CONTACTS. TH-Report 79-E-94. 1979. ISBN 90-6144-094-7

95) Hajdasinski, A.K. and A.A.H. Damen
REALIZATION OF THE MARKOV PARAMETER SEQUENCES USING THE SINGULAR VALUE DECOMPOSITION OF THE HANKEL MATRIX. TH-Report 79-E-95. 1979. ISBN 90-6144-095-5

96) Stefanov, B.
ELECTRON MOMENTUM TRANSFER CROSS-SECTION IN CESIUM AND RELATED CALCULATIONS OF THE LOCAL PARAMETERS OF Cs + Ar MHD PLASMAS. TH-Report 79-E-96. 1979. ISBN 90-6144-096-3

97) Worm, S.C.J.
RADIATION PATTERNS OF CIRCULAR APERTURES WITH PRESCRIBED SIDELOBE LEVELS. TH-Report 79-E-97. 1979. ISBN 90-6144-097-1

98) Kroezen, P.H.C.
A SERIES REPRESENTATION METHOD FOR THE FAR FIELD OF AN OFFSET REFLECTOR ANTENNA. TH-Report 79-E-98. 1979. ISBN 90-6144-098-X

99) Koonen, A.M.J.
ERROR PROBABILITY IN DIGITAL FIBER OPTIC COMMUNICATION SYSTEMS. TH-Report 79-E-99. 1979. ISBN 90-6144-099-8